Contents

1 INTRODUCTION

1.1 ALUMINIUM

1.1.1 The element

Aluminium is the thirteenth element of the periodic table and it belongs to group 13. It was discovered by Davy in 1805 and it was isolated for the first time by Örsted in 1825. Approximately 8 % of Earth crust contains Aluminium, and this element is the third most abundant element after oxygen (47%) and silicon (28%). Table 1.1 lists some properties of Aluminium.

Table 1.1: Aluminium properties

Atomic mass (m.a.u.)	26.982
Atomic ray (calc.) (pm)	125
Electronic configuration	$[Ne]3s^23p$
Oxidation states	III
Melting point (°C)	660.33
Boiling point (°C)	2467
Evaporation heat (kJ/mol)	293.4
Fusion heat (kJ/mol)	10.79
Electro-negativity	1.61
Natural isotopes	26, 27
Synthetic isotopes	23, 24, 25, 28, 29, 30

The element in its lowest oxidation state (zero) is very reactive; for this reason it can be found in nature just as Al^{3+}, forming compounds like oxides, silicates, sulphates and phosphates which can be found mostly in clays, feldspar, cryolite and bauxite. Bauxite is the raw material used to extract aluminium for its industrial production. Thanks to its corrosion resistance (due to the formation of an oxide protective film) and to its ability to form light alloys, aluminium in its metallic form can be used in

several applications. Even its ionic form is important for many applications: aluminium sulphate is used as a flocculant in water purification, alkyls-aluminium are involved in the catalytic process in Ziegler–Natta polymerizations, aluminium chloride is contained in deodorants as antiperspicant, aluminium hydroxide is used in toothpastes as abrasive, and several aluminium compounds are found in anti-acid medicines and in the treatment of hyperphosphatemia, a disease which affects patients with chronic renal deficiency [Willis 1983].

In natural water the concentration of Al^{3+} is very low, about 10^{-8} M in neutral conditions; this value increases by changing the pH and with the presence of complexing agents, like inorganic anions (fluoride and phosphates) or organic compounds (humic and fulvic acids). Aluminium solubility especially increases with decreasing pH, as evidenced by the greater dissolution extent of the metal from minerals observed in recent decades due to the increase of rain acidity. This phenomenon has increased aluminium bioavailability in natural water [Zatta 1995].

1.1.2   Aluminium speciation in aqueous solutions

Several studies were carried out to study aluminium speciation in aqueous solutions, but results are often very different each other, due to the multiplicity of compounds forming in the solution, the slowness of reactions, and the formation of metastabile species.

At acidic pH, Al^{3+} is found exclusively as $[Al(H_2O)_6]^{3+}$, an octahedral exahydrate ion usually written as Al^{3+}. Starting from pH above 3.5, Al^{3+} is involved in hydrolysis reactions which lead to the loss of H^+ ions from the coordinated water molecules. The species $Al(OH)^{2+}$, $Al(OH)_2^+$, $Al(OH)_3$ and $Al(OH)_4^-$ [Martin 1986] are formed. $Al(OH)_3$ is slightly soluble , so it undergoes precipitation at pH about 4, but it dissolves again at basic pH (about 11) after the formation of tetrahydroxoaluminate. If Al^{3+} concentration is high enough, at neutral pH the formation of several polymeric species can occur, in which hydroxyl ions connect two or more metal ions; the formation kinetics of these polymers is very slow (months or years). For this reason, these species have not been univocally characterized yet. The most reliable speciation model is the one proposed by Öhman, referred to an environment of NaCl 0.6 M [Ohman 1988]. Table 1.2 reports the stoichiometry and formation constant of the identified aluminium hydroxo-complexes.

Table 1.2: stoichiometry and formation constant of identified aluminium hydrolysis products, and solubility product of amorphous and crystalline aluminium hydroxide [Ohman 1988]. (Constants refer to the equilibrium $m\text{Al} + n\text{H}_2\text{O} \rightleftharpoons \text{Al}_m(\text{OH})_n + n\text{H}^+$)

Species	$\log \beta$
$\text{Al}(\text{H}_2\text{O})_6^{3+}$	---
$\text{Al}(\text{OH})^{2+}$	-5.52
$\text{Al}(\text{OH})_2^+$	-11.3
$\text{Al}(\text{OH})_3$	-17.3
$\text{Al}(\text{OH})_4^-$	-23.46
$\text{Al}_3(\text{OH})_4^{5+}$	-13.57
$\text{Al}_{13}(\text{OH})_{32}^{7+}$	-109.2
$\text{Al}(\text{OH})_{3(\text{amorphous})}$	$pK_s = 10.8$
$\alpha-\text{Al}(\text{OH})_3$	$pK_s = 9.2$

Observed pK_a referring to consecutive hydrolysis of Al^{3+} are lower than the ones expected by electrostatic and statistic considerations. This can be explained on the basis of the progressive decrease of the Al^{3+} coordination number of from 6 ($\text{Al}(\text{H}_2\text{O})_6^{3+}$) to 4 ($\text{Al}(\text{OH})_4^-$), which shortens the Al-O bond. Consequently, the deprotonation of coordinated water molecules is facilitated, because of their higher acidity [Martin 1986]. The proved pentacoordination of aluminium in the complex $\text{Al}(\text{OH})^{2+}$ [Swaddle 2005] further confirms this hypothesis.

1.1.3 Complex formation between aluminium(III) and ligands: thermodynamic aspects

In the presence of a ligand, Al^{3+} can form many complexes, in addition to the ones previously mentioned. Thanks to its strong localized charge and small ionic radius, aluminium(III) is considered a hard Lewis acid. Therefore it presents a good affinity for Lewis bases of the same type, which include, in particular, functional groups containing negatively charged oxygens. The strongest interactions are observed with organic species like alkoxides (R-O$^-$), phenoxides (Ar–O$^-$), hydroxamic acids (N–O$^-$) and carboxylate (COO$^-$) ions; interactions with carboxy groups are significant only if oxygen is significantly negatively charged thanks to the resonance form C–O$^-$. As regards inorganic ions, Al^{3+} affinity is high towards SO_4^{2-}, SiO_4^{4-}, and especially

towards PO_4^{3-} and F^-. The stability of the complexes increases with the number of coordination sites of the binder: the stability can be very high if the ligand is able to form a polydentate chelation ring with 5 or 6 terms. However, at basic pH all complexes are destabilized due to the formation of the species $Al(OH)_4^-$.

1.1.4 Complex formation between aluminium (III) and ligands: kinetic aspects

The complexation reactions involving Al^{3+} go generally to completeness within some seconds. This time value is much larger than that required for many other metal ions (usually 10^{-6}–10^{-7} seconds), but it is lower than that of Cr^{3+} and Co^{3+} (10^6 and 10 seconds, respectively), which are the most inert metal ions. The kinetics of substitution of the solvent from the metal depends also on the type of the ligand [Kiss 1996]. The substitution of the ligand from the metal centre seems to follow an interchange dissociative mechanism (*D*), whereby a dissociation is required before a new ligand molecule may coordinate. This mechanism agree with the small dimensions of Al^{3+} [Hugy 1985]. In the first step a ionic couple is formed; this is the rate determining step. The loss of a water molecule, and the formation of the complex (1.1), occur after the first step:

$$Al(H_2O)_6^{3+} + HL \rightleftharpoons Al(H_2O)_6(HL)^{3+}$$

$$Al(H_2O)_6(HL)^{3+} \rightarrow Al(H_2O)_5(HL)^{3+} + H_2O \tag{1.1}$$

$$Al(H_2O)_5(HL)^{3+} \rightarrow Al(H_2O)_5L^{2+} + H^+$$
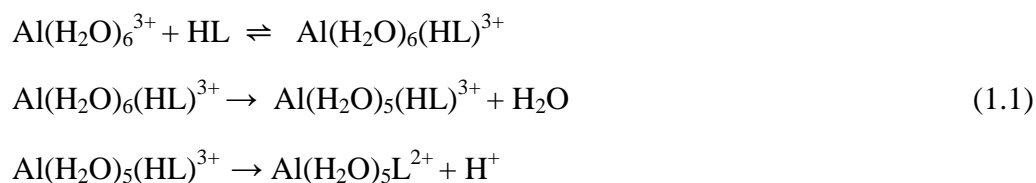
It is worth nothing that the only available kinetic information in aluminium-ligand reactions have been obtained at acidic pH, or regards very strong mononuclear complexes. This because at neutral pH, and/or if the complexes are not very stable, hydroxo-complexes and metastabile species can form (see paragraph 1.1.2), which strongly complicates the speciation in solution.

1.1.5 Biochemistry and toxicity of aluminium

Aluminium is commonly present in beverages such as tea, coffee and water (thanks to the depuration processes with aluminium sulphate). Aluminium can also be assimilated through cooking food in aluminium pans, vaccines and body deodorants which contain aluminium chlorohydrates [Crisponi 2012 (a)]. The daily amount of aluminium introduced with diet is about 5–50 mg [Ganrot 1986]. A higher amount is introduced with antiacids drugs, gel for hyperphosphatemia treatment, and food additives such as E173 (metallic aluminium), E541 (sodium and aluminium

phosphate), E554 (sodium and aluminium silicate), E556 (Calcium and aluminium silicate).

When aluminium enters the circulatory system, it is complexed by transferrin, a protein devoted to transport iron inside the organism. The ion is then removed through kidney dialysis and, in a little amount, through feces excretion. The remaining part is accumulated mainly in brain, bones, lungs and milt [Zatta 1995].

Several clinical and epidemiological studies evidenced a correlation between aluminium storage in the organism and the onset of some human diseases; these affect almost exclusively uremic patients who undergo dialysis, and they are dialysis dementia, vitamin D-resistant osteomalacia, and microcytic anemia (not dependent on iron).

Dialysis dementia is a neurological disease characterized by the increase of aluminium in the brain up to 20-30 times compared to a healthy person. [Alfrey 1980]. It leads to personality changes, psychosis and dementia until death, which may occur even in few months. At the base of the disease there is the inability to eliminate aluminium by renal excretion, so the accumulation increases up to toxic levels. Furthermore, in dialysis patients the metal also comes from the gel used to control hyperphosphatemia and dialysis water, which enters directly into the bloodstream without passing through the gastro-intestinal barrier. To avoid this problem, deionized dialysis water and filters are being used nowadays.

Vitamin D-resistant osteomalacia is a disease characterized by bone fragility and musculo-skeletal pain, caused by the increased amount of aluminium in bones and brain [Alfrey 1980]. In the bone tissue level, the ion is gradually internalized in osteoblasts, which have several exposed transferrin receptors on their plasma membrane. Inside these cells, the metal plays an antiproliferative role by inhibiting the synthesis of bone matrix, to which osteoblasts would be devoted in healthy organisms [Silverthorn 2007].

Microcytic anemia is a disease that affects the hematopoietic system of patients with uremia. It causes a significant reduction in the size of red blood cells. This anemia is called "iron independent" because it is not caused by iron deficiency.

1.2   ZINC

1.2.1   The element

Zinc is present on Earth crust at an amount equal to 132 ppm and it is the 24th most abundant element. Crustal Zn is mainly bound with sulphur as zinc sulphide (ZnS).

Its structure is similar to the diamond one, with half of the positions occupied by S, and half by Zn.

Zinc is mainly used as antirust metal: a thin zinc layer covers iron and other metals to avoid rust. Zinc is used also to obtain alloys: the most common zinc alloy is brass (Cu/Zn containing 20-50% of zinc). Among the ionic compounds, ZnO is the commercially important one, because it is used as white pigment in paints, in cosmetics, as deodorizing and antibacterial agent in baby powders, and as zinc source in food. Some properties of Zinc are listed in Table 1.3.

Table 1.3: zinc properties

Atomic mass (m.a.u.)	65.409
Atomic ray (calc.) (pm)	142
Electronic configuration	$[Ar]3d^{10}4s^2$
Oxidation states	II
Melting point (°C)	420
Boiling point (°C)	907
Evaporation heat (kJ/mol)	115.3
Fusion heat (kJ/mol)	7.322
Electro-negativity	1.65
Natural isotopes	64, 66, 67, 68, 70
Synthetic isotopes	65, 72

Zinc has two electrons belonging to an *s* orbital, and a full *d* orbital. The removal of the s electrons gives compounds with the characteristic oxidation state (+II). There is no evidence for the existence of oxidation states higher than (+II), because the removal of more electrons would destroy the symmetry of a complete *d* shell. Zinc is a soft metal, probably because *d* electrons do not participate to metallic bond.

Zinc is a silvery metal, and it is oxidized easily by humid air; it dissolves in diluted non-oxidant acids forming hydrogen; it reacts with oxidant acids like concentrated HNO_3 and H_2SO_4, forming salts, sodium oxides and SO_2. Furthermore, zinc has amphoteric properties and it is soluble in alkali forming zincates with formulas

$[Zn(OH)_4]^{2-}$ and $[Zn(OH)_3]^-$. By heating, the metal forms the oxide ZnO, the insoluble sulphide ZnS, and halides ZnX_2. [Lee 1996]

1.2.2 Zinc speciation in aqueous solutions

The hydrolysis behaviour of Zn^{2+} is not completely sure due to some inconsistencies existing in the extensive literature on this ion. Some of the apparent disparity, is probably due to small complexing effects in the different media employed. While there is a general consensus (among the potentiometric studies) for the existence of $ZnOH^+$ and Zn_2OH^{3+} in small amounts, the solubility and solvent extraction results indicate the possible formation, with very different stabilities, of $Zn(OH)_2$, $Zn(OH)_3^-$, $Zn(OH)_4^{2-}$ and $Zn_2(OH)_6^{2-}$. In any case, Zn^{2+} hydrolyzes only sparingly before precipitation of the poorly soluble $Zn(OH)_2$ which commences in the neutral region. The fresh precipitates produced from zinc salt solutions are usually the amorphous $Zn(OH)_2$ or ZnO, which will subsequently change to a more stable form upon aging. In some cases mixed precipitates which have not been well characterized can form. The formation constants of zinc hydroxo-complexes estimated in perchlorate media at 25 °C are listed in Table 1.4.

Table 1.4: formation constants of zinc hydrolysis products, and solubility product of zinc oxide and hydroxide. [Charles 1976] (constants refer to the equilibrium
$$m\text{Zn} + n\text{H}_2\text{O} \rightleftharpoons \text{Zn}_m(\text{OH})_n + n\text{H}^+)$$

Species	Log β
$ZnOH^+$	−8.96
$Zn(OH)_2$	−16.9
$Zn(OH)_3^-$	−28.4
$Zn(OH)_4^{2-}$	−41.2
Zn_2OH^{3+}	−9.0
$Zn_2(OH)_6^{2-}$	−57.8
ZnO(prec.)	pK_s=11.31
$Zn(OH)_2$(amorphous)	pK_s=12.45

1.2.3 Complex formation between zinc (II) and ligands: structural and thermodynamic aspects

Zn^{2+} ion does not have stabilizing effects of the ligand field, because its d shells are complete. The stereochemistry of its compounds is then governed only by size,

electrostatic forces, and covalent bonding forces. As regards the coordination number, it can be noted that ZnO crystallizes in a lattice in which the Zn^{2+} ions are situated in tetrahedral cavities surrounded by four oxide ions. Similarly, $ZnCl_2$ crystallizes in not less than three allotropic forms, at least two of which contain tetracoordinated zinc atoms. A commercially available Zn^{2+} compound is nitrate, which can be obtained with different hydratation forms, among which $Zn(NO_3)_2 \cdot 6H_2O$ is the most common. Similarly, it is possible to isolate salts containing $[Zn(NH_3)_6]^{2+}$ from reactions done in liquid NH_3, e.g. $ZnCl_2 \cdot 6NH_3$. So, the coordination number 6 is common. Anyway the coordination number 4 is also often observed; for example in aqueous solutions, $[Zn(NH_3)_6]^{2+}$ exists in equilibrium with tetrahedral $[Zn(NH_3)_4]^{2+}$. As well, coordination number 5 can occur in several salts, as e.g. $Zn(acac)_2 \cdot H_2O$ in which the coordination of Zn^{2+} is square-based pyramidal [Housecroft 2005].

Zinc dithiocarbamates complexes and other sulfur compounds are important accelerators in the vulcanization of rubber with sulfur. Dithiocarbamates form 1:1 pentacoordinated complexes with amines [Coates 1967]. The zinc β-dichetonates also form 1:1 pentacoordinated adducts with nitrogenous bases [Graddon 1964]. Examples of high coordination numbers for Zn^{2+} are rare, but include pentagonal bipyramidal $[Zn(15\text{-crown-5})(H_2O)_2]^{2+}$, and dodecahedral $[Zn(NO_3)_4]^{2-}$ [Albert 1967]. Some examples of the different structures and coordination numbers displayed by Zn^{2+} complexes are reported in Table 1.5 [Albert 1967]. As regards thermodynamics, Zn^{2+} is a borderline hard/soft ion and readily complexes with ligands containing a range of donor atoms, e.g. borderline N-, hard O- and soft S-donors. At the same time, the complexes formed by this metal ion are generally not extremely stable.

Table 1.5: zinc stereochemistry [Albert 1967]

Coordination number	Geometry	Examples
2	Linear	$Zn(CH_3)_2$
4	Tetrahedral	$[Zn(CN)_4]^{2-}$, $ZnCl_2(s)$, $Zn(NH_3)_2Cl_2$
5	Distorted trigonal-based bipyramidal or square-based pyramidal	$ZnCl_2$, $Zn(acac)_2 \cdot H_2O$
6	Octahedral	$[Zn(NH_3)_6]^{2+}$ (crystals)

1.2.4 Complex formation between zinc (II) and ligands: kinetic aspects

There are relatively few data for substitution reactions involving Zn^{2+}. Some measurements, e.g. those for the Zn^{2+}-bpy system, strongly evidence the I_d character in the substitution. When the interchange is concerted and there is partial, and equal, association and dissociation of the entering and leaving groups, the mechanism is termed I. This will rarely occur and more likely there will be a preference for I_a or I_d, in which the entering and leaving groups are either firmly (I_a) or weakly (I_d) embedded in the coordination sphere of the metal. In the interchange mechanism, there is an interchange of H_2O and L perhaps within an outer-sphere complex ($MH_2O\cdots L$) which is very rapidly formed from the reactants as shown in scheme (1.2) [Wilkins 2002]:

$$ZnH_2O + L \rightleftharpoons ZnH_2O\cdots L \qquad k_1, \text{ fast}$$

$$ZnH_2O\cdots L \rightleftharpoons ZnL\cdots H_2O \qquad k_2 \qquad\qquad (1.2)$$

$$ZnL\cdots H_2O \rightleftharpoons ZnL + H_2O \qquad \text{fast}$$
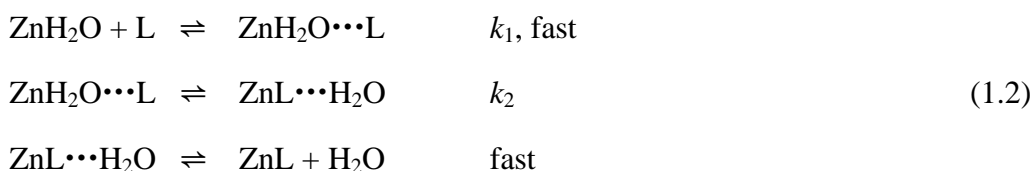
The water exchange rate constants for several metal ions are shown in Figure 1.1. The water exchange constant for Zn^{2+} is about 10^7 s^{-1}, which represents a mean value compared with those of many other metal ions. However, it is 10^7 larger than that of Al^{3+}.

Figure 1.1: rate constants (s^{-1}) for water exchange of metal cations, measured directly by NMR or estimated from the rate constants for complex formation [Wilkins 2002].

1.2.5 Biochemistry and toxicity of zinc

Since the 1920-1930s the essentiality of this element for the growth of plants and animals had been recognized. However, only in the '60s it was shown that this element is essential also fo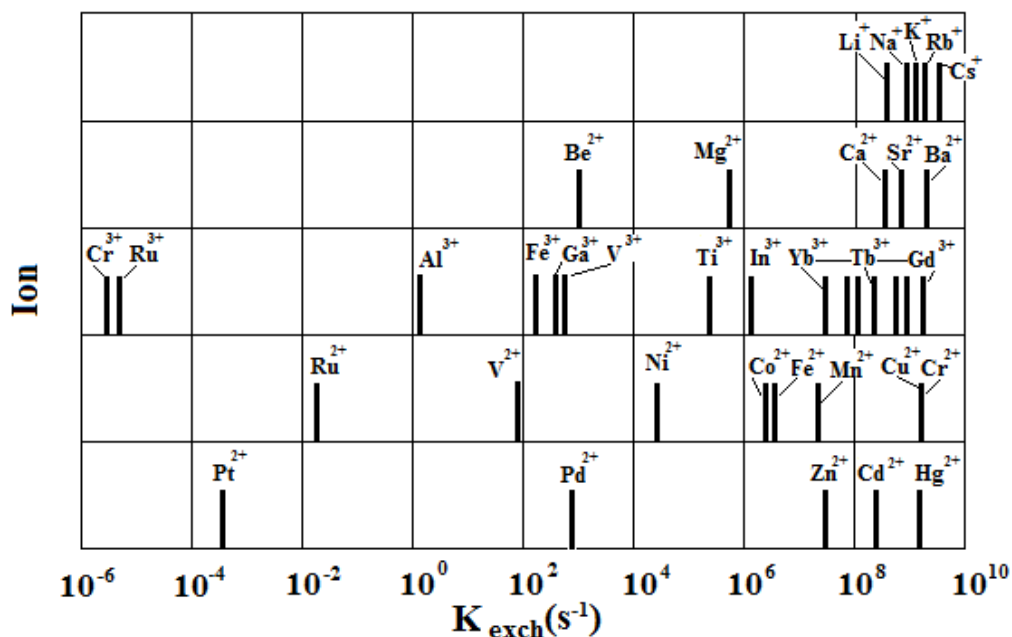r humans [Pories 1966]. It is a component of many enzymes in the liver, pancreas, kidney and other organs. It is estimated that more than one-third of human enzymes contain metals [Guengerich 2009]. They participate in a wide variety of biochemical processes in the cells. The equilibrium distribution of metal ions is crucial for many physiological functions. Enzymes containing Zn take part in many metabolic processes like synthesis and degradation of carbohydrates, lipids, proteins and nucleic acids.

Some human disease, such as delays and abnormalities in the growth, appear to be linked to zinc deficiency. It was also demonstrated the therapeutic importance of zinc in the treatment of dermatitis enteropathica. Some recent studies suggest a protective effect of zinc against the action of some toxic heavy metals [Abdulla 1979]. The total body content of zinc is about 2-2.5 g. The highest concentrations are present in the choroid of the eye, in the prostate, and about 20% of the total content is contained in the skin. This element is present in blood mainly in red blood cells (80%), but also in white blood cells and platelets. About 60% of the plasmatic zinc is bound weakly to albumin and performs the function of protein carrier, while less than 10% is bound to amino acids (hystidine and cysteine) and only a small fraction is bounded to transferrin.

Ingestion is the most common way to assume zinc and its absorption occurs in the duodenum at an amount of 20-30 % of the ingested. The absorption, as for most of the metal ions, is influenced by age, sex, state of nutrition, level of zinc in the diet, and also by the presence of certain antagonists such as calcium, phosphates, and chelating agents. Most of the zinc that is not absorbed is excreted with faeces.

In addition to the protective action previously cited, zinc also acts by blocking the formation of free radicals resulting from the oxidation of iron: according to recent studies, Zn^{2+} is interposed, during the oxidation of iron, between the latter and thiol groups, thus preventing the formation of free radicals [Wilson 1987]. In dependence of this (but it has not been shown in which way) zinc deficiency would be related to some tumour diseases [Wilson 1977].

Despite the essentiality of zinc, in high doses it becomes toxic and disturbs the metabolism beginning with inhibition of mitochondrial respiration leading to cell failure. Experimental studies reveal that metallothionein, a protein that binds to heavy metal through the thiol group of cysteine residues, favours zinc adsorption. Metallothionein binds copper stronger than zinc, but in excess of zinc, copper absorption is low. In the case of excess of zinc intake, copper deficiency is possible

[Brilla 2005]. The antagonistic effect between Zn and Cu or Fe is confirmed by several studies, which show that copper and iron concentration decreases after zinc excess administration [Prejbenau 2011].

1.3 COPPER

1.3.1 The element

Copper is rather abundant as it is the 25th element on the Earth. Its mean concentration on Earth crust is 68 ppm by weight. The most common mineral is chalcopyrite $CuFeS_2$, but also basic cuprum carbonate $CuCO_3 \cdot Cu(OH)_2$, cuprous oxide Cu_2O and Cu_5FeS_4 are found. Sulphide minerals are often poor in metal concentration and can contain only 0.4 % of copper; for this reason minerals are extracted and exposed to air. CuS it slowly oxidized to $CuSO_4$, which is washed away with water or diluted H_2SO_4. Copper is separated from the resulting solution of copper sulphate by the addition of scrap iron, which forms metallic copper according to the reaction 1.3.

$$Fe + Cu^{2+} \rightarrow Fe^{2+} + Cu \qquad (1.3)$$

The metal is used in the electrical industry for its high conductivity, and is also used for water pipes due to its low reactivity. Over than 1,000 different copper alloys are known: the most used is brass. Different copper compounds are used in agriculture to prevent the attack of fungi or insecticides. Some properties of copper are listed in Table 1.6.

Table 1.6: copper properties

Atomic mass (m.a.u.)	63.546
Atomic ray (calc.) (pm)	145
Electronic configuration	$[Ar]3d^{10}4s^1$
Oxidation states	I, II, (III)
Melting point (°C)	1083
Boiling point (°C)	2570
Evaporation heat (kJ/mol)	300.3
Fusion heat (kJ/mol)	13.1

Electro-negativity	1.9
Natural isotopes	63, 65
Synthetic isotopes	64

The metals belonging to the copper group have the highest known electrical and magnetic conductivity, and are the most malleable and ductile. These properties are due to their cubic compact structure: when a sufficient force is applied, a floor can slip over another one; thanks to the simplicity of the structure, after the relative movements of the floors, the structure is again a cubic compact one.

Copper has one *s* electron in its external orbital. Nevertheless, the oxidation state (+I) is not very stable and Cu^+ undergoes disproportionation in water (see also below) unless this ion is strongly stabilized in a suitable chemical form. Cu^{2+} is reduced to Cu_2O by weak reducing agents. Cu_2O is a basic oxide, that reacts with halohydric acids HCl, HBr and HI, resulting in insoluble CuCl, CuBr and CuI. Cu^+ forms many polymeric complexes, with a cluster made of four Cu atoms at the vertices of a tetrahedron, but without metal-metal bonds.

The state (+III) is not common for copper. In alkaline solutions, Cu^{2+} can be oxidized to $KCu^{III}O_2$; if a molten mixture of $KCl/CuCl_2$ is fluorinated, $K_3[Cu^{III}F_6]$ is formed. Strong oxidation with periodic acid (H_5IO_6) gives $K_7Cu^{III}(IO_6)_2 \cdot 7H_2O$.

The state (+II) is the most common and stable for copper. Rameic ion Cu^{2+} has the electronic configuration d^9 and has an unpaired electron: therefore, its compounds are paramagnetic and thanks to *d-d* transitions they are also coloured. Most copper complexes like halides CuX_2, and complexes formed with ammonia and amines in aqueous solution, have an octahedral distorted structure. This is due to the Jahn-Teller effect.

1.3.1.1 Jahn-Teller effect

When the metal cation Cu^{2+} is surrounded by six ligands placed on the Cartesian axes at the vertices of an octahedron, an electrostatic attraction between the metal ion and ligands can be supposed. However, there is also a repulsive interaction between electrons in the *d* orbitals and the ligand charges. If the electrostatic field (the crystal field) were spherical, then the energies of the five $3d$ orbitals would be raised (destabilized) by the same amount. However, since the d_{z^2} and $d_{x^2-y^2}$ atomic orbitals point directly at the ligands while the d_{xy}, d_{yz} and d_{xz} atomic orbitals point between them, the d_{x^2} and $d_{x^2-y^2}$ atomic orbitals are destabilized to a greater extent than the d_{xy}, d_{yz} and d_{xz} atomic orbitals (Figure 1.2). Thus, the d_{z^2} and $d_{x^2-y^2}$ atomic orbitals

are destabilized while the d_{xy}, d_{yz} and d_{xz} atomic orbitals are stabilized. The Jahn-Teller theorem states that any non-linear molecular system in a degenerate electronic state will be unstable and will undergo distortion to form a system of lower symmetry and lower energy, thereby removing the degeneracy [Housecroft 2005].
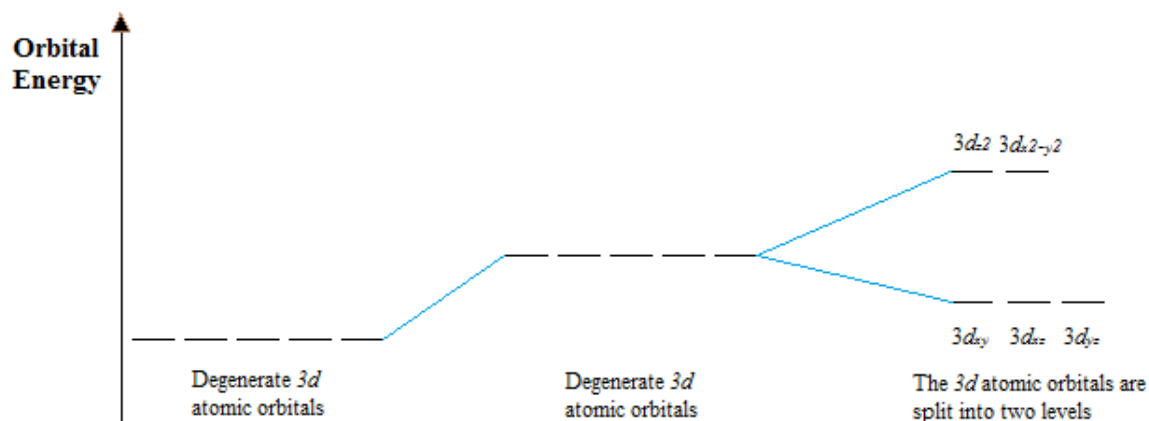
Figure 1.2: the changes in the energies of the electrons occupying the *d* orbitals of an M^{n+} ion when the latter is in an octahedral crystal field. The energy changes are shown in terms of the orbital energies [Housecroft 2005].

From the O_h character table, it can be deduced that the d_{z2} and d_{x2-y2} orbitals have e_g symmetry, while the d_{xy}, d_{yz} and d_{xz} orbitals posses t_{2g} symmetry. The energy separation between them is Δ_{oct}. The magnitude of Δ_{oct} is determined by the strength of the crystal field, the two extremes being called *weak field* and *strong field*.

Octahedral complexes of d^9 ions are often distorted, e.g. CuF_2 (the solid state structure of which contains octahedrally sited Cu^{2+} centres), so that two metal-ligand bonds (axial) have different lengths with respect to the remaining four bonds (equatorial). This is shown in Figure 1.3 (a) (elongated octahedron) and in Figure 1.3 (b) (compressed octahedron).

(a) Bond length a > e   (b) Bond length a < e
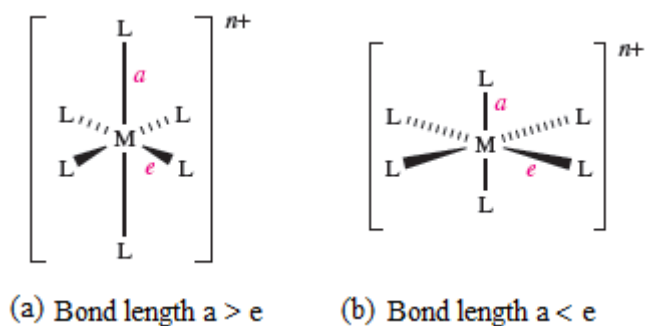
Figure 1.3: effect of Jahn-Teller distortion

For a d^9 configuration the two orbitals in the e_g set are occupied by one and two electrons respectively. If the doubly occupied orbital is in the d_{z^2} , most of the electron density in this orbital will be concentrated between the cation and the two ligands on the z axis. Thus, there will be greater electrostatic repulsion associated with these ligands than with the other four, and the complex will suffer elongation (Figure 1.3 (a)). Conversely, if the doubly occupied orbital is in the $d_{x^2-y^2}$, it would lead to elongation along the x and y axes (Figure 1.3 (b)). The corresponding effect when the t_{2g} set is unequally occupied is expected to be much smaller since the orbitals are not pointing directly at the ligands. Distortions of this kind are called *Jahn–Teller* distortions.

1.3.2 Copper speciation in aqueous solutions

The +3 oxidation state is known in solids such as Cu_2O_3, but such compounds are powerful oxidizing in water and are not stable. The speciation data for copper regard therefore only the oxidation states (I) and (II). However, the equilibrium constant for the Cu^+ disproportionation reaction in water, according to (1.4),

$$2Cu^+ \rightleftharpoons Cu^{2+} + Cu^0 \qquad\qquad (1.4)$$

is 10^6, and therefore only small amounts of Cu^+ can exist in water if this ion is not stabilized.

Cupric ion with its d^9 configuration has a ligand field stabilization in its complexes, and usually the Jahn-Teller effect is observed. This causes the hydrated ion $Cu(H_2O)_6^{2+}$ to have a distorted octahedral structure with weak absorption in the visible [Cotton 1968]. Two of the water molecules in trans position are more distant from the Cu^{2+} ion than the other four, which are coplanar. The Cu^{2+} ion is stable at acidic pH. Above pH 4 it begins to hydrolize, and it precipitates as oxide or hydroxide soon thereafter. The formation constants of copper hydroxo-complexes estimated in 3 M perchlorate media at 25°C are shown in Table 1.7.

Table 1.7: formation constants of copper hydrolysis products, and solubility product of the most important copper oxide [Charles 1976]. Constants refer to the equilibrium
$$m\text{Cu} + n\text{H}_2\text{O} \rightleftharpoons \text{Cu}_m(\text{OH})_n + n\text{H}^+$$

Species	Log β
$CuOH^+$	< -8
$Cu(OH)_2$	< -17.3
$Cu(OH)_3^-$	< -27.8

$Cu(OH)_4^{2-}$	-39.6
$Cu_2(OH)_2^{2+}$	-10.36
$CuO(s)$	$pK_s=7.62$

The only important hydrolysis product of Cu^{2+} is CuO, which is insoluble enough to limit the concentration of Cu^{2+} which can exist in solution as the pH is increased. Cu^{2+} hydrolyzes only to a slight extent at moderate concentrations ($\sim 10^{-3}$m) before precipitation occurs. The principal hydrolysis product is the dimer $Cu_2(OH)_2^{2+}$. A series of mononuclear species, from $CuOH^+$ to $Cu(OH)_4^{2-}$, are formed as well. The first three should be important only in very diluted solutions between pH 8 and 12, and the last forms only in very alkaline solutions. In spite of several estimates, the stability of $CuOH^+$ is only approximately known. Presently, it can be said that its $\log\beta$ is less than -8. As well, the stabilities of $Cu(OH)_2$ and $Cu(OH)_3^-$ are reported but are also not precisely known. The reason is that this species coexist at very low concentration with the solid. On the other hand, the stability of $Cu(OH)_4^{2-}$ is fairly well established by measurements of the solubility of CuO in basic solutions.

1.3.3 Complex formation between copper(II) and ligands: structural and thermodynamic aspects

A very large number of Cu^{2+} complexes are known. Cupric copper forms neutral, anionic and cationic complexes both of non-chelate and chelate kind. Complexes containing N- and O-donor ligands are very common, and coordination numbers of 4, 5 and 6 predominate. For example both the aqua species $[Cu(H_2O)_6]^{2+}$ and $[Cu(H_2O)_4]^{2+}$ exist. The most common coordination geometry is the distorted octahedral, but the square pyramidal, the trigonal-bipyramidal, and the distorted tetrahedral, are sometimes observed. Since the electron population of the Cu^{2+} ion is d^9, in any complex with regular octahedral symmetry the Jahn-Teller effect decreases the energy of the d_{z^2} orbital. It is therefore occupied by two electrons (while the $d_{x^2-y^2}$ orbital is occupied by one), and the approach of a nucleophilic ligand on the z axis is inhibited by the presence of a higher electron density. Consequently the distances Cu-L along the z axis are greater than the four Cu-L distances in the xy plane. In the limit, a square planar complex can be derived from an octahedral complex by the removal of two ligands on the z axis.

Among the ligands, the major copper binder contain oxygen atoms, or oxygen atoms and nitrogen atoms. In relatively few complexes the binding is assured by only nitrogen atoms, as in the very stable $[Cu\ en_2]SO_4$, and in even fewer cases by sulphur atoms.
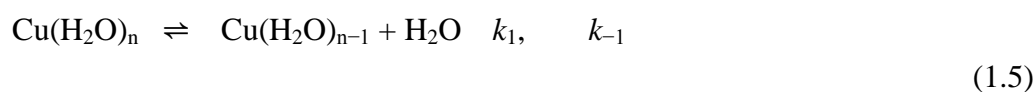
Copper can form many neutral dichelate complexes with β-diketones and similar compounds. They are insoluble in water, but soluble in organic solvents including hydrocarbons. Other neutral poorly soluble complexes are formed by aminoacids. The Cu^{2+}-glycine (H_2NCH_2COOH) complex is deep violet-blue. Cupric disalicyldioxime is also very insoluble.

Negatively charged complexes are formed e.g. by carbonate and oxalate: their sodium salts, e.g. $Na_2[Cu(C_2O_4)_2]\cdot 2H_2O$, have been isolated.

Positively charged complexes, on the other hand, are commonly formed when Cu^{2+} coordinates to amines, as e.g. forming the dichelate and trichelate ethylenediamine derivative [Durrant 1970].

1.3.4 Complex formation between copper(II) and ligands: kinetic aspects

As seen, the six water molecules are arranged around Cu(II) ion in a tetragonally distorted octahedron [Hunt 1983]. Water substitution can easily occur at the very labile axial positions. Rapid inversion of the axial and equatorial ligands leads then to apparent easy substitution in the equatorial position [Eigen 1963]. The resulting water exchange speed is so rapid ($k = 10^{10}$ s^{-1}) that for example it cannot be determined accurately by ^{17}O NMR [Hunt 1983]. The Cu(II)-methanol system is more amenable to study. The mean lifetime at 25 °C of a particular tetragonal distortion in $Cu(MeOH)_6^{2+}$ is $12\cdot 10^{-11}$ s while that for CH_3OH is $1.4\cdot 10^{-8}$ s; thus the six coordinated methanols are indistinguishable. From thermodynamic data and from a comparison of CH_3OH exchange with $M(CH_3OH)_6^{2+}$, M = Mn^{2+}, Fe^{2+}, Co^{2+}, Ni^{2+} and Cu^{2+}, it is concluded that electronic occupancy of d-orbitals and effective radius dictates the dissociative mode (D). This means that the mechanism involves an intermediate having a lower coordination number than in the reactant, as explained in the scheme (1.5):

$$Cu(H_2O)_n \rightleftharpoons Cu(H_2O)_{n-1} + H_2O \quad k_1, \qquad k_{-1}$$

$$(1.5)$$

$$Cu(H_2O)_{n-1} + L \rightleftharpoons Cu(H_2O)_{n-1}L \quad k_2, \qquad k_{-2}$$

The speed of substitution of the solvent from the metal depends also on the concentration and the type of the ligand. If the concentration of L is low, $k_2[L] < k_{-1}[H_2O]$ so that M is scavenged by H_2O preferentially; otherwise M is scavenged by both L and H_2O, or preferentially by L.

Furthermore, ligand exchange reaction has been studied. When the Cu complex has one or more coordinated water e.g. in reaction (1.6)

$$CuL(H_2O)_m^{(2-n)+} + cyclamH^+ \xrightarrow{k} Cu(cyclam)^{2+} + H^+ + L^{n-} + mH_2O \qquad (1.6)$$
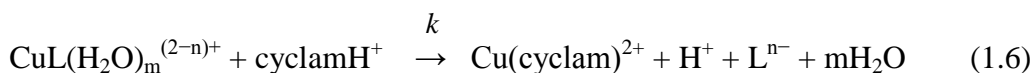
The following relationship of $\log k$ with $\log K_{CuL}$ (1.7) is followed:

$$\log k = \log [k_0/(1 + K_{CuL}K_0^{-1})] \qquad (1.7)$$

with $k_0 = 1.1 \cdot 10^7 \, M^{-1} \, s^{-1}$ and $K_0 = 2.3 \cdot 10^{10} \, M^{-1}$ at 25 °C and $I = 1.0$ M (KNO$_3$). This means that for the weaker Cu^{2+} complexes ($\log K_{CuL} < 10.4$), k is independent on the nature of L, and unwrapping of the coordinated L is not a prerequisite for interchange. For very stable Cu complexes ($\log K_{CuL} \gg 10.4$), there is an inverse relationship between the stability of CuL and its reactivity in ligand exchange reactions [Wilkins 2002].

1.3.5 Biochemistry and toxicity of copper

The essentiality of this element is known since the 1930s, when the need of copper in the production of heme A, a component of cytochromeoxidase, was demonstrated [Cohen 1934]. Subsequent studies have shown that this element is an essential trace metal used as a catalytic cofactor for many enzymes.

Homeostasis of metal ions is critical for life and is maintained within strict limits [Bertini 2008]. In particular, redox active metals likely play a major role in altered redox balance. For example, superoxide dismutase is an enzyme that contains copper and has antioxidant capacity against the formation of superoxide radicals [Wilson 1987]: this enzyme is inhibited by low levels of the element, but on the other hand an excess of copper ions catalyses the formation of free radicals [Floyd 1933], by undergoing redox cycling and causing oxidative stress by increasing the formation of reactive oxygen species (ROS) like superoxide ion, hydrogen peroxide, and hydroxyl radical. This will eventually result in the damage of many biomolecules in the cells [Arnal 2012]. Copper ions *in vivo* exist in Cu$^+$ and Cu^{2+} oxidation states and can undergo electron transfer reactions in living system. In the reductive environment of the cell, Cu^{2+} can be reduced to Cu$^+$ by ascorbate or glutathione, and the reduced Cu$^+$ can be oxidised to Cu^{2+} through the Fenton reaction. The reduced metal ion Cu$^+$ generates extremely reactive hydroxyl radicals from hydrogen peroxide like in reaction (1.8) [Suzuki 1981].

$$Cu^+ + H_2O_2 \rightarrow Cu^{2+} + OH^\bullet + OH^- \qquad (1.8)$$

Some scientists believe that environmental factors are responsible for the increased copper uptake. The metal ion might be more bioavailable because it is leached from copper plumbing in homes or ingested as inorganic copper from vitamin/mineral

supplements. Cu overload is implicated in the pathogenesis of a variety of human diseases like cancer, cirrhosis, atherogenesis and neurodegenerative diseases [Arnal 2012].

On the other side, copper deficiency is associated with anaemia, osteoporosis, abnormal pigmentation of the skin (as experimentally tested on animals), whereas some human diseases, such as Wilson's disease and some forms of cirrhosis, are related to an alteration of copper metabolism. The total content in the human body is normally between 80 and 120 mg. About 1/3 of this quantity is in liver and brain, while another third is located in the skeleton. The normal level in the plasma, where almost all copper (90-95% of it) is bound to ceruloplasmin is approximately 1 mg/L. Copper assumed with the diet is absorbed in the duodenum to an extent of about 30%. The daily requirement is 1.5-3 mg. Generally, a balanced diet provides adequate amounts of copper. Deficiencies have been observed in malnourished children and may occur in patients who undergo parenteral nutrition for a long time.

1.4 ALZHEIMER'S DISEASE

Alzheimer's disease (AD) is the most common cause of progressive dementia in the elderly population. It is a chronic neuro-degenerative disorder that leads to progressive disturbances of cognitive functions including memory, judgement, decision-making, orientation to physical surroundings and language [Nussbaum 2003]. The disease has no doubt existed for millennia, but it was often confused with other syndromes that also presented as "senile dementia", that is, progressive cognitive decline after middle age. The description of the clinic-pathological syndrome by the Bavarian psychiatrist, Alois Alzheimer, in 1906 established a neuropathological phenotype that has enabled considerable diagnostic specificity, although until recently only at the end of the patient's life.

Progress in elucidating the biology of AD first arose from the compositional analyses of *amyloid plaques* and *neurofibrillary tangles* in the mid-1980s.

Alzheimer's disease (AD) is characterized by innumerable deposits of extracellular amyloid plaques. A small peptide, amyloid-β peptide (Aβ), plays a critical role in the initial build up of these amyloid plaques and is the main constituent of the amyloidal deposits [Masters 1985]. Amyloid-β peptide can be between 39 and 43 residues in length, of which Aβ-(1-40) and Aβ-(1-42) are the most abundant fragments. Aβ_{42} is more prone to aggregation and more toxic to neurons than Aβ40. The β-amyloid peptides can react together to form soluble oligomers, protofibrils, fibrils or insoluble extracellular aggregates. In particular, soluble oligomers appear to be responsible for the toxicological mechanisms, as they can directly damage neurons by oxidative

attacks; they are involved also in the alteration of electrochemical signals, for example by creating small membrane channels that unbalance the ionic gradients of Ca^{2+}.

Neurofibrillary tangles are generally intraneuronal cytoplasmic bundles of paired, helically wound ~10 nm filaments (PHFs), often interspersed with straight ~10 nm filaments [Geser 2008]. Neurofibrillary tangles usually occur in large numbers in AD brains, particularly in entorhinal cortex, hippocampal formation, amygdala, association cortices of the frontal, temporal and parietal lobes, and certain subcortical nuclei that communicate with these regions. The subunit protein of the PHF is the microtubule-associated protein, tau. This plays a central role in maintaining the structural integrity of neuronal microtubules, that are polymers of tubulin that form the cytoskeleton.

The two classical proteinaceous lesions of AD can occur independently in humans. There are some cases of AD itself that are "tangle-poor", that is, very few neurofibrillary tangles are found in the neocortex together with abundant Aβ plaques [Terry 1987]. The main risk factors for AD include exogenous factors, like brain trauma, smoking, obesity, diabetes, hypertension, hypercholesterolemia, exogenous exposure to metals (especially Pb, Hg, and Al). Estimates of the proportion of AD cases that are genetically based have varied widely from as low as 10% to as high as 40% or 50%, and some investigators believe that, in the fullness of time, virtually all cases will be shown to have some genetic determinants.

1.4.1   Effects of Zn^{2+}, Cu^{2+} and Al^{3+} associated with Alzheimer's disease

Some metal ions appear to have a role in the disease. Analysis of the autopsy of AD patients shows abnormally high levels of specific metal ions in the senile plaques (Cu^{2+}, 25 µg/g, ~393 µM; Zn^{2+}, 69 µg/g, ~1055 µM). Al^{3+} has also been detected in amyloid fibers in cores of the senile plaques [Yumoto 2009]. These metal ions are Lewis acids, and for this reason they are able to coordinate Aβ, thanks to the interaction with nitrogen and oxygen atoms, Lewis bases, belonging to the amino acid residues situated in the portion of amyloid peptide 1-16, with the formation of complexes with the stoichiometric ratio of 1:1. The complex formation is supposed to lead to stabilization and/or induction of β-amyloid oligomers formation. An independent support of this metal ion role comes from the experimentally evidence that the imbalance of cellular Zn^{2+} and/or Cu^{2+} homeostasis modulates AD pathology [Zatta 2009], and dietary Cu^{2+} and Al^{3+} are risk factors for AD [Frisardi 2010]. Zn^{2+} and Cu^{2+} have been shown to accelerate Aβ deposition *in vivo* forming amorphous aggregates [Bush 1994], even if Zn^{2+} affinity for Aβ is significantly weaker than that of Cu^{2+}. Al^{3+} promotes Aβ fibrils or oligomer formation [Zatta 2009].

On the other side, Cu^{2+} and Zn^{2+} are essential cofactors for the activity of many α-secretase and some protease involved in the cleavage of *β*-amyloid in small peptides. It is clear, therefore, that a defect of these metals in the body lead to accumulation of amyloid peptides. Several attempts were made to obtain efficient chelators with moderate affinity towards copper and zinc that participate to the amyloid aggregation, in order to prevent the formation of plaques [Kozlowski 2012].

As mentioned above, copper takes part in the Fenton reaction, according to the reaction (1.8). A healthy organism can ensure a homeostasis condition between production and elimination of ROS. Thanks to the enzymes proposed to antioxidant defense, the organism can eliminate these radical species. Two categories of enzymes have been mentioned, belonging to the family of oxidoreduttase: superoxidodismutase (SOD) and catalase; they act according to the reactions (1.9) and (1.10) respectively.

$$2\,O_2^{\bullet-} + 2\,H^+ \;\rightleftharpoons\; O_2 + H_2O_2 \qquad\qquad (1.9)$$

$$2\,H_2O_2 \;\rightleftharpoons\; O_2 + 2\,H_2O \qquad\qquad (1.10)$$

Other radicals, known to be harmful to the body, are the RNS (Reactive Nitrogen Species). RNS derive from the nitric oxide radical (NO •), produced by the nitric oxide synthase (NOS) enzyme. This radical is an important cellular messenger and plays a key role in the body's immune system of a healthy organism. However, the reaction (1.11) takes place in the presence of a superoxide anion radical, leading to a very reactive species, peroxynitrite ($ONOO^-$). This is responsible for the nitrosylation of proteins, DNA and mitochondrial metabolism damage, and for a series of reactions that are known as condition of nitrosative stress.

$$^\bullet NO + O_2^{\bullet-} \;\rightarrow\; ONOO^- \qquad\qquad (1.11)$$
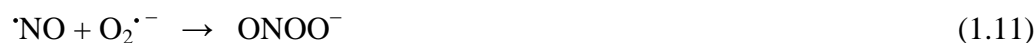
Oxidative stress seems to be one of the main causes of Alzheimer's disease, because the mitochondrial functionality related to it, gradually decreases with age. The central role of metals in the pathogenesis of the disease can derive from an imbalance between free ions and ions bound to enzymes. More precisely, if the pool of free metals prevails over that of bound metals, the condition of oxidative stress is much more favored: on one side, an accumulation of ROS and RNS thanks to the Fenton reaction is observed, on the other hand a deficit of detoxification mechanisms is verified, due to the lack of metal cofactors in the reactive sites of SOD and catalase.

2 CHELATION THERAPY

2.1 INTRODUCTION

The only therapy that has been proven to be effective in the treatment of acute and chronic intoxications due to excessive absorption of metal ions is based on the administration of chelating agents able to selectively complex the metal. This therapeutic approach is named *chelation therapy*, and is currently employed for the detoxification of several metals. The objective of chelation therapy is the removal of toxic metal ions from human body or attenuation of their toxicity by transforming them into less toxic compound or dislocating them from the site at which they exert a toxic action [Crisponi 2012 (b)].

An ideal chelating agent should have some specific requisites, that can be summarized as follows:

- Selectivity toward the target metal ion and not towards other essential ions;
- Stability of the complexes, i.e. higher stability constants than those with endogenous ligands;
- Fast kinetic exchange of the toxic metal ion between chelator and endogenous ligands;
- Lack of toxicity both of the chelating agent and of its complexes;
- The chelating agent, once in the body, should not promote redox reaction like the Fenton (1.8);
- Good oral absorbability and intestinal absorption and good bioavailability to the target cells;
- Slow rate of metabolism, to permit the complete formation of the complexes before their excretion;
- Favorable excretion of the complexes formed;
- Low production costs.

Selectivity and stability of a chelator *in vivo* can be estimated if the stability constants of the metal-chelator complexes are known. As the complex formation is a competitive reaction between proton and metal ion for the same basic sites of the ligand, a more general parameter, different than the stability constants, is needed to

compare the selectivity and stability of different chelators. This parameter can be the pM. It is defined as $-\log[M]$ at $[M]_{Tot} = 1 \cdot 10^{-6}$ molL^{-1} and $[L]_{Tot} = 1 \cdot 10^{-5}$ molL^{-1} at pH 7.4, where $[M]$ is the concentration of the free metal ion and $[M]_{Tot}$ and $[L]_{Tot}$ are the total concentrations of metal and ligand, respectively. pM values are key parameters in order to chemically evaluate a chelator.

It is well known that any toxic metal chelating agent can complex and therefore remove from body also essential metal ions, thus causing toxic side effects due to metal ion deficiency. Copper, and especially zinc, appear to be the most affected essential metal ions during the chelation therapy regiments; for example, zinc deficiency problems are sometimes experienced in the Deferiprone therapy of aluminium and iron overload pathologies [Kontoghiorghes 1995]. On one side, the evaluation of the complexation strength of a chelator towards Cu^{2+} and Zn^{2+} can allow to predict the extent of essential metal ion removal during the chelation therapy. On the other hand, several studies have been carried out in order to find efficient chelators with moderate affinity towards metal ions such as Cu^{2+} and Zn^{2+}, that cause toxic effects if present in high levels in the organism, and that may participate of the amyloid aggregation [Kozlowski 2012] within Alzheimer disease. Therefore, the Cu(II) and Zn(II) complex formation of a chelator should always be known.

Another key requirement of a chelator is the oral absorbability, because it would allow the best comfort for the patient, and lower health care therapy costs, compared to any other way of administration. Lipinski has listed the requirements that a molecule must possess in order to be bioavailable in the gut [Lipinski 1997]:

1. Molecular mass lower than 500 Dalton;
2. Log$P$ < 5, where P is the n-octanol/water partition coefficient. The value of log$P$ indicates how much the molecule is lipophilic;
3. Presence of less than 10 hydrogen bond donors;
4. Presence of less than 10 hydrogen bond acceptors.
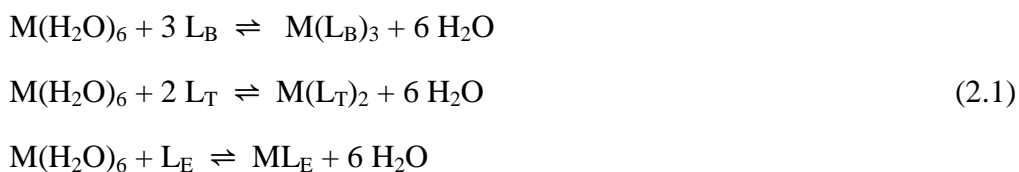
Although the " Lipinski rules" are generally valid, it should be noticed that one of them, the requirement of lipophilicity, is controversial. It is essential that the chelator has an appropriate lipophilicity, in order to be able to cross the cellular membranes, but at the same time, it requires a certain degree of hydrophilicity, in order to be transported in plasma.

2.1.1 Metal coordination number in metal complexes

The metal coordination number (CN) is very important for the determination of structure and properties of metal complexes with chelating agents. As seen in chapter 1, the preferred CN for several metal cations is ambiguous (e.g., for both Cu^{2+} and Zn^{2+} CN=4, 5, or 6 [Rotzinger 2005, Dudev 2000]), and the factors determining the metal CN are often not fully understood. The CN depends on (1) metal size, charge, charge-accepting ability and (2) ligand size, charge, charge-donating ability, denticity (number of coordinating groups which can bind the metal ion at the same time) [Dudev 2006].

The metal size plays a role in determining the CN. The CN in hydrated complexes often increases by increasing the size of the metal, even if with many exceptions. Metal charge and charge-accepting ability do not seem to be the major determinants of the metal CN in complexes containing neutral ligands such as water. Al^{3+}, Cu^{2+} and Zn^{2+} are in fact all hexacoordinated in water, despite their difference charges and charge-accepting abilities.

Ligand net charge and charge-donating ability, rather than the ligand size, have an important role in determining the metal CN. For example, when two water molecules are replaced by two negatively charged monodentate ligands such as Cl^- or Br^-, the CN of Cu^{2+} and Zn^{2+} is lowered from 6 to 4. Negatively charged ligands, which are good charge donors, affect the metal CN more than neutral ligands. Also the denticity of a ligand plays an important role in determining the CN of the metal. Denticity also significantly affects the metal-ligand complexation strength. At constant metal-ligand bond strength, the stability of complexes formed is maximum for hexadentate chelating agents, due to the greater entropy resulting from the complexation reaction (2.1):

$$M(H_2O)_6 + 3\ L_B \ \rightleftharpoons \ M(L_B)_3 + 6\ H_2O$$

$$M(H_2O)_6 + 2\ L_T \ \rightleftharpoons \ M(L_T)_2 + 6\ H_2O \qquad\qquad (2.1)$$

$$M(H_2O)_6 + L_E \ \rightleftharpoons \ ML_E + 6\ H_2O$$

(L_B is a bidentate ligand, L_T is a tridentate and L_E is a hexadentate one).

As another disadvantage of the bidentate and tridentate ligands, they can form multiple complexes *in vivo*, whose concentration depends on total ligand and on metal-to-ligand ratio, thus complicating the speciation model. On the other hand, bidentate and tridentate ligands have an important advantage over hexadentate ligands, because they can be orally more active thanks to their lower molecular

weight. Furthermore, chelating molecules with molecular mass lower than 300 Da can also cross the membrane of the brain [Gaeta 2005].

2.2 CHELATING DRUGS FOR IRON AND ALUMINIUM INTOXICATIONS

Aluminium and iron are currently the most important among the different metal ions involved in chelation therapy, due to the relatively high occurrence of their overload-produced diseases. Chelators used for iron can be used for aluminium, and vice versa, because of the very similar coordination chemistry which is displayed by the two hard M^{3+} ions.

Chelating drugs existing for aluminium and iron overload are Deferoxamine and Deferiprone. Exjade is a new drug which presently is used for iron chelating therapy only, but it can in principle be proposed also for aluminium.

Deferoxamine (DFO) (Figure 2.1(a)) is a tris-hydroxamic derivative produced by the bacterium *Streptomyces pilosus* as growth agent [Keberle 1964]. It was introduced in 1970 in iron intoxication's therapy and, some years later, the use has been extended in the aluminium chelation therapy. DFO is an hexadentate ligand which forms very stable 1:1 complexes with Al^{3+} and Fe^{3+}. Six oxygen atoms are involved in the coordination (three pairs of O-N-C=O), forming with the metal three chelated rings with five terms each. DFO has several disadvantages. Firstly, its complexes have a low lipophilicity which inhibits the penetration in human cells thus allowing the only chelation of blood iron. Furthermore, DFO has a high molecular mass (> 500 Da), that prevents its oral intake, and it is rapidly metabolized towards non-complexing derivatives. For this reasons, very slow subcutaneous infusions of the drug are necessary (from 8 to 12 hours), for five up to seven times per week, compromising the life of the patient. Moreover it was observed that since DFO forms more stable complexes with iron than with aluminium, patients taking this drug for aluminium intoxications may undergo iron deficiency. Finally, there are important side effects of this chelator, such as abnormalities in the eye (cataracts), growth delay, sleep disorders, allergies, anaphylactic reactions, as well as renal and pulmonary complications.

Deferiprone (L1) has been proposed as alternative drug in order to overcome problems related to the DFO therapy. It is a bidentate ligand able to form strong complexes with stoichiometric metal-to-ligand ratio 1:3 (at physiological pH) both with Fe^{3+} and Al^{3+} (Figure 2.1(b)). Thanks to its low molecular mass, L1 can be orally administrated, two or three times per day. Moreover, L1 affinity for aluminium is only slightly lower than that of DFO. However, the chelator causes several side effects such as gastrointestinal complications, skeletal pains and zinc deficiency. The

latter is a consequence of the ability of L1 to complex also zinc(II) [Kontoghiorghes 2000]. Another disadvantage of L1 is its rapid hepatic metabolism, due to the conjugation of the hydroxyl group in the ring position 3 with glucuronide, and the resulting loss of its chelation ability. This forces the administration of high doses of the drug, thus causing more severe toxic side effects. Despite these drawbacks, the therapeutic use of L1 is licensed in India since 1995 and in Europe since 2000, where it is still administered in patients who have experienced allergic or toxic effects towards DFO.

Exjade (ICL670, Figure 2.1(c)) and some of its triazole derivatives have received considerable attention in recent years [Lattmann 1997]. ICL670 has two oxygen atoms and one nitrogen atom acting as charge donors, therefore it is considered a tridentate ligand. Currently, it is only used for iron chelation therapy. ICL670 has a good oral bioavailability but, because of its high hydrophobicity, it is able to cross membranes easily, inducing the redistribution of toxic metals in the tissues. Furthermore, the presence of a nitrogen atom between the chelating groups, probably promotes the complexation of other essential metals [Liu 2002]. This disadvantage is typical of tridentate ligands, which contain always at least one nitrogen donor atom having larger affinity towards essential metal ions.

Besides DFO; L1 and ICL670, there is a number of other ligands which have been proposed, or are currently under study, for the chelation therapy of aluminium and iron. Next paragraphs lists some of these compounds.
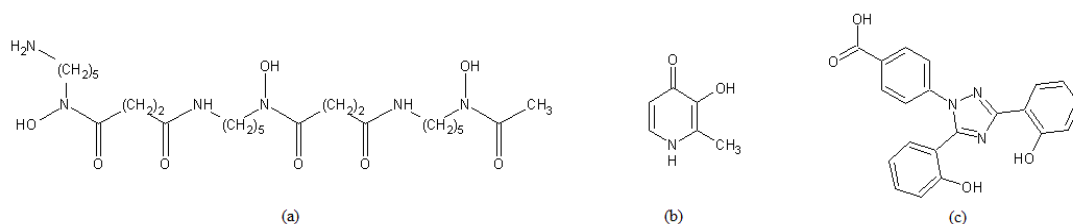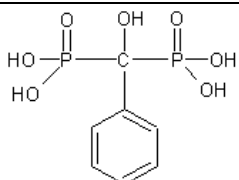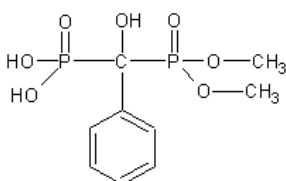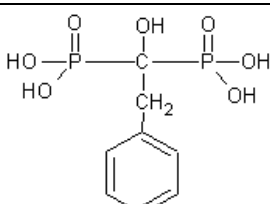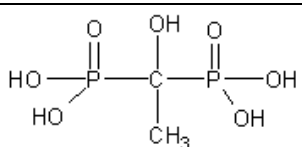
Figure 2.1: (a) Deferoxamine (DFO), (b) Deferiprone (L1), (c) Exjade (ICL670)

2.2.1 Bisphosphonates derivatives
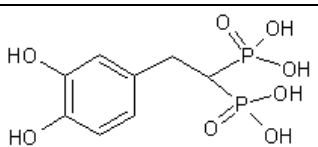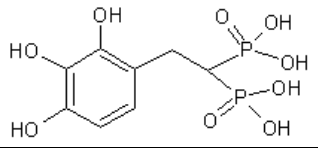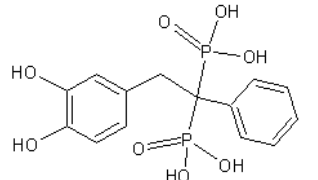
Bisphosphonates (Table 2.1) have long been studied to investigate their chelating properties towards iron and aluminium. It was established that they form extremely stable complexes, even more stable than those formed by L1. They also have a good toxicity profile and their low molecular weight enables good intestinal adsorption.
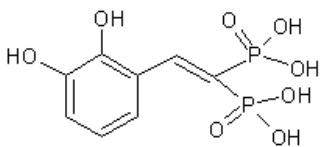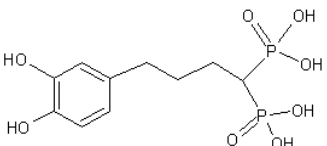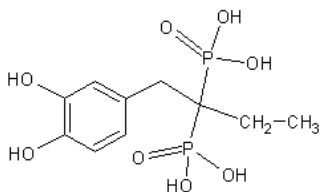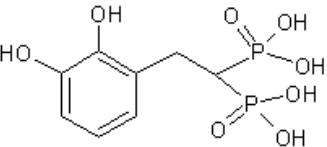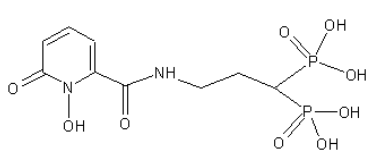
Table 2.1: 1-Phenyl-1-hydroxymethylene bisphosphonate and three derivatives [Crisponi 2012 (b)]

Formula	Full name
	1-Phenyl-1-hydroxymethylene-1,1 bisphonic acid
	[1-(Diethoxyphosphinyl)-1-hydroxybenzyl]-1-phosphonic acid
	1-Benzyl-1-hydroxymethylene-1,1-bisphosphonic acid
	1-Hydroxyethane-1,1-bisphosphonic acid

Other two families of derivatives were synthesized (Table 2.2), in which the bisphosphonate units are connected to a catechol or pyridinone unit; both of them in fact are strong iron and aluminium chelators.

Table 2.2: catechol and hydroxypyridinonate-bisphosphonate derivatives [Crisponi 2012 (b)]
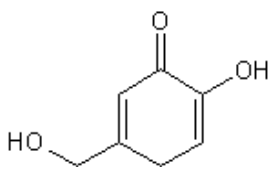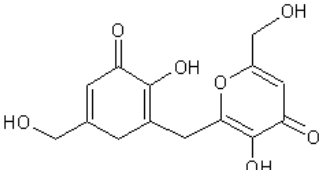
Formula	Full name
	3,4-Dihydroxy phenyl ethylidene bisphosphonic acid
	2,3,4-Trihydroxy phenyl ethylidene bisphosphonic acid
	1-(3,4-Dihydroxybenzyl)-1-phenyl methylene bisphosphonic acid

Formula	Full name
	2,3-Dihydroxy phenyl ethenylidene bisphosphonic acid
	3,4-Dihydroxy phenyl butylidene bisphosphonic acid
	1-(3,4-Dihydroxybenzyl)-1-ethyl methylene bisphosphonic acid
	2,3-Dihydroxy phenyl ethylidene bisphosphonic acid
	3-([(1-Hydroxy-6-oxo-1,6-dihydro-2-pyridinyl) carbonyl]amino-1-phosphonopropylphosphonic acid

2.2.2   Kojic acid derivatives

Kojic acid (5-hydroxy-2-(hydroxymethyl)-4-pyrone) is a natural derivative of 4-pyrone, produced by some species of mould. Kojic acid and its derivatives (Table 2.3) are good chelating agents for hard metal ions such as Fe^{3+} and Al^{3+}.

Table 2.3: chemical structure of kojic acid derivatives [Crisponi 2012 (b)]

Formula	Full name
	5-Hydroxy-2-hydroxymethyl-pyran-4-one
	6-[5-Hydroxy-2-hydroxymethyl-pyran-4-one]-5-hydroxy-2-hydroxymethyl-pyran-4-one

	2,2'−[(2-Hydroxy-3-methoxyphenyl)methanediyl]bis[3-hydroxy-6-(hydroxyl methyl)-4H-pyran-4-one]
	2,2'−[(4-Hydroxy-3-methoxyphenyl) methanediyl]bis[3-hydroxy-6-(hydroxyl methyl)-4H-pyran-4-one]

Several studies have shown that both Kojic acid and its dimer are able to bind Al^{3+}, forming very stable mono and binuclear species, variously protonated. The study of these chelators is still in progress, with the aim to determine their behavior towards essential metal ions such as Cu^{2+}, Zn^{2+}, Ca^{2+}, and Mg^{2+}.

2.2.3 Hydroxypyridinecarboxylic acids

In recent years, the studies conducted by the research group in which this thesis work is included, focused on a new class of compounds for Fe^{3+} and Al^{3+} chelation therapy: hydroxypyridinecarboxylic acids (HPCs). The HPCs state of art is summarized in a recent review paper [Crisponi 2012 (b)].

The two simplest unsubstituted derivatives are 3–hydroxy–4–pyridinecarboxylic acid (DT0) and 4–hydroxy–3–pyridinecarboxylic acid (DQ0) shown in Figure 2.2 (a) and Figure 2.2 (b) respectively. Ring substitution of DT0 and DQ0 gives the DTs and DQs derivatives, respectively. DTs and DQs possess two oxygenated *ortho* functional groups, the carboxylic acid (–COOH) and the phenol (–OH). As they behave as Lewis hard bases, in their deprotonated forms they are capable to bind metal ions of the same type, forming a strong six-membered metal chelation ring. The pyridine nitrogen has a significant effect in enhancing the metal ion complexation strength compared with hydroxybenzenecarboxylic acids (i.e. salicylic acid derivatives) because of the strong electron-attracting effect of the charged pyridinic-N^+. This effect has been experimentally proven by comparing the pK_A value of –OH in DTs without a N-methyl substituent with those in N-substituted DTs: it has been observed that for the latter pK_A is much lower ($pK_A \sim 11$ for N-unsubstitued DTs, $pK_A \sim 7$ for N-methyl derivatives).
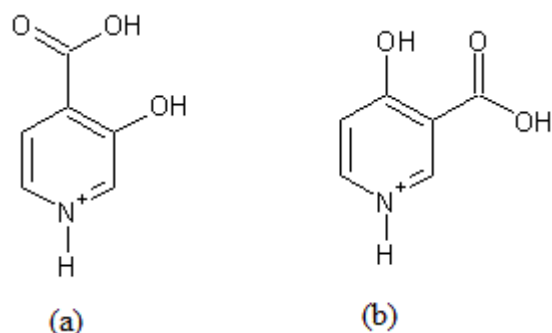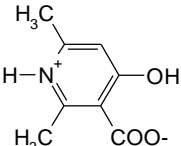
Figure 2.2: (a) 3–hydroxy–4–pyridinecarboxylic; (b) (DT0) and 4–hydroxy–3– pyridinecarboxylic acid (DQ0).

HPCs have several advantages with respect to the other existing or proposed aluminium and iron chelators. Above all, they have a low molecular mass, which should allow a good oral bioavailability, and they have very low toxicity *in vitro*. Toxicity *in vivo* is still unknown as no systematic work has been performed up to now; however, there is one important example, pyridoxic acid (POA), that allows to assume that HPCs are non-toxic *in vivo*, too. POA is a derivative of DT0 (so it is structurally very similar to the ligands examined) and it is a non-toxic metabolite of vitamin B6 . As another important advantage of HPCs over L1, the hydroxyl in POA (and presumably in all HPCs) does not undergo conjugation *in vivo*; here also more systematic studies are needed to confirm that the POA data can be generalized to all HPCs. HPCs studied so far have also expressed modest or low affinity for divalent essential ions in the organism, such as Zn^{2+}, Cu^{2+} and Fe^{2+}. Therefore, HPCs should not interfere with the biochemistry of these metals [Dean 2009]. However, although the complexes formed with hard metal ions are very stable, DT0 and DQ0 affinity for Al^{3+} and Fe^{3+} is appreciably weaker than that generated by drugs currently in use, such as L1. For this reason several DT0 and DQ0 derivatives have been synthesized and studied, in order to increase the strength of complexes with the two metals, without changing the other positive properties. The possibility which has been hitherto studied was the insertion of methyl substituents on the free positions of the pyridine ring, i.e. in position 1, 2, 5, and/or 6: this moderate electron-donating functional group was expected to increase the basicity of chelating oxygens and, therefore, to increase the complexing affinity towards hard metal ions.

Table 2.4 shows the methyl derivatives of DT0 (DTs) and DQ0 (DQs) that have been synthesized and studied so far.

Table 2.4: hydroxypyrdinecarboxylic acids studied so far [Crisponi 2012 (b)], and abbreviations adopted. Compounds are shown in their neutral form.

Formula	Full name	Abbreviation
	3–hydroxy–1–methyl–4–pyridinecarboxylic acid	DT1
	4–hydroxy–1–methyl–3–pyridinecarboxylic acid	DQ1
	3– hydroxy–2–methyl–4–pyridinecarboxylic acid	DT2
	4– hydroxy–2–methyl–3–pyridinecarboxylic acid	DQ2
	4– hydroxy–5–methyl–3–pyridinecarboxylic acid	DQ5
	4– hydroxy–6–methyl–3–pyridinecarboxylic acid	DQ6
	1,2–dimethyl–3– hydroxy–4–pyridinecarboxylic acid	DT712
	1,5–dimethyl–4– hydroxy–3–pyridinecarboxylic acid	DQ715
	1,6–dimethyl–4– hydroxy–3–pyridinecarboxylic acid	DQ716
	2,6–dimethyl–3– hydroxy–4–pyridinecarboxylic acid	DT726

	2,6–dimethyl–4– hydroxy–3– pyridinecarboxylic acid	DQ726

Studies of these new derivatives have highlighted positive kinetic, toxicological (*in vitro*), and electrochemical properties, which are similar to those of the two not-substituted HPCs.

The stability constant studies performed on the methyl derivatives allowed to draw some conclusions. First, the stability of DTs and DQs complexes with Fe^{3+} is almost the same. Instead, it seems that DQs form more stable complexes with Al^{3+} compared to DTs. Second, considering the behavior of each member of the DQs class, in relation to its interaction with Fe^{3+}, it has been observed that the effect of the electron-donating methyl substituent on the complex stability is maximum when the methyl is introduced in position 1, by a N-substitution on the pyridine ring. Otherwise it is appreciable but minor when the methyl is in positions 5 and 6. Furthermore, the effect of $-CH_3$ is additive, since dimethylated derivatives (DQ715 and DQ716) form stronger complexes than monomethylated ones (DQ1, DQ5 and DQ6). On the contrary, studies concerning the stability of DQs-Al^{3+} complexes showed a minimal methyl effect in position 1, and a higher one in positions 5 and 6. The insertion of a methyl in *ortho* to the carboxylic group (DQ2) has instead generated a negative effect, i.e. a considerable decrease in the complexing strength. This can be explained by the steric hindrance of the methyl group, which prevent the co-planarity between the –COOH and the pyridine ring. Consequently, a distortion of the chelate ring occurs and, as a result, a decrease in the complex stability arises. For this reason, DQ2 is the weakest chelator among the HPCs examined so far, whereas DQ726 complexes are stronger than those formed by DQ2 but weaker than those of DQ6.

Third, results obtained for DTs-Fe^{3+} are very similar to those obtained for DQs-Fe^{3+}. In particular, DT712 forms the complexes having the highest stability with Fe^{3+} among HPCs investigated so far. In DTs-Al^{3+} complexes, the substitutions of the pyridine ring with one or more methyl groups do not increase the complexation strength with the metal. There is in fact no big difference among DT0, DT1, DT2 and DT712 ability in binding Al^{3+}.

Although suitable methyl substitutions eventually enhanced the complex stability of HPC complexes, that the complexing strength of even the best HPC prepared so far does not reach that of L1: pAl and pFe values are always one or more orders of

magnitude lower than the corresponding values of L1. Therefore, a different strategy is needed to design HPCs that can form stronger Al(III) and Fe(III) complexes.

2.2.4 Other proposed molecules

Several alternative molecules have been studied for a possible improvement as chelating drugs. Their structures are shown in Figure 2.3. These molecules have been subjected to clinical trials, but in the most cases toxic effects and/or low efficiency has been stated, so that they have been abandoned

Hydroxybenzilethylenediaminodiacetic acid (HBED) is an aminocarboxylic phenolic chelating agent which has a higher chelating efficiency for metal ions than DFO. However, despite its low molecular mass, the drug must be administered by intramuscular injections because the oral administration is not efficient [Bergeron 1993]. Some derivatives of HBED have been studied (in particular the monoethyl ester) as orally active prodrugs. Their advantage is the ability to easily cross the gastro-intestinal membrane, due to their hydrophobicity. After the enzymatic hydrolysis of the ester bond, they gain a pharmacological activity and an increased hydrophilicity. Therefore, the metal-ligand complex just formed is easily removed and poorly permeate into cell membranes, so that the redistribution of the toxic ion in tissues is limited. The biggest disadvantage of HBED and of its derivatives is that their complexes with metals are toxic. Moreover, the presence of two nitrogen atoms in this ligands class is responsible for the strong coordination of essential metal ions.

Desferrithiocin (DFT) is a tridentate ligand able to form strong complexes with Fe^{3+} and Al^{3+} [Hahn 1990]. The presence of the nitrogen atom favors also the formation of complexes with essential metals [Anderegg 1990]. Furthermore, DFT has several side effects, including neurotoxicity, nephrotoxicity and loss of body weight [Wolfe 1990].

Pyridoxal isonicotinoyl hydrazone (PIH) is a tridentate ligand with strong affinity towards Al^{3+} and Fe^{3+}, but it has an excessively slow kinetic of complexation. For this reason other derivatives have been studied which, however, are more toxic than the starting compound [Edward 1995].

Other interesting molecules investigated are some derivatives of L1. The insertion of substituents on L1 was tested in order to optimize its chelating properties and reduce adverse effects and the kinetic of degradation *in vivo*. Among these derivatives CP502 is the most important one. It has an amide group in position 2 and a methyl in position 6 of the pyridine ring. This molecule is able to complex Fe^{3+} with a stability about hundred times higher than L1 at physiological pH [Liu 2002]. A similar positive effect in chelating the metal has been obtained with the introduction of a hydroxyalkyl group (for example $-CH_2OH$) in position 2. The effect of both

substituents (amide and hydroxyalkyl) in position 2 leads to a decrease of the affinity of the ligand towards the proton, reducing the competition with the metal ion. The acidity of the hydroxyl group in position 3 is increased thanks to the electron-attracting property of the substituent in position 2, and thanks also to the energy stabilization induced by the ionized molecule: this is the result of the deprotonation process, and leads to an intramolecular hydrogen bond (which does not interfere with the metal coordination) between the –OH and the substituent in position 2.
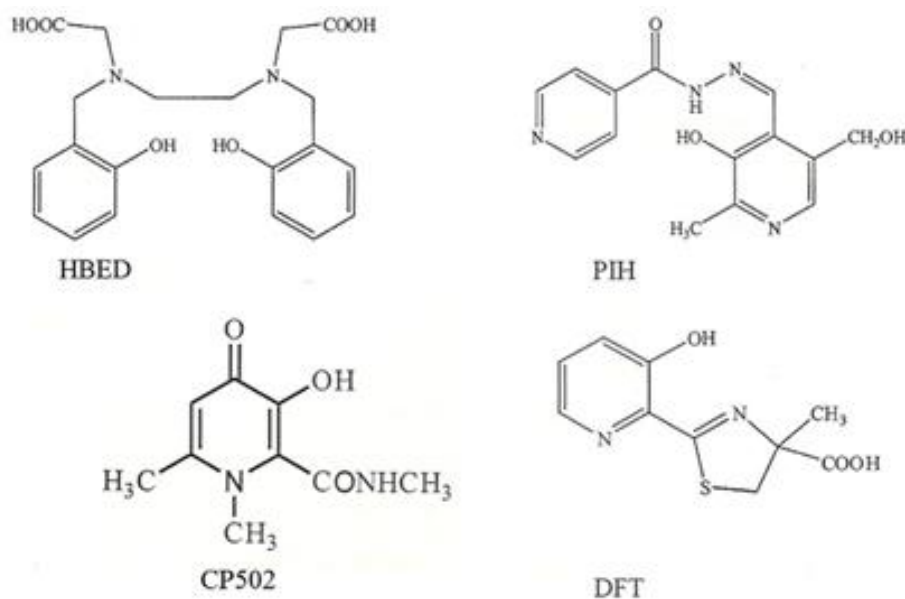
Figure 2.3: other proposed molecole for the Al and Fe chelation therapy

2.3 AIM OF THIS THESIS WORK

This thesis is included in a work project which focuses on the evaluation of selected HPCs as possible chelating agents for iron and aluminium. The involved research groups are the ones coordinated by dr. Valerio Di Marco, dr. Maria Grazia Ferlin and prof. Cristina Marzano from the University of Padova, and by prof. Tamás Kiss from the University of Szeged (Hungary).

As seen, the only but important disadvantage of the HPCs studied so far is that their Al^{3+} and Fe^{3+} complex stability, despite being very high, is still lower than that of available chelators such as L1. The methyl substitution of the pyridine ring demonstrated to be beneficial to increase the complex stability, but was not enough as it did not allow to at least reach the pM values displayed by the chelators presently in use, such as L1.

To this connection, an alternative strategy to synthesize stronger HPC chelators could be the insertion of another chelating group, e.g. a second carboxylate, on the pyridine ring. This second COOH should be added in *ortho* to the hydroxy group. In this way, a more probable coordination is expected towards the toxic metal ion (statistical effect). Furthermore, the second carboxylate group should favour the deprotonation of the hydroxy group, by both an electronwithdrawing effect and an intramolecular hydrogen bond formation. In this way, the Lewis basicity of the phenolic group should be enhanced, and complex formation should eventually be favoured. It is also interesting to evaluate if the simultaneous methyl-carboxy substitution would be beneficial to enhance the complex stability.

In order to evaluate both the second carboxylate and the double carboxylate – methyl effects on complex formation, two new HPC derivatives have been synthesized and studied: 4-hydroxy-3,5-pyridinedicarboxylic acid (DQ58) and 4-hydroxy-1-methyl-3,5-pyridinedicarboxylic acid (DQ71508). These new compounds are shown in Figure 2.4.

A parallel work was conducted in Padova and in Szeged on these ligands. In Padova, the complex formation of DQ58 and DQ71508 was performed with Al^{3+} and Fe^{3+}, in order to evaluate their complexation strength towards these toxic metal ions. In Szeged, the complex formation of the same ligands was performed with Cu^{2+} and Zn^{2+}, in order to evaluate their complexation strength towards the selected essential metal ions. This thesis work regards the DQ58 and DQ71508 complexation towards Zn(II), and the DQ58 complexation towards Cu(II).

Furthermore, the work in Szeged regarded also the complex formation study of 4-pyridoxic acid (Figure 2.4) (POA) with Al^{3+}, Cu^{2+} and Zn^{2+}. Despite being an important metabolite of vitamine B6, the complex formation properties of this HPC derivative have been never investigated so far. Another study performed within this thesis is the coordination chemistry of POA towards Al(III) and Zn(II).
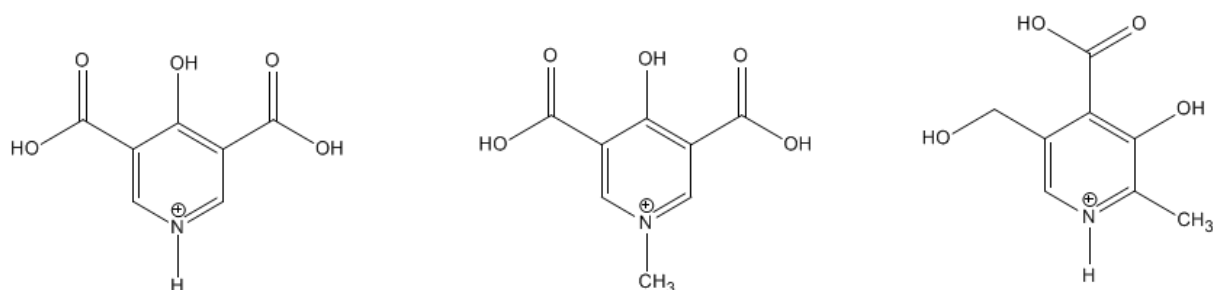
Figure 2.4: 4-hydroxy-3,5-pyridinedicarboxylic acid (DQ58); 4-hydroxy-1-methyl-3,5-pyridinedicarboxylic acid (DQ71508); 3-hydroxy-5-(hydroxymethyl)-2-methyl-4-pyridinecarboxylic acid (POA). All ligands are shown in their completely protonated forms (H_4L^+, H_3L^+ and H_3L^+, respectively)

3 STUDY OF COMPLEX EQUILIBRIA

There are several techniques available for the study of complex equilibria. In the following paragraphs, the methods which have been used in the frame of this thesis will be described: potentiometry, UV-Vis, NMR, EPR.

3.1 POTENTIOMETRY

3.1.1 Introduction

Protonation constants of the ligands, $\beta(H_rL)$, and the overall stability constants of the metal complexes, $\beta(M_pL_qH_r)$, can be determined by pH-potentiometric titrations at equilibrium. Whereas the proton is a product or a reagent of the acid-base reaction under study, no proton may appear in the stoichiometry of the complex formation. In this case, pH-potentiometry can anyway give the requested information, because there is a competition between H^+ and metal ion for the binding sites of the ligand (e.g. 3.1):

$$q\mathrm{HL} + \mathrm{M}^{m+} \rightleftharpoons \mathrm{ML}_q^{(m-q)+} + q\mathrm{H}^+ \tag{3.1}$$

Therefore, the stability of the metal complex can be measured via the H^+ (pH) changes. Equilibrium equations for the formation of the metal complex can be described by the following general chemical equation (3.2):

$$p\mathrm{M} + q\mathrm{L} + r\mathrm{H} \rightleftharpoons \mathrm{M}_p\mathrm{L}_q\mathrm{H}_r \tag{3.2}$$

where M denotes the metal ion, L the completely deprotonated ligand and H the proton (charges are omitted for simplicity). The overall stability constants of the species can be defined according to equation (3.3):

$$\beta_{pqr} = \frac{[M_pL_qH_r]}{[M]^p[L]^q[H]^r} \tag{3.3}$$

3.1.2 Glass electrode

The electrode potential difference between a reference electrode and a reversible working electrode inserted in the solution is measured in the potentiometric measurements. The reference electrode is generally a Ag/AgCl/KCl, whereas the working electrode in pH-potentiometric measurements is practically always the glass electrode. Nernst equation (3.4) provides the relationship between the potential (E) of the glass electrode and the concentration of the electrode active component H^+:

$$E = E^0 + (RT/nF) \ln[H^+] \tag{3.4}$$

Where: E^0 is the standard potential of the electrode. It is a constant that includes various contributes: the standard potential of the internal $Ag/AgCl/Cl^-$ electrode, the one of the external reference, and the asymmetry potential of the membrane;

R is the universal gas constant (8.314 J/mol K);

T is the absolute temperature (K);

n is the number of moles of electrons transferred in the cell reaction or half-reaction;

F is the Faraday constant (96487 C/mol).

RT/F is called the *Nernst slope*. Changes of the electrode potential is measured as a function of the volume of the titrant and the titration curve is recorded (cm^3-pH data pairs).

Combination glass electrode (Figure 3.1) can be used for the measurements, in which the indicator (H ion-selective) and the reference (Ag/AgCl/KCl(3M)) electrodes are conveniently placed in one single housing.

pH range 2-12 can be usually measured precisely by a H ion-selective electrode. However, two errors may influence and eventually reduce this pH range. In the presence of Na^+ or K^+ ions (which can be added e.g. with the titrant NaOH or KOH), the electrode response is non-linear at the alkaline pH range, and the pH measured is lower than the actual value. This phenomenon is called *alkaline error*, and it generally appears at pH > 11 in the case of Na^+ ions. The glass electrodes currently used are made of special types of glass, which significantly reduces the alkaline error; the value of the latter can in any case be determined by dedicated experiments. Another error can be due to absorption of acidic molecules by the gel layer at very acidic pH, leading to a decrease in the hydrogen ion activity in the gel layer. This error is called *acidic error*, and the pH measurement shows a higher pH than the actual value of the solution.

wires to pH meter

filling hole

Ag/AgCl
reference electrode

reference electrode
internal solution

junction

AgCl covered
silver wire

glass electrode
internal solution
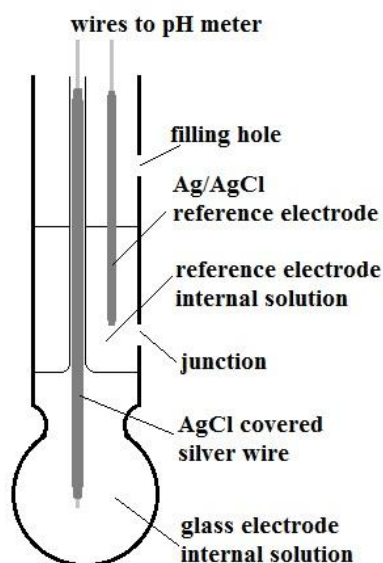
Figure 3.1: schematic representation of the combination glass electrode

3.1.3 The ionic strength control

Complexation measurements typically require the use of an inert electrolyte, that is present in large excess compared to the other species, to ensure a constant ionic strength during the experiment. This allows to assume constants, at least as a first approximation, the activity coefficients of the species at equilibrium. Therefore, in the determination of the formation constants, it is sufficient to know only the species concentrations. The so obtained constants are defined "stoichiometric", as they are dependent on the environment in which the measurement is performed. They are different from the thermodynamic constants which need the activity values instead of concentration ones.

The electrolyte should not interact with the species in solution (metal and ligand), because it is rather impossible to determine any complex formed between the electrolyte and these species; for this reason, salts of alkali metals and single charged anions are usually used [Rossotti 1961], such as sodium perchlorate, potassium chloride, sodium chloride, etc. In this thesis work KCl 0.2 M was used. K^+ was chosen because the titrant KOH is less subjected to carbonation than NaOH and Cl^- was chosen due to its physiological and environmental importance; the 0.2 M value represents a compromise between a physiological and environmental (sea water) solution, and it has been used since long time by the research group of Szeged.

3.1.4 The experimental titrations

The titrations are generally performed by mixing a strong acid and the ligand (and/or the metal ion), so that to obtain an acidic (ca. pH = 2) starting solution. The samples also contain KCl providing the constant ionic strength (0.2 M). This solution is then titrated by a strong base. The titrations are generally performed by automatic titrators, which add a suitable volume of titrant in a vessel containing the acidic starting solution, measure the pH, wait until equilibrium is reached (i.e. until pH is stable), then perform another addition of titrant. These procedures are repeated until titration end, which is generally represented by a basic pH values (e.g.12). Therefore, the almost entire pH region from acidic to basic pH is covered by pH-potentiometric titrations. The stability constants are obtained by using suitable computer programs.

3.1.5 Determination of the ligand protonation constants

For the ligand titrations, the stability constants are obtained using the computer program HYPERQUAD vers.2008. HYPERQUAD needs the following input data:

- ✓ V_0: starting volume of the sample (cm^3);
- ✓ n_{ligand} (mmol): amount of ligand; estimated value based on its weight and molecular weight;
- ✓ n_H (mmol): amount of acidic protons; estimated value is given by $r \times n_{ligand} + n_{HCl}$, where r is the proton content of the ligand, and n_{HCl} is the amount of strong acid added;
- ✓ V_{KOH} *vs.* pH points: data points of the titration curves; the pH values are corrected by the Irving factor;
- ✓ c_{KOH}: concentration of the titrant (mol/dm^3);
- ✓ Irving factor (IRV): it is the difference between the measured and calculated pH during a strong base-strong acid titration, when concentrations are known and the pH contribution given by the autoprotolysis of water is negligible;
- ✓ pK_w: autoprotolysis constant of water;
- ✓ $\log\beta$ (H_rL) presumed.

The HYPERQUAD program solves the following equation system (3.5):

$$\beta(H_rL) = \frac{[H_rL]}{[H]^r[L]}$$

$$c_L = [L] + \sum_{i=1}^{n} \beta(H_rL)[L]_i[H]_i^r \qquad (3.5)$$

$$c_H = [H] + \sum_{i=1}^{n} r_i\beta(H_rL)[L]_i[H]_i^r$$

(*n* is the number of the species)

The presumed protonation constants and the values of c_L and c_H are refined by the program in order to find the best fit between the measured and calculated titration curves. This non-linear fitting is performed through an iteration procedure.

The proton dissociation constants (pK_r) can be calculated easily from the protonation constants. For example, in the case of a ligand containing three dissociable protons, the relations are (3.6):

$$\log\beta_{HL} = pK_3; \log\beta_{H2L} = pK_3 + pK_2; \log\beta_{H3L} = pK_3 + pK_2 + pK_1 \tag{3.6}$$

3.1.6 Determination of the metal-ligand complex formation constants

For the determination of the stoichiometry and stability constants of metal-ligand complexes, the two computer programs PSEQUAD and HYPERQUAD were used. When they have been used together, identical stability constant values (within the experimental uncertainty) have been obtained. The input data for PSEQUAD are the same listed before for SUPERQUAD, and in the case of metal-ligand mixtures they include also the amount of metal ion.

The overall stability constants are calculated by solving the mass balance equations (3.7):

$$c_M = [M] + \sum_{i=1}^{n} p_i \beta_{pqr} [M]_i^p [L]_i^q [H]_i^r$$

$$c_L = [L] + \sum_{i=1}^{n} q_i \beta_{pqr} [M]_i^p [L]_i^q [H]_i^r \tag{3.7}$$

$$c_H = [H] + \sum_{i=1}^{n} r_i \beta_{pqr} [M]_i^p [L]_i^q [H]_i^r$$

The correct speciation (i.e. the number and the stoichiometry of the species) is obtained indirectly, by comparing the fitting results of different speciation models: the model giving the best fit corresponds to the correct speciation in solution.

3.1.7 Limitations of pH-potentiometry

In potentiometry, as seen, the concentration of $[H_3O]^+$ is only indirectly affected by the metal-ligand complex formation. Therefore, while in simple systems the interpretative model is unique, in systems with multiple complexes it may happen that some of them change the pH only marginally. Therefore, many speciation models can be acceptable, and the correct choice requires a large number of titrations at very different conditions.

Another disadvantage of the method is that it is unable to provide reliable results when the pH is less than 2. This is not only due to the acidic error described previously, but also to the impossibility to discriminate the [H] change due to the complexation equilibria when [H] is very high. Furthermore, the liquid junction potential of the reference electrode is not more negligible at acidic pH, thus inaccurate pH value measurements are obtained.

Finally, the technique requires the analyzed system to be in equilibrium conditions during the titration; otherwise, the measured pH cannot be directly correlated to the composition of the solution. Consequently, the speed of the reactions must be sufficiently high (usually within minutes, exceptionally few hours), since the calibration parameters of the glass electrode (E^0 and Nernst slope) slowly change over time and may introduce systematic errors if the titration times become too large.

3.2 UV-VIS SPECTROSCOPY

3.2.1 Introduction

Photons of UV and visible light can have enough energy to cause transitions between the different electronic energy molecular levels. These transitions result in very broad absorbance bands as they are due to vibrational and rotational energy levels superimposed on the electronic ones. The broadening is even more evident in solutions because of solvent-solute interactions. The amount of light absorbed by a sample is expressed as either transmittance (3.8) or absorbance (3.9) according to the following equations:

$$T = I/I_0 \quad \text{or} \quad \% \, T = 100 \, I/I_0 \tag{3.8}$$

$$A = -\log T \tag{3.9}$$

where I_0 is the intensity of the incident radiation, and I is the intensity of the transmitted radiation. For most applications, absorbance values are used since the relationship between absorbance and both concentration and path length, known as Lambert-Beer equation, is linear in most experimental conditions (3.10).

$$A = \varepsilon \, b \, c \tag{3.10}$$

where ε is the molar absorptivity [L mol^{-1} cm^{-1}], b is the path length of the sample [cm], and c is the concentration of the compound in the solution [mol L^{-1}].

Absorbance by organic compounds results from the presence of a chromophore in the molecule. A chromophore is a molecular group usually containing conjugate π bonds, but it can also have different characteristics. The main transitions responsible for the chromophore character are $\pi \rightarrow \pi^*$, n $\rightarrow \sigma^*$, and n $\rightarrow \pi^*$. These absorptions typically fall in the 185-1000 nm wavelength range.

As UV-visible spectra generally show only few broad absorbance bands they provide a limited amount of qualitative information. However, the presence of an absorbance band at a particular wavelength can be a good indicator of the presence of a specific chromophore, despite the exact position of the absorbance maximum is not fixed but depends partially on the molecular environment of the chromophore and on the solvent in which the sample is dissolved. Other parameters, such as pH and temperature, also may cause changes in both the intensity and the wavelength of the absorbance maxima. The conjugation of more double bonds increases both the intensity and the wavelength of the absorption band.

There can be more than one type of electronic transitions, or excitations, taking place depending upon the nature of the chromophore(s) involved: the spectrum obtained is the combination of the different types of transitions occurring within the compound. For instance, if the ligand of a metal-ligand complex contains a chromophore which is not directly engaged in the metal binding, the ligand can absorb UV-Vis radiation in the same way as it would do on its own. The absorption due to the ligand therefore forms part of the spectrum for the particular complex. Transition metal ions, have peculiar electronic energy levels that cause absorption at 400–700 nm.

Four different types of electronic transitions in metal complexes can occur:

- *d-d* transitions: they are related to excitation of an electron from the lower to the upper *d* level of the metal ion;
- *f-f* transitions: caused by the electrons in the *f* levels with the same mechanism as for *d-d* transitions. Bands are of extremely low intensity; furthermore *f* orbitals, being deeply buried in the interior of the metal atoms, are very little affected by any ligand crystal field effects;
- LMCT (Ligant-to-Metal Charge Transfer) transitions: charge transfer (CT) transitions involve the movement of a charge from one atom to another during the electronic transition. If an electron is in a molecular orbital (MO) that is primarily located on the ligand and gets excited to a MO that is located

on the metal cation, there is a ligand-to-metal charge transfer transition. Such transitions are usually very intense;

- MLCT (Metal-to-Ligand Charge Transfer) transitions: if the CT band in an electronic spectrum is associated with an excitation of an electron from a *d* orbital (metal-centered) to a ligand-centered MO (in most cases an antibonding MO), a metal-to-ligand charge transfer transition occur.

3.2.2 UV-Vis spectra evaluation

The processing of spectrophotometric data is conducted similarly to that of the potentiometric data (see paragraphs 3.1.5 and 3.1.6) and by the same computer programs. The only difference is that in this case the theoretical and experimental magnitude which is compared during the fitting procedure is the absorbance *A*, which is additive in a mixture. For example, in a solution containing metal and ligand, A is given by the relation (3.11):

$$A = \varepsilon_\mathrm{M}\, b\, [M] + \varepsilon_\mathrm{L}\, b\, [L] + \sum \varepsilon_i\, b\, (\beta_{pqr})_i\, [M]^p\, [L]^q\, [H]^r \qquad (3.11)$$

where:

- ε_i is the molar absorptivity (at the selected wavelength λ) of the species *I*, which might be zero for certain compounds;
- $(\beta_{pqr})_i$ are the overall formation constants as defined by equation (3.3), which include also the protonation constants of the ligand and the hydrolysis constants of the metal ion.

Hence, the fitting procedure requires to the values for ε in addition to those of β.

3.2.3 A comparison between potentiometry and UV-Vis spectroscopy

UV-visible spectroscopy has some advantages when compared with potentiometry. For example there is the possibility to operate at lower analytical concentrations than in potentiometric titrations: whereas the latter requires at least an analyte concentration equal to $2 \cdot 10^{-4}$ M (as below this value data are not interpretable), UV-visible spectroscopy allows to work at concentrations as low as about 10^{-5} M, provided that the relevant ε values are high enough. Spectroscopy techniques allow to operate at very acidic (or very basic) pH, because no electrode is required. Furthermore, UV-visible measurements are not limited by the speed of the complexation reactions, because there is no problem to wait even very long times before performing the measurement. Another important advantage of UV-visible

measurements is that they might give structural information about the complex. Finally, these measurements are generally faster and simpler than potentiometric ones.

The only, but very important, disadvantage of UV-visible spectroscopy is that data obtained are generally less accurate than data obtained with potentiometry. This is due to the intrinsic poor resolution of the UV-visible spectra, since absorption bands of the ligand, and/or metal complexes are usually overlapped, making it difficult to separate the various components of the signal. Another problem which affect the accuracy of the fitted data is that more parameters have to be fitted for UV-Vis data than for potentiometric titrations, as also the ε values and not only the stability constants are unknown. The situation is much worse if many complexes coexist in solution, and if the spectra of metal-ligand complexes, as commonly happens, are very similar each other and to those of the free ligand or of the free metal.

For this reason, the UV-visible spectroscopy is usually used mostly to verify potentiometric data, or to study solutions with very slow kinetics, or at extreme pH values.

3.3 EPR

3.3.1 Introduction

Electron paramagnetic resonance (EPR) spectroscopy allows to detect electron spin transitions of permanent or temporary paramagnetic species, which include organic and inorganic free radicals, molecules in the triplet electronic state, metals and semiconductors with conduction and/or valence bands, defects in crystals and systems containing transition metals ions.

According to quantum mechanics, the angular momentum of the electron spin is associated with an angular momentum quantum number $S = ½$. The two spin eigenstates of the electron, denoted by |α> and |β> respectively, are degenerative in the absence of an external magnetic field. The application of a magnetic field causes the two energies to become different, because of the *Zeeman* interaction.

The separation in energy between the two states depends on the intensity of the magnetic field according to the equation (3.12):

$$\Delta E = E_\alpha - E_\beta = g_e \mu_B B_0 \tag{3.12}$$

where μ_B and g_e are the Bohr magneton ($\mu_B = 9.72 \cdot 10^{-23}$ J T^{-1}) and the g factor ($g_e = 2.0023$ for the free electron) respectively, and B_0 is the magnetic field.

An unpaired electron can pass from one energy level to another absorbing or emitting an amount of energy equal to the energy gap between states α and β, in order to verify the resonance condition described by equation (3.12) and schematized in Figure 3.2.

In EPR technique with a continuous wave, this condition is obtained by varying the magnetic field and irradiating the sample at a constant frequency.
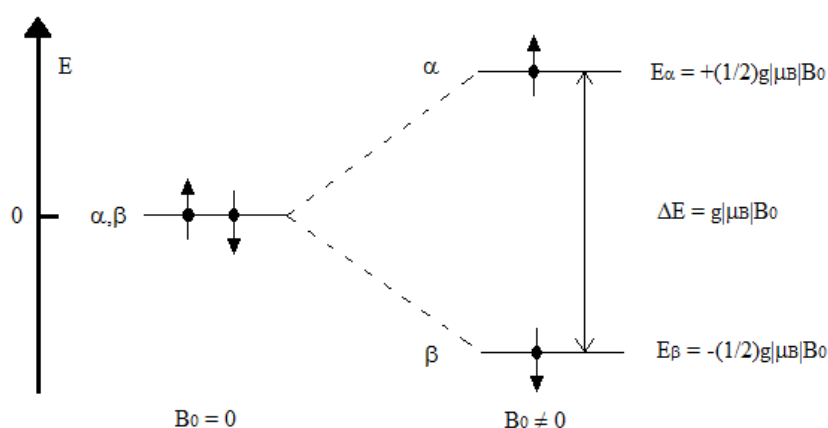
Figure 3.2: schematic representation of Zeeman effect, that is the separation in energy of electronic states α and β in the presence of an external magnetic field.

In molecules there are no individual unpaired electrons, because they are associated with one or more atoms, and the value of g can differ considerably from that of the free electron. This is due to the interaction of the spin magnetic moment **S** with the orbital angular momentum **L**. This coupling is known as *spin-orbit coupling*. As a consequence, a local magnetic field is generated, that is added vectorially to the external field. The spin-orbit coupling is very important in solid state EPR, as only in solid samples (polycrystalline powder or frozen solution) anisotropy is preserved and the paramagnetic species can experiment all possible orientations with respect to the field. Therefore, the principal values of the tensor **g** can be determined. In solution, where paramagnetic molecules move rapidly and erratically, only an average value of **g** can be measured.

Another information which can be obtained from an EPR spectra comes from the *Hyperfine coupling*. Some nuclei possess an intrinsic spin angular momentum (**I**) associated with a magnetic moment. Consequently, the effective magnetic field which affects the electrons is also a function of the magnetic field generated by the nuclei. If the electron magnetic moment is coupled with the magnetic moment of a nucleus, the possible electronic transitions are $2I+1$ (**I** is the nuclear quantum

number). The relationship between the intensity of lines in the spectra arise from the Tartaglia triangle, and the separation between them is given by the hyperfine coupling constant, *A*. The constant *A* depends on the orientation of the paramagnetic molecules relative to the direction of the magnetic field.

3.3.2 EPR signals of copper

Among the metal ions considered in this thesis work, Cu^{2+} gives EPR signals because its electron configuration is d^9, so it has an unpaired electron in a *d* orbital and electronic spin $S = ½$. Copper is present as a mixture of isotopes ^{63}Cu (69.2%) and ^{65}Cu (30.8%), having nuclear spin $I = 3/2$. Its EPR spectrum in continuous wave (CW-EPR) is reported in Figure 3.3. Thanks to the hyperfine interaction, four lines separated by the constant A// are obtained. The hyperfine coupling A⊥, which originates from the nuclear magnetic moment of Cu^{2+} for g⊥, is normally very small, so this part of the spectrum does not show any splitting. The parallel region has typically $g = 2.2\text{-}2.3$, while for the perpendicular region *g* varies from 2.03 to 2.06.
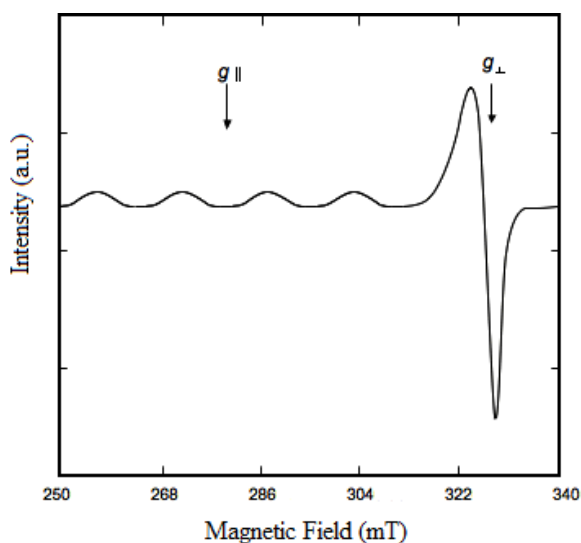
Figure 3.3: CW-EPR spectrum of a Cu(II) compound

3.3.3 EPR spectra evaluation

The EPR spectra can be simulated using suitable programs, and the relevant stability constants can be obtained, similarly as described before, by comparing the simulated and the experimental spectra. The complete procedure is described in the papers of Rockenbauer et al., who first proposed to use EPR for the copper complexation studies [Rockenbauer 2001].

Differently than for potentiometric and UV-Vis elaborations, here the anisotropic EPR parameters and the orientation dependent linewidth parameters should be fitted in addition to the stability constants. Due to this large numbers of parameters,

potentiometric and other spectroscopic results must be available to allow the fitting procedure on EPR data to succeed, i.e., EPR cannot be used as independent technique in complexation studies.

The elaborations of the EPR spectra obtained during this work is still in progress. Therefore, no EPR results can be presented at this stage.

3.4 NMR SPECTROSCOPY

3.4.1 Introduction

The NMR (*Nuclear Magnetic Resonance*) phenomenon is produced if a nucleus having magnetic properties (nuclear spin) is inserted in a magnetic field B_0. The nuclear magnetic moment of a nucleus aligns with B_0 in $2I+1$ ways, either with or against the applied field. For example, for a single nucleus with $I = ½$ two new energy levels are generated, named α (lower energy level) and β. The rotational axis of the spinning nucleus cannot be orientated exactly parallel (or anti-parallel) with the direction of the applied field, but must precess about this field at an angle, with an angular velocity given by the expression (3.13):

$$\omega_0 = \gamma B_0 \qquad\qquad (3.13)$$

Where ω_0 is the precession rate which is also called the Larmor frequency. The magnetogyric ratio (γ) relates the magnetic moment (μ) and the spin number (I) for a specific nucleus (3.14):

$$\gamma = 2\pi\mu/hI \qquad\qquad (3.14)$$

Each nucleus has a characteristic value of γ. For example, for ^{1}H, $\gamma = 2.674 \cdot 10^4$ gauss^{-1} sec^{-1}. This precession process generates an electric field with frequency ω_0. If the sample is irradiated with radio waves in the MHz frequency range, the nucleus absorbs the energy and is promoted to less favorable higher energy state thus causing a magnetic transition.

3.4.2 Sigma electrons and electronic shielding

Electrons are negatively charged particles that surround nuclei within a molecule. It is well known that moving charged particles generate a magnetic field. In NMR spectroscopy, the lines of force of this electron-generated magnetic field run in the opposite direction as the lines of force generated by the external magnetic field B_0.

This has the effect of reducing the net magnetic moment affecting the nuclei. The electronic magnetic field effect causes nuclei with different chemical environments to yield resonance frequencies perturbed from the frequency defined by the applied external field B_0.

The Larmor frequency can be re-written to include the electronic effect (3.15):

$$\omega_0 = \gamma \, (B_0 - S) \tag{3.15}$$

where S represents the change in magnetic field caused by the opposing electron magnetic moment, that is, all electrons making up the sigma bonding around the nuclei generate a magnetic field that is anti-parallel to the external magnetic field force lines. This causes the NMR signal generation to occur at higher external magnetic field setting. NMR signals are shifted upfield, and nuclei are said to be electronically shielded. The sharpness of the NMR signals (at least for nuclei with $I = \frac{1}{2}$), and the sensitivity of the shifts on the chemical surroundings of the atom, allow the powerful use of NMR as a qualitative tool for the identification of the molecule under exam.

The shift is generally measured relative to the signal of a reference compound, which is usually tetramethylsilane (TMS) or similar compounds, as e.g. the analogous water-soluble trimethylsilane-propionic acid. The association with the reference signal is called *chemical shift* and it is measured in parts per million (ppm).

3.4.3   NMR spectroscopy in the study of complex formation

NMR spectroscopy can be applied to the study of metal-ligand complex formation, since it allows a qualitative (and sometimes semi-quantitative) analysis of the complexation. NMR spectra can provide the number of species existing in solution and in some cases their structure, while the signal integration is related to the relative abundance of the particular complex. These information can be acquired either through the evaluation of the electronic effects exercised by the ligand on the metal (by nuclear spectroscopy of the metal) or, on the opposite, considering the effects generated by the metal on the ligand (by NMR studies of e.g. [1]H nuclei of the ligand).

In complexometric analysis in which aluminium is involved, there is the possibility to study directly the metal center, because the isotope [27]Al is very sensitive to this technique, thanks to its high gyromagnetic ratio and to its large isotopic abundance, close to 100%. Despite this, ^{27}Al NMR spectra are often difficult to interpret, because aluminium nucleus has a quadrupole moment which broaden NMR peaks when, as usually happens, the metal ion is in the center of an asymmetric electronic

distribution. Therefore, ^{1}H spectroscopy on the ligand is better suitable to study aluminium complex formation. A specific advantage of aluminium is its kinetic inertia, that allows to obtain ^{1}H spectra with very narrow lines for each of the species formed in solution. For Zn^{2+} and for many other atoms, on the other hand, the very high complex formation speed does not allow to obtain separate NMR lines: one single line is rather obtained for each proton, and its chemical shift is a weighted average between the chemical shifts due to that proton in the different complexes. For Cu^{2+} and for other paramagnetic atoms, finally, the technique is even less suitable, because the magnetic field generated by unpaired electrons shorten the relaxation times of the nuclear spins, leading to a consequent widening of the signals. This can be so pronounced, that the signals themselves may disappear.

3.4.4 Isotopic effects

If ^{1}H-NMR spectra have to be obtained in water, it is advisable to minimize the strong interference due to the water protons by using heavy water (D_2O) as solvent. This, however, introduces isotopic effects, which mainly affect equilibrium constants if H_3O^+ is directly involved in the reaction (primary isotope effects), and to a lesser extent all the other constants in solution through a "solvent effect".

Although the metal-ligand complexation constant is not directly affected by the deuterated solvent, the effective strength of the complex changes significantly in heavy water because the competition for the ligand of H^+ is different than that of D^+. On the other hand, the similarity of the two solvents makes it very improbable that qualitative changes occur, hence the number and the stoichiometry of the species present are generally identical. NMR study of metal-ligand complexes in D_2O is therefore expected to provide reliable qualitative information.

4 EXPERIMENTAL

4.1 INSTRUMENTS

- Orion 710A pH-meter
- Metrohm combined electrode (type 6.0234.1000)
- Automatic titrator Metrohm 665 Dosimat equipped with 1 mL and 5 mL burettes
- Measuring cells of 20 mL and 10 mL
- Thermostat which provides a constant temperature $25.0 \pm 0.1°C$
- Analytical balance
- Technical balance Gibertini TM 560–2R (Padova)
- BRUKER EleXsys E500 spectrometer (microwave frequency ~9.7 GHz, microwave power 13mW, modulation amplitude 5 G, modulation frequency 100 kHz).
- Heidolph Pumpdrive 5101 peristaltic pump to circulate the solution from the titration pot through a capillary tube into the cavity of the EPR instrument.
- Hewlett Packard 8452A diode array spectrophotometer
- 1 cm quartz cuvette
- Crison glass electrode, calibrated with two buffer solutions:
  - ➢ stabilized solution of sodium and potassium phosphates, "Labochimica", pH=7 ± 0.02 (20°C)
  - ➢ stabilized citric acid, HCl and NaOH solution, "Titolchimica", pH = 4.00 ± 0.02 (20 ° C)
- NMR Bruker DRX-400 spectrometer, frequency 400.13 MHz

4.2 REACTANTS

- Potassium hydrogen phthalate (Sigma Aldrich >98%)
- Hydrochloric acid (Merck, 36 % m/m)
- Potassium hydroxide (Merck, > 86%)
- Potassium chloride (Sigma Aldrich, > 98%)

- 4-hydroxy-3,5-pyridinedicarboxylic acid (DQ58), synthesis product of the research groups of D. Marton and M. Grazia Ferlin, University of Padova
- 4-hydroxy-1-methyl-3,5-pyridinedicarboxylic acid (DQ71508), synthesis product of the research groups of D. Marton and M. Grazia Ferlin, University of Padova
- 2-Methyl-3-hydroxy-4-carboxy-5-hydroxymethylpyridine, or 3-hydroxy-5-(hydroxymethyl)-2-methyl-4-pyridinecarboxylic acid (POA), Aldrich
- Zn(II) solution, prepared by dissolution of anhydrous $ZnCl_2$ (SigmaAldrich) in a known amount of HCl (Merck, 36%). $[Zn^{2+}]_0 = 0.09721$ M, $[H^+]_0 = 0.00669$ M
- Cu(II) solution, prepared from $CuCl_2 \cdot 2H_2O$ (Reanal, > 98%) dissolved in doubly distilled water. $[Cu^{2+}]_0 = 0.08828$ M
- Al(III) solution prepared by dissolution of $AlCl_3$ (Sigma Aldrich) in doubly distilled water. $[Al^{3+}]_0 = 0.100992$ M, $[H^+]_0 = 0.0216$ M
- Ethylenediaminetetraacetic acid (EDTA) (Sigma Aldrich, > 99%)
- methyltimol blue indicator
- hexamethylenetetramine buffer
- Deuterium oxide, "Aldrich", nominal concentration 99.9% deuterium atoms
- DCl, Janssen Chemical, 20 wt% solution in D_2O, 99% deuterium atoms
- NaOD, Aldrich, 40 wt% solution in D_2O, 99.9% deuterium atoms
- Zinc oxide, Aldrich 99.9%
- Aluminium trichloride hexahydrate, "Aldrich", nominal concentration 99%
- 3–(trimethylsilyl) propionic acid, sodium salt (TMSP), "Aldrich", minimum concentration 99%

4.3 PREPARATION OF THE SOLUTIONS

All the solutions used for pH-potentiometric titrations, UV-Vis and EPR measurements were prepared by dissolving the reagents in a known volume of doubly-distilled Milli-Q water, and the temperature was set at 25 °C. The exact concentrations (expressed in molarity M, mol/L) of the stock solutions prepared were determined by potentiometric titrations, using the programs HYPERQUAD and PSEQUAD for data evaluation. The solutions used for NMR measurements were prepared by direct weighing of the analytes and the solvent.

To all ligand stock solutions (except those for NMR measurements) an appropriate quantity of hydrochloric acid and kalium chloride was added, in order to reach a pH of around 2 and a ionic strength of KCl 0.2 M.

4.3.1 Potassium hydrogen phthalate solution

Two different solutions of potassium hydrogen phthalate were prepared. The first one was prepared at an accurate concentration of 0.05 M and it was used as standard buffer solution to calibrate the pH-meter: at this concentration and at $T = 25\ °C$, pH = 4.01 by definition. This solution was prepared every 2-3 days to ensure the maintenance of the exact concentration.

The second potassium hydrogen phthalate solution was prepared by diluting the first one with doubly distilled water, and adding KCl to obtain a ionic strength of 0.2 M. This solution was used repeatedly to titrate the KOH solution, in order to obtain its exact concentration.

4.3.2 KCl solution

The strong electrolyte KCl was used to keep the ionic strength (I) constant in all samples. I was imposed to be 0.2 M and it was adjusted by suitable additions of 1 M KCl solution.

The KCl 1 M stock solution was prepared by solubilising a weighed amount of salt in a known volume of water.

4.3.3 HCl solution

This solution was prepared by dilution of commercial HCl (37% m/m) with double-distilled water. The HCl concentration was determined by potentiometric titrations with standardized KOH 0.1 M using Gran's method, and it resulted 0.228 M $\pm$ 0.001. The HCl solution was used in HCl-KOH titrations, to acidify all the ligand and metal-ligand solutions, and to vary the pH (if needed) in UV-Vis measurements.

4.3.4 KOH solution

0.1 M carbonate-free KOH solutions were used. They were prepared by dissolution of KOH pellets in freshly boiled double-distilled water, which was left to cool to room temperature under argon bubbling. An approximately double amount of KOH pellets was weighted, and its surface was washed out in order to remove the carbonate-layer before adding it in the solution flask. In order to keep the ionic strength constant, KCl has been added to the KOH solution to set the K^+ - concentration = 0.2 M. A small amount of KOH solution was quickly titrated by HCl solution with known concentration to check the correctness of the 0.1 M KOH concentration, and after the solution was diluted accordingly if necessary. The

solution was poured into the burette under argon. The capillaries and the piston of the burette had to be rinsed with the titrant several times and its concentration was determined after 24 h storage. The KOH solution was than standardized against hydrogen phthalate, and it was used for *ca.* 3 weeks; after that time, a new titrant solution was prepared.

4.3.5   Aluminium, zinc and copper solutions

The aluminium, zinc, and copper solutions were prepared by dissolution of $AlCl_3$, $ZnCl_2$, and $CuCl_2$ respectively in acidic aqueous solutions. Zn^{2+} solution was directly titrated by EDTA standard solution in order to obtain its exact metal concentration. Al^{3+} solution cannot be directly titrated by EDTA, as the complex formation reaction is fairly slow. Therefore, an excess EDTA and aluminium are allowed to react in a hot solution for several minutes. The reaction is allowed to proceed at acidic pH (2-3) to avoid the metal hydrolysis. When almost all Al(III) is bound to EDTA, the pH is increased to ~9 in order to complete the complex formation. After several minutes extra boiling, the solution is cooled down, and the excess of EDTA is titrated by a Zn(II) titrant solution.

This procedure is called *back titration*. The titration by Zn^{2+} is performed at pH ~ 5 (hexamethylenetetramine buffer) in the presence of methyltimol blue indicator. The H^+ concentration was obtained by direct titration of the metal solution by standardized KOH solution.

4.3.6   DQ58 solutions

Four DQ58 solutions were prepared, one for each different technique employed. All solutions were prepared by careful weighing of the ligand and dissolving it in doubly distilled water. The following concentrations were achieved: ~2 mM for pH-potentiometric, EPR and UV-Vis measurements and ~1.5 mM for NMR measurements. The solubility of DQ58 in water is slightly larger than $2 \cdot 10^{-3}$ M. The exact concentration of the potentiometric, UV-Vis and EPR solutions was determined by repeated titrations with the standardized KOH solution. DQ58 solutions, when not in use, were stored in the refrigerator.

4.3.7   DQ71508 solutions

Five DQ71508 solutions were prepared. Two of them were used for pH-potentiometric studies, the other three for UV-Vis, EPR and NMR measurements respectively. All solutions were prepared by accurately weighing the ligand and dissolving it in water. Solutions for pH-potentiometric studies were prepared at concentration 1.3 mM (to study the system DQ71508-Cu(II)) and 1.6 mM (to study the system DQ71508-Zn(II)). The concentrations for the UV-Vis, EPR and NMR

studies were ~1.3 mM. The solubility of DQ71508 in water is around $2.5 \cdot 10^{-3}$ M. As for DQ58, the exact concentration of the potentiometric, UV-Vis and EPR solutions was determined by repeated titrations with the standardized KOH solution. DQ71508 solutions, when not in use, were stored in the refrigerator.
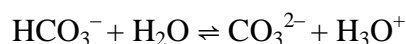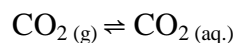
4.3.8 POA solutions

Three POA solutions were used. All solutions were prepared by accurately weighing the ligand and dissolving it in water. The concentration reached for pH-potentiometric and UV-Vis measurements was ~2 mM, while the concentration reached for NMR measurements was ~2.5 mM. The solubility of POA in water was not determined, but it overcomes 2.5 mM. The exact concentration of the potentiometric and UV-Vis solutions was determined by repeated titrations with the standardized KOH solution. POA solutions, when not in use, were stored in the refrigerator.

4.4 EXPERIMENTAL PROCEDURE FOR pH-POTENTIOMETRIC TITRATIONS

pH-potentiometric measurements were performed for solutions containing the ligands alone (DQ58, DQ71508 or POA), and for solutions containing one ligand and one metal ion. The following metal-ligand solutions were studied: DQ58-Zn(II), DQ71508-Zn(II), DQ71508-Cu(II), POA-Zn(II), and POA-Al(III). DQ58-Cu(II) and POA-Cu(II) complexes have been studied in the frame of a different thesis work [Suba 2013]. The pH-metric measurements were carried out at an ionic strength of 0.2 M KCl in aqueous solution. The titrations were performed in the pH range 2-11 or until precipitation occurred in the samples.

4.4.1 Instrumental apparatus

The potentiometric measurements were performed in a galvanic cell, whose temperature is stabilized at 25.0 ± 0.2 °C, thanks to a water circulation cooling system. A 20 mL cell was used to titrate DQ58 and DQ71508, a 10 mL one was used for POA. Titrations were performed with a carbonate-free KOH solution of know concentration (ca. 0.1 M); the samples were in all cases deoxygenated by bubbling purified and saturated argon for some minutes before the measurements, and argon was also passed across the solutions during the titrations. The use of the argon flow is necessary in the cell when the solution reaches neutral or alkaline pH. In these situations, the carbonation would result in a constant drift of the pH to more acidic values, due to (4.1):

$$CO_{2\,(g)} \rightleftharpoons CO_{2\,(aq.)}$$

$$CO_{2\,(aq.)} + 2\,H_2O \rightleftharpoons HCO_3^- + H_3O^+ \tag{4.1}$$

$$HCO_3^- + H_2O \rightleftharpoons CO_3^{2-} + H_3O^+$$

Before each titration, the glass electrode was calibrated with hydrogen phthalate, and the pH readings were corrected according to Irving *et al.* (strong acid vs. strong base titrations) [Irvin 1967].

A homemade computer program enables the automatic management of the instrument, controls the addition of the titrant, and monitors the pH when the equilibrium is reached according to the given parameters.

The following information and titration parameters are set:

- ✓ Dosing unit: it specify which burette is working if many are connected to the PC and pH-meter
- ✓ Name of the file
- ✓ Concentration of the base solution
- ✓ Initial volume of the sample
- ✓ Cycle time: the pH has to be stabilized within pH $\pm$ 0.002 unit during a given period
- ✓ Maximum cycle number: the pH is checked *e.g.* maximum 15 times
- ✓ Volume of the first addition
- ✓ Minimum volume of the titrant added
- ✓ Maximum volume of the titrant added
- ✓ Dose limit: the titration runs until a certain value of pH or Volume of titrant is added
- ✓ pH difference: pH interval between one measurements and the following
- ✓ waiting time before starting the titration

An automatic titration is performed, and an output file is obtained reporting the pH values (from which the Irving factor must be subtracted) as a function of the titrant volume. This file is then used as input file by the computer programs HYPERQUAD and PSEQUAD.

4.4.2 Sequence of potentiometric titrations

The calculation of the metal-ligand complex formation constants by potentiometric titrations, and therefore the titrations of metal-ligand solutions, require to be performed by sequential steps.

First of all, the KOH solution has to be standardized with potassium hydrogen phthalate. This KOH solution is then used to standardize HCl, the metal and the ligand, and finally the metal-ligand solutions.

4.4.3 KOH standardization with potassium hydrogen phthalate

3 mL of a 0.05 M standard hydrogen phthalate solution were added to 13 mL of water and to 4 mL of KCl 1 M in order to obtain a ionic strength 0.2 M; this solution was then titrated with KOH. Table 4.1 shows the parameters chosen for all the KOH standardizations:

Table 4.1: parameters for KOH standardization

Cycle time (s)	10
Max. cycle number	8
Volume of the first addition (mL)	0.1
Minimum volume of the titrant added (mL)	0.01
Maximum volume of the titrant added (mL)	0.1
Final pH	11.5

4.4.4 Strong acid-strong base titrations

The HCl-KOH titrations were performed once or twice a day in order to check the correct functioning of the potentiometric system. From these titrations, the exact concentration of the strong acid (HCl) solution, the Irving factor (IRV), and the water ionization constant (pK_w) can be determined. The requirement for a correct functioning of the potentiometric system is that the same IRV and pK_w values should be obtained in different titrations.

The 20 mL titrated solution was composed by 0.6 mL of HCl, 15.4 mL of water and 4 mL of KCl. Table 4.2 shows the parameters chosen for the titrations.

Table 4.2: parameters for the strong acid-strong base titrations

Cycle time (s)	10
Max. cycle number	8
Volume of the first addition (mL)	0.1
Minimum volume of the titrant added (mL)	0.01
Maximum volume of the titrant added (mL)	0.1
Final pH	11.5

4.4.5　Titrations of solutions containing DQ58, DQ71508 or POA

Titrations of each ligand were carried out either by directly titrating each stock solution (prepared as described in previous paragraphs), or by diluting it in a 1:1 v/v ratio and adding KCl in order to keep the ionic strength constant.

Table 4.3 shows the parameters chosen for all the ligand titrations.

<div align="center">

Table4.3: parameters for the ligand titrations

Cycle time (s)	15
Max. cycle number	15
Volume of the first addition (mL)	0.05
Minimum volume of the titrant added (mL)	0.005
Maximum volume of the titrant added (mL)	0.1
Final pH	11.5
Waiting time before starting (s)	60

</div>

4.4.6　Titrations of DQ58-Zn(II) solutions

The ligand stock solution was added with a known volume of zinc solution and, if necessary, doubly distilled water and KCl, in order to obtain a 20 mL solution. The chosen ligand-to-metal ratios were 2:0.5, 2:1, 2:1.4, 1:0.5 and 1:0.9. Experimental parameters of the titrations are shown in Table 4.4. The starting acidic solutions were titrated with KOH; titrations were stopped when a precipitate was observed. Precipitation occurred at pH 6.4, 5.1, 4.8, 6.8 and 5.8 at the above listed ligand-to-metal ratios, respectively.

<div align="center">

Table 4.4: parameters for the Zn(II)-ligand and Cu(II)-ligand titrations

Cycle time (s)	15
Max. cycle number	15
Volume of the first addition (mL)	0.05
Minimum volume of the titrant added (mL)	0.005
Maximum volume of the titrant added (mL)	0.1
Final pH	11.5
Waiting time before starting (s)	180

</div>

The waiting time before the titration start was set at a value larger than zero to permit the complete complexation between the ligand and the metal after their mixing.

4.4.7　Titrations of DQ71508-Cu(II) and DQ71508-Zn(II) solutions

The ligand stock solution was added with a known volume of metal solution (copper or zinc) and, if necessary, doubly distilled water and KCl, in order to obtain a 20 mL solution. The chosen ligand-to-metal ratios were 2:0.5, 2:1, 2:1.8, 1:0.5 and 1:0.75 for copper, 2:0.5, 2:1, 2:1.75, 1:0.5 and 1:0.8 for zinc. Like before, the starting

solution was titrated with KOH, and titrations were stopped when precipitation occurred. For copper, a precipitate formed at pH 4.4, 3.4, 3.0, 4.1 and 3.4, respectively, at the above listed ligand-to-metal ratios. For zinc, precipitation occurred at pH 8.5, 8.3, 7.9, 8.3 and 7.7, respectively. Experimental parameters are listed in Table 4.4.

4.4.8   Titrations of POA-Zn(II) and POA-Al(III) solutions

The ligand stock solution was added with a known volume of metal solution (aluminium or zinc) and, if necessary, doubly distilled water and KCl, in order to obtain a 10 mL solution. The chosen ligand-to-metal ratios were 2:0.5, 2:1, 2:1.8, 1:0.5 and 1:0.9. For POA-Zn(II) solutions, precipitation occurred respectively at pH 7.8, 7.7, 7.5, 7.7 and 7.6. For POA-Al(III) solutions, precipitation was not observed for the 2:0.5 ratio, whereas for the other ratios it occurred at pH 7.4, 5.1, 6.5 and 5.6, respectively. Experimental parameters of the POA-Zn(II) titrations are shown in Table 4.4. Experimental parameters of the POA-Al(III) titrations are reported in Table 4.5. The latter are different from those used for the other metal-ligand titrations, because the complexation kinetic of Al(III) is much slower than that of Zn(II) and Cu(II).

Table 4.5: parameters for the POA-Al(III) titrations

Cycle time (s)	25
Max. cycle number	15
Volume of the first addition (mL)	0.05
Minimum volume of the titrant added (mL)	0.005
Maximum volume of the titrant added (mL)	0.1
Final pH	11.5
Waiting time before starting (s)	320

4.5   EXPERIMENTAL PROCEDURE FOR UV-VIS MEASUREMENTS

UV-vis spectrophotometric measurements were performed for DQ58-Cu(II) and DQ71508-Cu(II) solutions in order to obtain additional complexation data. Aqueous solutions at 25.0 ± 0.1 ^{o}C and at ionic strength 0.20 M (KCl) were analyzed.

4.5.1   Instrumental apparatus

A Hewlett Packard 8452A diode array spectrophotometer was used to collect the UV-**v**is spectra in the interval 200–400 nm. The spectra were recorded under argon atmosphere. In the acquisition of all spectra the blank is represented by a solution of potassium chloride 0.2 M, and each solution contains KCl 0.2 M.

Protonation and stability constants and the individual spectra of the species were calculated by the computer program PSEQUAD.

4.5.2 DQ58 solutions

Starting from the DQ58 stock solution prepared, as explained in paragraph 4.3.6, a more diluted solution (0.081 mM) was prepared to be employed for all UV-Vis measurements.

The free ligand solution was analyzed by UV-Vis by varying the pH from 2.164 to 11.611 by 0.1-0.2 pH units intervals. The base solution used for this purpose (0.1 M) had to be diluted when the pH was close to each pK_A because otherwise a too big change in the absorbance value was observed even with very small additions of the titrant. The dilution due to base additions was taken into account during data evaluation.

4.5.3 DQ58-Cu(II) solutions

Two different experiments were carried out for DQ58-Cu(II) solutions. In the first experiment, two solutions were prepared, containing ligand-to-metal ratios 1:1 and 1:0.5 ($[L]_0$ = 0.081 mM and $[M]_0$ = 0.066 mM, $[L]_0$ = 0.081mM and $[M]_0$ = 0.04 mM, respectively). The pH was varied in the range 2.170-11.307 for the first solution, and 2.171-11.613 for the second one. The absorbance spectra were registered every 0.1-0.2 pH units. The second experiment was carried out to check the presence of the bis-complex (CuL_2). A ligand solution (0.081 mM) was prepared, and the pH was set at ~6.1 by adding KOH 0.1 M. This intermediate pH was chosen in order to favor the formation of the bis-complex without causing precipitate formation. The absorbance was registered in the absence of the metal, and for metal concentrations ranging from 0.007 mM to 0.064 mM, keeping constant the pH at 6.1 $\pm$ 0.1 by small additions of the base solution when necessary. The ligand dilution due to the additions was taken into account during data evaluation.

Table 4.6 reports the Cu^{2+} and KOH additions (the latter to keep the pH constant), the measured pH value, and the Cu^{2+} concentration obtained in each experiment.

Table 4.6: Volumes, pH and concentrations of the UV-Vis measurements performed at constant pH and different ligand-to-metal ratios. The starting solution contained starting volume = 10 mL, $[DQ58]_0$=0.081 mM.

Experiment n°	Cu^{2+} addition (μL)	KOH addition (μL)	pH	Cu^{2+} concentration (mmol/L)
1	---	---	6.147	0
2	40	---	6.132	0.007
3	40	15	6.145	0.014
4	40	10	6.131	0.021
5	40	13	6.125	0.028
6	40	15	6.121	0.034
7	40	15	6.139	0.041
8	40	12	6.122	0.048
9	40	12	6.107	0.054
10	40	12	6.101	0.061
11	40	10	6.122	0.064

4.5.4 DQ71508 solutions

Solutions containing DQ71508 only were prepared and analyzed in an analogous way as described for DQ58. The DQ71508 concentration was 0.08 mM. The measurements were carried out varying the pH from 2.190 to 9.242 by 0.1-0.2 pH units intervals.

4.5.5 DQ71508-Cu(II) solutions

As before, two different experiments were carried out for DQ71508-Cu(II) solutions. In the first experiment, two solutions containing $[L]_0 = 0.080$ mM and $[M]_0 = 0.070$ mM, $[L]_0 = 0.080$ mM and $[M]_0 = 0.040$ mM, respectively, were prepared. The pH was varied in the range 2.203-9.318 for the first solution, and 2.207-7.230 for the second one. The absorbance spectra were registered every 0.1-0.2 pH units. The second experiment was carried out starting from a 0.08 mM ligand solution added with increasing amounts of a metal solution at a constant pH ~ 6.1. Metal concentrations ranged from 0.007 mM to 0.065 mM.

Table 4.7 reports the Cu^{2+} and KOH additions (the latter to keep the pH constant), the measured pH value, and the Cu^{2+} concentration obtained in each experiment.

Table 4.7: Volumes, pH and concentrations of the UV-Vis measurements performed at constant pH and different ligand-to-metal ratios. The starting solution contained starting volume = 10 mL, $[DQ71508]_0 = 0.08$ mM.

Experiment n°	Cu^{2+} addition (μL)	KOH addition (μL)	pH	Cu^{2+} concentration (mmol/L)
1	---	---	6.181	0
2	40	2	6.120	0.007
3	40	15	6.143	0.014
4	40	10	6.198	0.021
5	40	10	6.143	0.028
6	40	10	6.123	0.034
7	40	10	6.125	0.041
8	40	10	6.128	0.048
9	40	10	6.121	0.054
10	40	10	6.131	0.061
11	20	---	6.131	0.064

4.6 EXPERIMENTAL PROCEDURE FOR ^{1}H-NMR SPECTROSCOPY

^{1}H NMR studies were carried out on a Bruker DRX-400 which works at 400.13 MHz. The sample temperature was set at 298 K during all data acquisitions. Chemical shifts are reported in ppm (δ_H) from $Me_3SiCH_2CH_2COOH$ (trimethylsilylpropionic acid, TMSP) as internal reference. The ^{1}H NMR measurements were performed through suppression of the water signal. Spectra were collected for all the three ligands and for DQ71508-Zn(II), DQ58-Zn(II) and POA-Al(III) solutions in D_2O mixtures at 1.3 mM (DQ71508), 1.5 mM (DQ58) and 2.5 mM (POA) ligand concentration.

KCl was not added, and therefore the ionic strength is not constant for the different solutions, since an excessive electrolyte concentration does not allow to obtain a good instrumental homogeneity. The ligand solutions were prepared directly by dissolving the solid in D_2O. The solutions containing Zn(II) or Al(III) and each ligand were prepared by dissolving the appropriate amount of ligand in the solvent and adding respectively ZnO or $AlCl_3 \cdot 6H_2O$ solids in the correct stoichiometric ratio. The DQ71508– Zn(II) ratio is 1:2; the DQ58-Zn(II) ratio is 1:2 and the POA-Al(III) ratio is 4:1. Table 4.8 shows the concentrations of the solutions.

Table 4.8: species concentrations for ^{1}H-NMR solutions

Solution	DQ58 (mmol/Kg)	DQ71508 (mmol/Kg)	POA (mmol/Kg)	Zn(II) (mmol/Kg)	Al(III) (mmol/Kg)
DQ58	1.478	---	---	---	---
DQ58-Zn(II)	1.478	---	---	2.866	---
DQ71508	---	1.357	---	---	---
DQ71508-Zn(II)	---	1.357	---	2.616	---
POA	---	---	2.525	---	---
POA-Al(III)	---	---	2.525	---	0.650

For each solution listed in Table 4.8 three aliquots at different pH values were prepared (Table 4.9). The pH of the solutions was measured with a glass electrode (Crison) calibrated with two standard solutions at pH = 4 and pH = 7. The pH was adjusted by addition of small volumes of DCl 3 M and NaOD 2 M. The pH values given by the pH-meter has to be added by 0.41 logarithmic units, because of the isotopic effects due to the two different solvents used in the calibration (H_2O) and in the measurements (D_2O). The values obtained in this way, should be more correctly defined as "pD", since they represent the concentration of free acid D_3O^+ in the heavy water solution; in the following, however, this magnitude will be indicated by the term "pH" for simplicity.

Table 4.9: pH values for ^{1}H-NMR measurements

	pH of solution 1	pH of solution 2	pH of solution 3
DQ58	2.54	3.88	6.36
DQ58-Zn(II)	---	3.90	6.34
DQ71508	3.23	5.24	6.36
DQ71508-Zn(II)	3.17	---	6.43
POA	2.76	4.22	5.16
POA-Al(III)	2.65	4.22	5.17

4.7 EXPERIMENTAL PROCEDURE FOR EPR MEASUREMENTS

All CW-EPR spectra were recorded with a BRUKER EleXsys E500 spectrometer (microwave frequency ~9.7 GHz, microwave power 13 mW, modulation amplitude 5 G, modulation frequency 100 kHz). The isotropic EPR spectra were recorded at room temperature in a circulating system during a titration. Three EPR spectra were recorded at 0.4 mM $CuCl_2$ and 1.3 mM DQ71508 ligand concentration, in the pH range 1.8-3.8. At higher pH values precipitation was detected. The 0.2 M ionic strength was adjusted with KCl. The solution pH was changed by KOH (2 M) or HCl (1 M) additions, and it was registered with an Orion 710A pH-meter equipped with a Metrohm 6.0234.100 glass electrode. A Heidolph Pumpdrive 5101 peristaltic pump was used to circulate the solution from the titration pot through a capillary tube into the cavity of the instrument. The titrations were carried out under nitrogen atmosphere. At various pH values, samples of 100 μL were taken from each solution and frozen in liquid nitrogen, to perform isotropic CW-EPR spectra. These were recorded under the same instrumental conditions as the room-temperature spectra described above. Table 4.10 schematizes the procedure.

Table 4.10: additions and withdrawal during EPR experiment; registered pH values before and after the acquisition of the spectra

Solution n°	V_{KOH} (mL)	V_{HCl} (mL)	Withdraw (mL)	pH
1	---	---	---	1.84
2	0.16	0.1	0.1	3.05
3	0.14	---	0.1	3.78

5 pH-POTENTIOMETRIC RESULTS AND DISCUSSION

5.1 KOH STANDARDIZATION

KOH solutions were standardized against hydrogen potassium phthalate. The equivalence point in these titrations was obtained with the best accuracy by using the *Gran method* (Gran plot) [Maccà 1995], which also gives an estimation of the KOH carbonate content from the different points of intersection of the Gran-plots at acidic and at basic pH (max. ~ 0.5 - 0.8 % of carbonate over base content was accepted). The concentrations of the KOH solutions used in this thesis are listed in Table 5.1.

Table 5.1: concentration values of KOH solutions used for the different systems investigated

System	KOH concentration (mol/L)
DQ58 + DQ58-Zn(II)	0.0928 ± 0.0003
DQ71508 + DQ71508-Zn(II)/Cu(II)	0.0998 ± 0.0002
POA + POA-Zn(II)/Al(III)	0.1185 ± 0.0002

5.2 HCl-KOH TITRATIONS

The exact concentration of the strong acid (HCl) solution, the Irving factor (IRV) and water ionization constant (pK_w) were determined by these titrations. The equivalence volume was obtained by the Gran method. The Irving factor (5.1) was calculated by subtracting the calculated pH values of the strong acid-strong base titration curve (computed from the known concentrations and volumes) from the measured values at pH < 3, when the pH contribution of water is completely negligible.

$$IRV = \Delta pH = pH_{measured} - pH_{calculated} \tag{5.1}$$

After the equivalence point, the pOH values can be calculated from the known concentrations and volumes, after correction with the Irving factor. Thus, pK_w is calculated from the data obtained in the alkaline pH range (5.2):

$$pK_w = -\log([H^+][OH^-]) = pH + pOH = (pH_{measured} - IRV) - \log[OH^-] \tag{5.2}$$

pK_w depends on the temperature and the ionic strength. The water ionization constant pK_w under the conditions employed (25 °C, 0.20 M (KCl)) was 13.76 ± 0.02. When the experimental value of pK_w differed, the sensitivity (or slope) of the electrode has to be changed. The apparent E^0 value of the glass electrode was determined through calibration with a 0.05 M potassium hydrogen phthalate solution (pH = 4.008 at 25 °C). The electrode was calibrated before each strong acid-strong base titration. The HCl concentration detected was 0.228 ± 0.001 mol/L.

5.3 LIGAND TITRATIONS

5.3.1 DQ58

Potentiometric titration of each ligand allowed the determination of the pK_A values, which are reported in Table 5.2. The pK_{A1} could not be determined by pH-potentiometric titrations, because it is too low. For other hydroxypyridinecarboxylic acids (HPCs) the pK_{A1} values were determined by UV-Vis [Crisponi 2012 (b)] and resulted to be below 1. In any case, the pK_{A1} value is unimportant as it does neither affect the ligand equilibrium at physiological conditions, nor does it influence the metal-ligand complex stability unless at extremely acidic pH values.

The deprotonation process of DQ58 is in principle relatively complicated, as the aromatic form of the ligand may coexist with the chinoid one, and each forms is in tautomeric equilibrium with the other. As result, many species can form at any pH value. However, data available till now suggest that the HPCs tautomeric keto-enolic equilibrium in aqueous solution is shifted towards the aromatic form [Crisponi 2012 (b)], and the exclusive formation of aromatic deprotonation products can be assumed for simplicity. Under this hypothesis, the pK_{A1} and pK_{A2} values can be attributed to the deprotonation of the two carboxylic groups, which are intrinsically more acidic than pyridinium and phenol. Among the latter two acidic groups, pyridinium has an intrinsic pK_A of *ca.* 5 and phenol of *ca.* 9. Furthermore, when one (or both) carboxylic groups deprotonate, an intramolecular hydrogen bond is formed between one carboxylate and the phenolic hydrogen. The stabilization induced by this bond not only lowers the pK_{A1} and pK_{A2} values, but also it is expected to decrease the acidic properties of phenol. Therefore, pK_{A3} can be attributed to pyridinium, and pK_{A4} to phenol. The possible processing of deprotonation in DQ58 is shown in Figure 5.1.
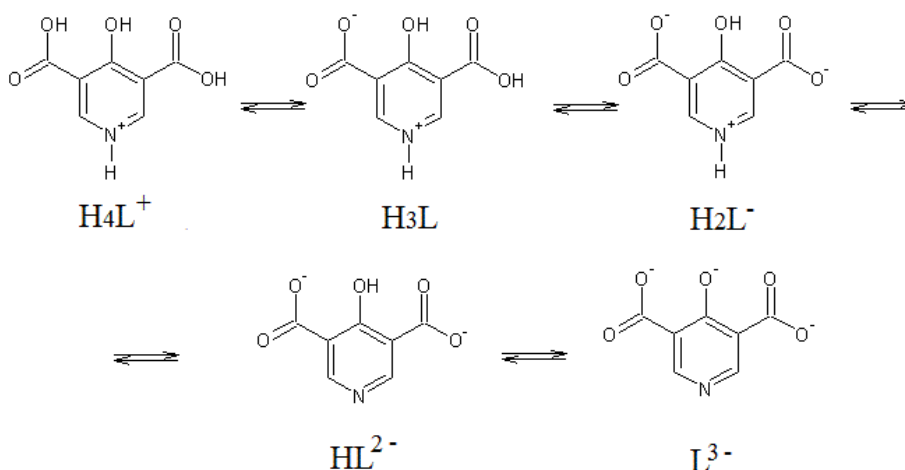
Figure 5.1: proposed deprotonation sequence of DQ58

5.3.2 DQ71508

pK_A values of DQ71508 are reported in Table 5.2.

The deprotonation sequence of this ligand is more sure than for DQ58, as no chinoid species can form. Similar considerations as for DQ58 can be done for the pK_A values of this ligand, except that no pyridinium deprotonation can be observed. The last proton is lost at pH~6.8 and belongs to the phenolic group. The significantly higher acidity of the phenolic group in DQ71508 with respect to DQ58 is due to the positive charge on nitrogen, which favours the deprotonation process. Similar phenolic pK_A values have been observed for all other 1-methylated HPC studied so far [Crisponi 2012 (b)]. The proposed deprotonation process is shown in Figure 5.2.
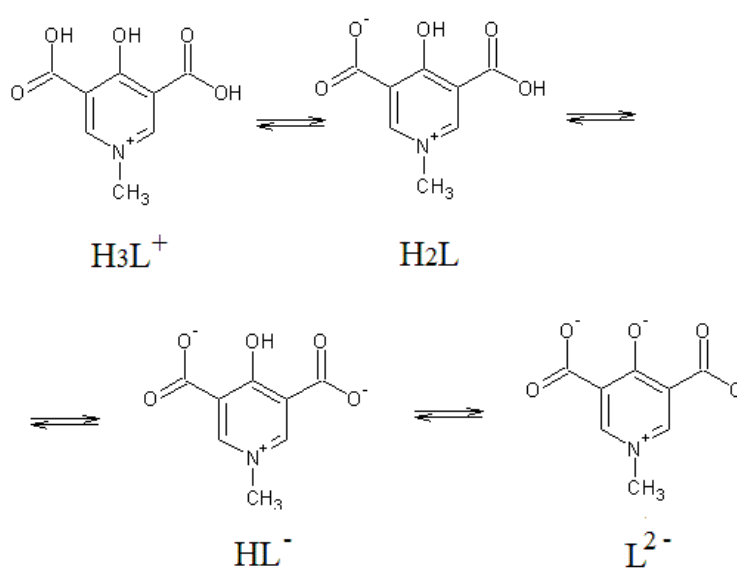
Figure 5.2: proposed deprotonation sequence of DQ71508

Finally, it is possible to state that the medium has a small but not negligible effect on the acidity of both ligands: when comparing the pK_A values detected in this work with those obtained in previous theses [Cassini 2012, Feltracco 2013], which have been measured in NaCl 0.6 mol/kg, it can be concluded that pK_A values decrease by ~0.3 log units upon increasing the ionic strength from 0.2 mol/L KCl to 0.6 mol/Kg NaCl.

5.3.3 POA

pK_A values of POA are reported in Table 5.2.

Like for DQ71508, also for this ligand no tautomeric equilibrium can occur, so that the deprotonation sequence of POA is rather certain and it is shown in Figure 5.3. The loss of the first proton is not detectable since it occurs at very low pH (< 1). The second proton to be lost belongs to the nitrogen and this deprotonation occurs at pH ~ 5. The last proton is lost at pH~9.8 and belongs to the phenolic group. pK_A values agree with those reported for other 3-hydroxy-4-pyridinecarboxylic acids studied so far [Crisponi 2012 (b)].
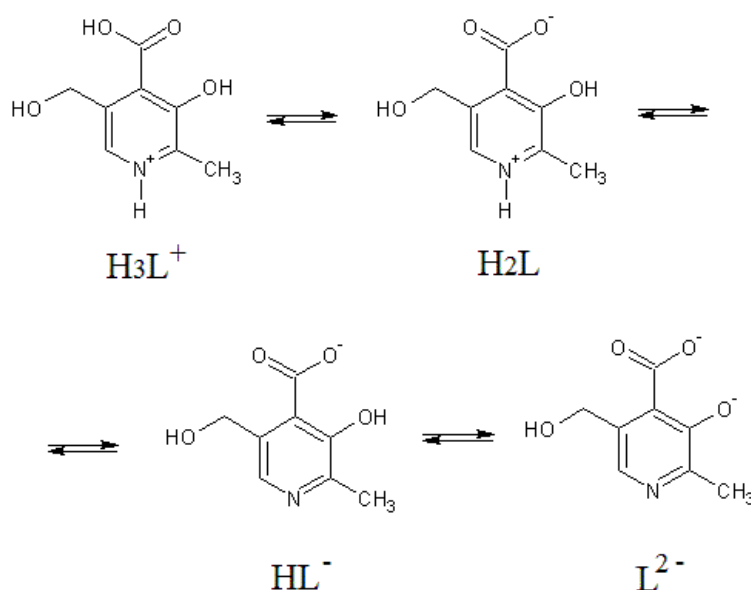

Figure 5.3: proposed deprotonation sequence of POA

Table 5.2: pK_A and logβ values (uncertainty*) of DQ58, DQ71508 and POA at 25 °C in aqueous KCl 0.2 mol/L

Stability constants	DQ58	DQ71508	POA
pK_{A1}	---	---	---
pK_{A2}	3.25 (2)	3.16 (6)	5.34 (3)
pK_{A3}	6.39 (1)	6.83 (2)	9.82 (2)
pK_{A4}	11.04 (1)	---	---
logβ_{HL}	11.04 (1)	6.83 (2)	9.82 (2)
logβ_{H2L}	17.43 (1)	9.99 (6)	15.16 (2)
logβ_{H3L}	20.68 (2)	---	---
logβ_{H4L}	---	---	---

* Three times the standard deviation

5.4 METAL-LIGAND COMPLEXES

5.4.1 DQ58-Zn(II) complexes

Solutions containing DQ58 and Zn(II) show the presence of only one complex, the neutral species having stoichiometry ZnLH (for the definition of "L" see caption of Figure 5.1). The stability constant of ZnLH, defined as seen in chapter 3 (equation 3.3), is reported in Table 5.3. The pH-potentiometric titration curves measured at 1:0.87 and 1:0.48 ligand-to-metal concentration ratios, and the species-distribution diagram for a typical DQ58-Zn(II) solution, are depicted in Figure 5.4.
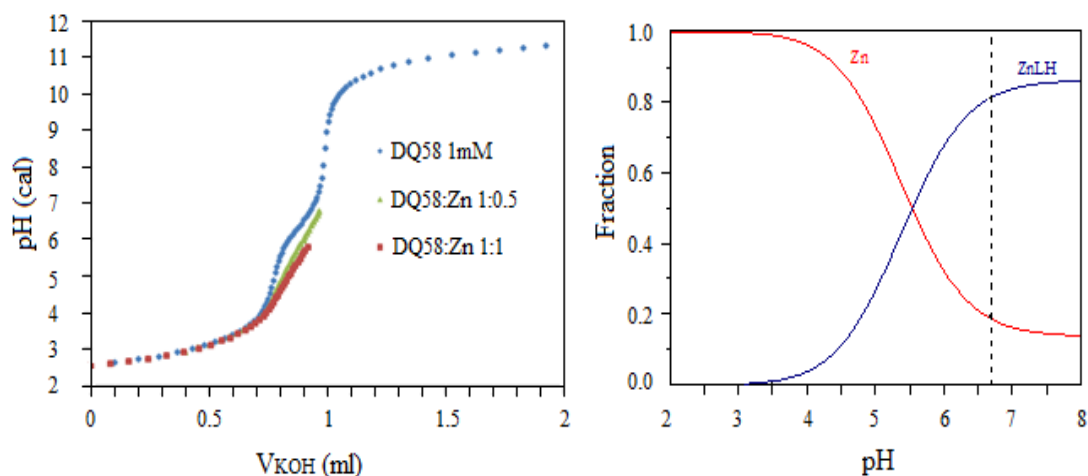

Figure 5.4: Left: pH-metric titration curves for DQ58-Zn(II) solutions ([DQ58]$_0$=1.00•10^{-3} M and [Zn^{2+}]$_0$=8.75•10^{-4} M or 4.86•10^{-4} M, respectively). Right: distribution diagram for a DQ58-Zn(II) solution ([DQ58]$_0$=1.00•10^{-3} M; [Zn^{2+}]$_0$=4.90•10^{-4} M; charges are omitted for simplicity).

Complex formation starts at pH ~ 4. In the presence of the metal ion, slight changes in the titration curves were observed. A sharp break on the titration curves occurs at pH~5.8-6.5 (depending on the ligand-to-metal ratio) as shown in the distribution diagram in the correspondence of the dashed vertical line. The solid which precipitates at this pH range is probably not the metal hydroxide ($Zn(OH)_2$ should precipitate at pH > 7). According to the potentiometric results, the solid might be ZnLH reaching its solubility limit, or it can be the bis-complex ZnL_2, which was not detected in solution and therefore should be assumed to have a very low solubility in water. The pH precipitation values listed in chapter 4 (paragraph 4.4.6) appear to be positively correlated with the metal concentration rather than with the ligand-to-metal ratio. Therefore, the precipitate is more likely ZnLH, and in this case its solubility is about $4 \cdot 10^{-4}$ M.

Table 5.3: stability constants of the DQ58-Zn(II) complexes as from potentiometric measurements at 25 °C in aqueous KCl 0.2 mol/L

Complex	logβ (uncertainty*)
ZnLH	15.09 (3)

* Three times the standard deviation

5.4.2 DQ71508-Zn(II) complexes

The elaboration of potentiometric titration data allowed the identification of two metal-ligand complexes, the protonated, charged $ZnLH^+$ and the neutral ZnL (for the definition of "L" see caption of Figure 5.2). The stability constants are reported in Table 5.4.

pH-potentiometric titration curves measured at 1:0.9, 2:1 and 4:1 ligand-to-metal concentration ratios and the species-distribution diagram for a typical DQ71508-Zn(II) solution are depicted in Figure 5.5.
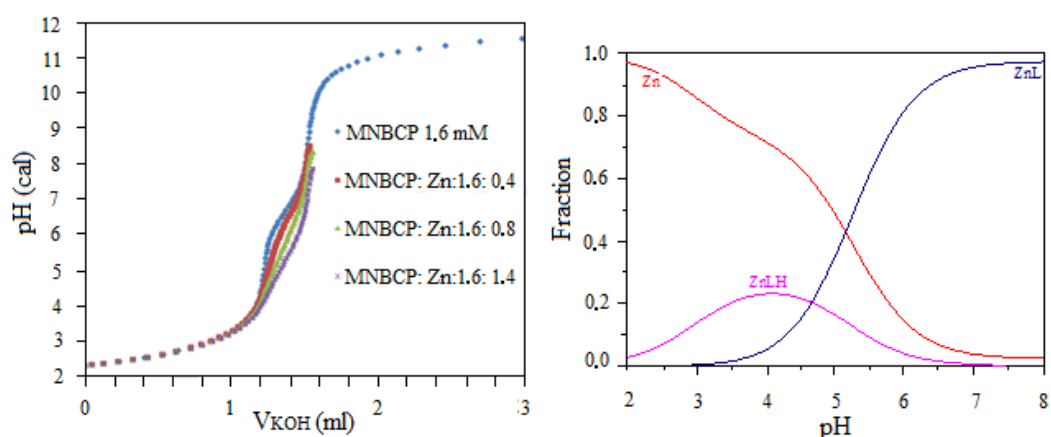
Figure 5.5: Left: pH-metric titration curve for DQ71508-Zn(II) solutions ([DQ71508]$_0$=1.50•10^{-3} M and [Zn^{2+}]$_0$=3.90•10^{-4} M, 7.70•10^{-4} M or 1.34•10^{-3} M, respectively). Right: distribution diagram for a DQ71508-Zn(II) solution ([DQ71508]$_0$=1.51•10^{-3} M; [Zn^{2+}]$_0$=3.87•10^{-4} M; charges are omitted for simplicity).

Complex formation starts at pH~3. In the presence of the metal ion, modest changes of the titration curves were observed. Two deprotonation steps are still observed on the titration curves, that means that there is free ligand in the solution, and indicating that the complexes are not very stable. The sharp break on the titration curve at ligand excess indicates that a precipitation process occurs at pH~8. The pH at which the precipitation occurs, the positive correlation of the precipitation pH and the ligand-to-metal ratio (see paragraph 4.4.7), and the appearance of the precipitate, all suggest that the solid is the metal hydroxide Zn(OH)$_2$.

Table 5.4: stability constants of DQ71508-Zn(II) complex as from potentiometric measurements at 25 °C in aqueous KCl 0.2 mol/L

Complex	logβ (uncertainty*)
ZnLH$^+$	9.25 (6)
ZnL	4.59 (6)

* Three times the standard deviation

The pK_A of ZnLH$^+$ can be computed from the difference between the logβ values of ZnLH$^+$ and ZnL, and it results to be 4.66. This should correspond to the deprotonation of the unbound carboxylate, which for the free ligand has a pK_A of 3.16. The larger value for the complex may be due to a more pronounced electron-donating effect of aquo-Zn^{2+} with respect to the proton, which destabilizes the deprotonated form; this electron-donation by Zn^{2+} is evident also from NMR spectra, see below.

5.4.3 DQ71508-Cu(II) complexes

The elaboration of potentiometric titration data allowed the identification of the same two metal-ligand complexes as observed for DQ71508-Zn(II), i.e. $CuLH^+$ and CuL. The stability constants of these complexes are reported in Table 5.5.

pH-potentiometric titration curves measured at 1:0.9, 2:1 and 4:1 ligand-to-metal concentration ratios, and a typical species distribution diagram for DQ71508-Cu(II), are depicted in Figure 5.6.
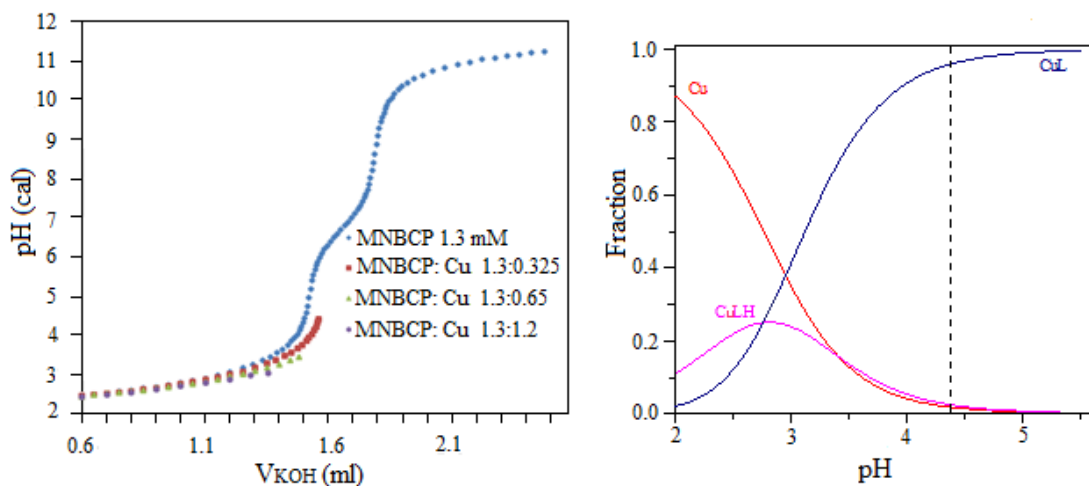

Figure 5.6: Left: pH-metric titration curves for DQ71508-Cu(II) solutions ($[DQ71508]_0=1.298 \cdot 10^{-3}$ M and $[Cu^{2+}]_0=3.60 \cdot 10^{-4}$ M, $7.20 \cdot 10^{-4}$ M or $1.29 \cdot 10^{-3}$ M). Right: distribution diagram for a DQ71508-Cu(II) solution ($[DQ71508]_0=1.30 \cdot 10^{-3}$ M; $[Cu^{2+}]_0=3.30 \cdot 10^{-4}$ M; charges are omitted for simplicity).

Complex formation starts at pH < 3 as it is clear both from the titration curves and the distribution diagrams. As just little differences are observed between the titration curves in the absence and in the presence of the metal ion, complexes that are forming are weak. The sharp break on the titration curve at ligand excess indicates occurs at a very low pH (3 < pH < 4), which is positively correlated with the metal concentration rather than with the ligand-to-metal ratio. The solid precipitating in this pH range is probably not the metal hydroxide ($Cu(OH)_2$ should precipitate at pH > 6), and could therefore be assigned to the neutral complex CuL.

Table 5.5: stability constants of the DQ71508-Cu(II) complex as from potentiometric measurements at 25 °C in aqueous KCl 0.2 mol/L

Complex	logβ (uncertainty*)
$CuLH^+$	10.02 (1)
CuL	7.26 (3)

* Three times the standard deviation

5.4.4 POA-Zn(II) complexes

The elaboration of potentiometric titration data did not allow the identification of any metal-ligand complexes. This was due to their extreme weakness, which is evident also from the pH-potentiometric titration curves measured at various ligand-to-metal concentration ratios depicted in Figure 5.7, which are very similar to the curves in the absence of metal ion. The sharp break on the titration curve at ligand excess indicates that a precipitation process occurs at pH~7.5. The pH at which the precipitation occurs and the appearance of the precipitate suggest that it is the metal hydroxide $Zn(OH)_2$.
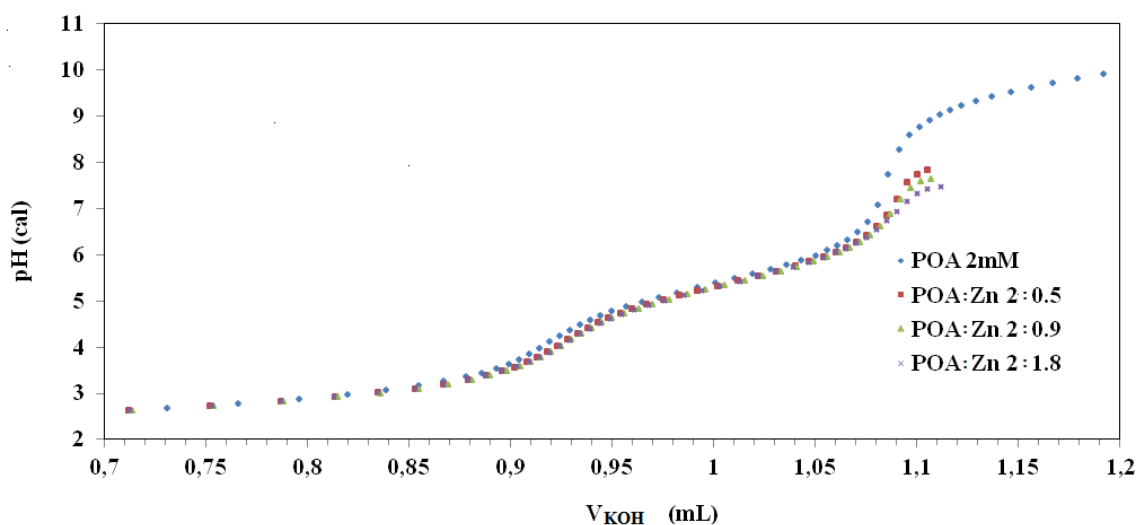
Figure 5.7: pH-metric titration curves for POA-Zn(II) solutions ([POA]$_0$=1.99•10^{-3} M and [Zn^{2+}]$_0$=4.98•10^{-4} M, 8.95•10^{-4} M or 1.79•10^{-3} M, respectively)

5.4.5 POA-Al(III) complexes

The elaboration of potentiometric titration data allowed the identification of a considerably large number of metal-ligand complexes with general metal-to-ligand stoichiometry 1:1, 1:2 and 1:3 and with different protonation states. The stoichiometry and the stability constants of these complexes are reported in Table 5.6. pH-potentiometric titration curves measured at various ligand-to-metal concentration ratios, and a typical species distribution diagram for Al(III)-POA solutions, are depicted in Figure 5.8 and Figure 5.9, respectively.
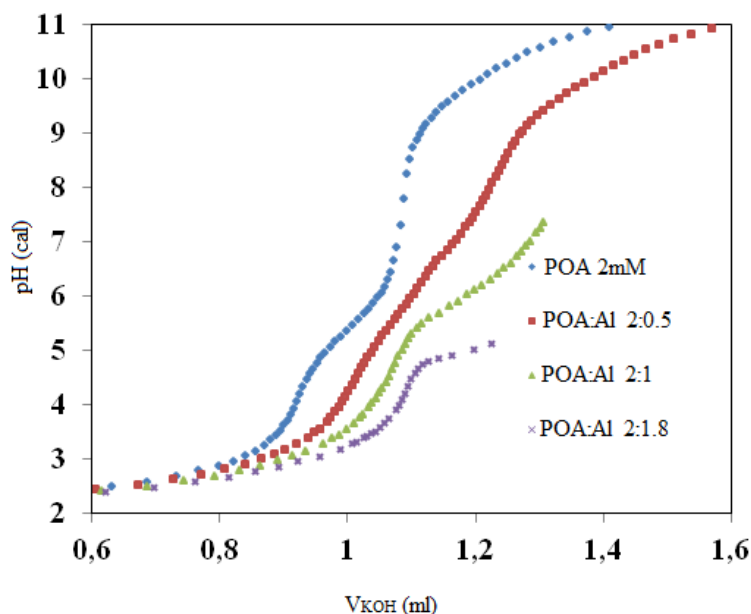
Figure 5.8: pH-metric titration curves for POA-Al(III) solutions ([POA]$_0$=1.858•10^{-3} M and [Al^{3+}]$_0$=5.05•10^{-4} M, 1.01•10^{-3} M or 1.81•10^{-3} M, respectively)

Complex formation starts at pH~2.5. The titration curves in the presence of the metal ion differ considerably from those of the free ligand, thus indicating that relatively strong complexes are formed. This is due to the hard character of the metal ion Al^{3+}, which has a large affinity towards the carboxylate and phenolate coordinating groups.
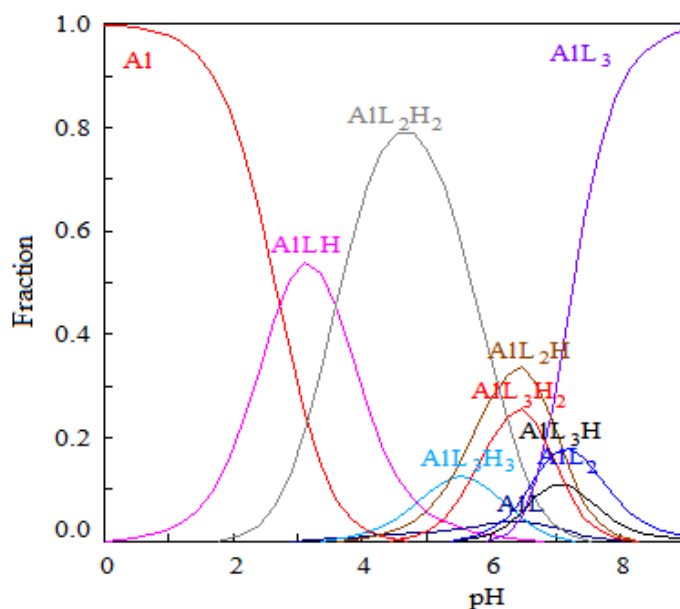

Figure 5.9: Distribution diagram for a POA-Al(III) solution ([POA]$_0$=2.50•10^{-3} M and [Cu^{2+}]$_0$=0.65•10^{-3} M; charges are omitted for simplicity).

The distribution diagram in Figure 5.9 shows that the free metal ion is present only at very acidic pH. By increasing the pH, the main complexes $AlLH^{2+}$, $AlL_2H_2^+$ and AlL_3^{3-} are forming. Many other minor species are formed in solution, especially at neutral pH, resulting from the deprotonation of the mono and bis-complexes and from the protonation of AlL_3^{3-}. While for the complex AlL_3H_3 the deprotonation must occur at the pyridinic nitrogen, in AlL_2H_2 it can occur more probably at the coordinating water. In fact, the pK_A relative to the loss of the pyridinic proton in free ligand is 6.20, and it is almost one order of magnitude higher than the pK_A of the hexa-aquoion hydrolysis, which is 5.52.

The precipitation of the aluminium hydroxide is not observed if solutions at sufficiently high ligand-to-metal ratios are titrated. At very basic pH values the POA-Al(III) complexes are destabilized due to the formation of the tetrahydroxoaluminate ion, $Al(OH)_4^-$. Such behavior at basic pH is always observed in Al(III) solutions containing any kind of ligand.

Table 5.6: stability constants of POA-Al(III) complexes as from potentiometric measurements at 25 °C in aqueous KCl 0.2 mol/L

Complex	logβ (uncertainty*)
$AlLH^{2+}$	9.56 (5)
AlL^+	15.10 (2)
$AlL_2H_2^+$	16.2 (4)
AlL_2H	23.3 (3)
AlL_2^-	29.46 (2)
AlL_3H_3	22.33 (6)
$AlL_3H_2^-$	28.91 (3)
AlL_3H^{2-}	36.05 (2)
AlL_3^{3-}	41.76 (3)

* Three times the standard deviation

6 SPECTROSCOPIC RESULTS AND DISCUSSION

6.1 UV-VIS MEASUREMENTS

Spectrophotometric measurements were performed both to confirm the potentiometric data, and to investigate the possible presence of additional complexes not determined by pH-potentiometric measurements. It was possible to obtain the ligand protonation constants, and the overall stability constants of the complexes detected in the solutions.

6.1.1 Solutions containing DQ58

The recorded spectra are shown in Figure 6.1 (from pH 2.164 to 3.656), Figure 6.2 (from pH 5.836 to 7.751), and Figure 6.3 (from pH 10.179 to 11.399). These pH ranges have been chosen according to potentiometric results, in order to show the presence of isosbestic points due to the presence of a pK_A. An isosbestic point indicates the coexistence of two species in equilibrium, which in these cases are H_3L-H_2L, H_2L-HL and HL-L, respectively (charges are omitted for simplicity). The absorption bands in the spectra are attributed to the $n \rightarrow \pi *$ electronic transitions of the carboxylic groups and to the $\pi \rightarrow \pi *$ transitions of the aromatic ring.
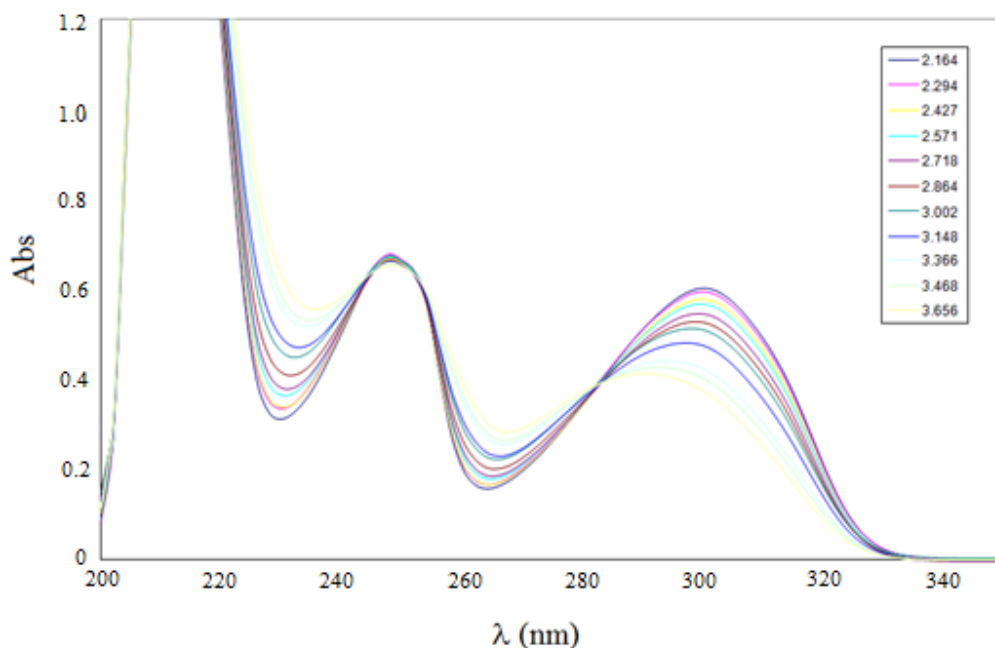

Figure 6.1: UV-Vis spectra of DQ58 ([DQ58]$_0$=0.08 mM) in KCl 0.2 M, registered from pH 2.164 to 3.656 with a 1 cm path length.
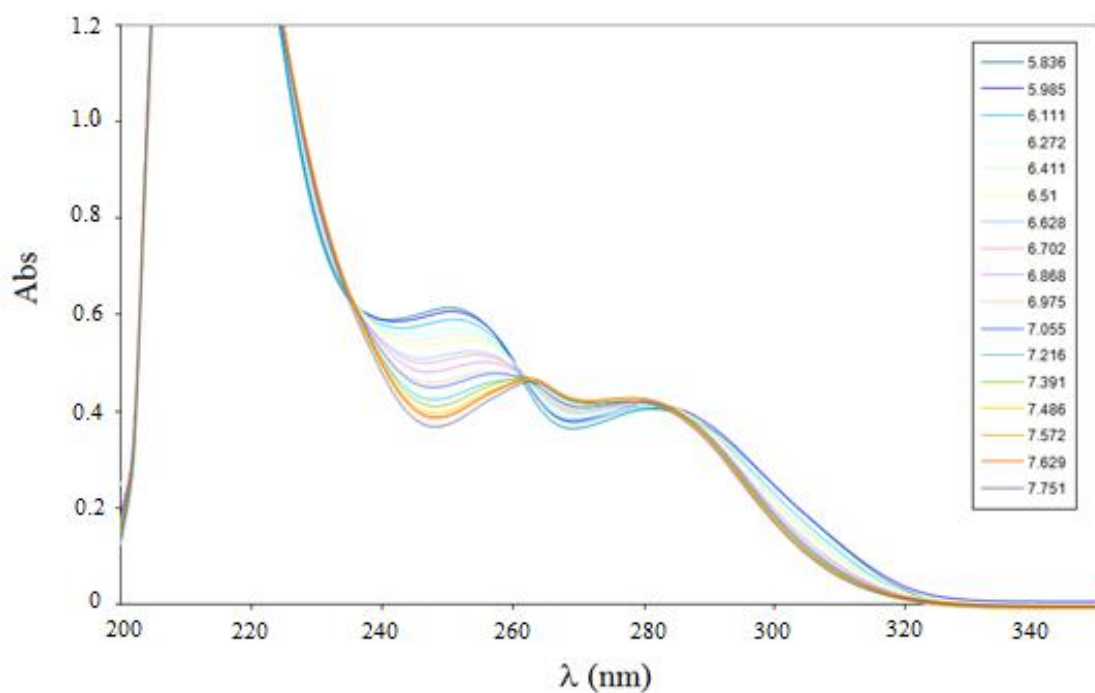
Figure 6.2: UV-Vis spectra of DQ58 ($[DQ58]_0$=0.08 mM) in KCl 0.2 M, registered from pH 5.836 to 7.751 with a 1 cm path length.
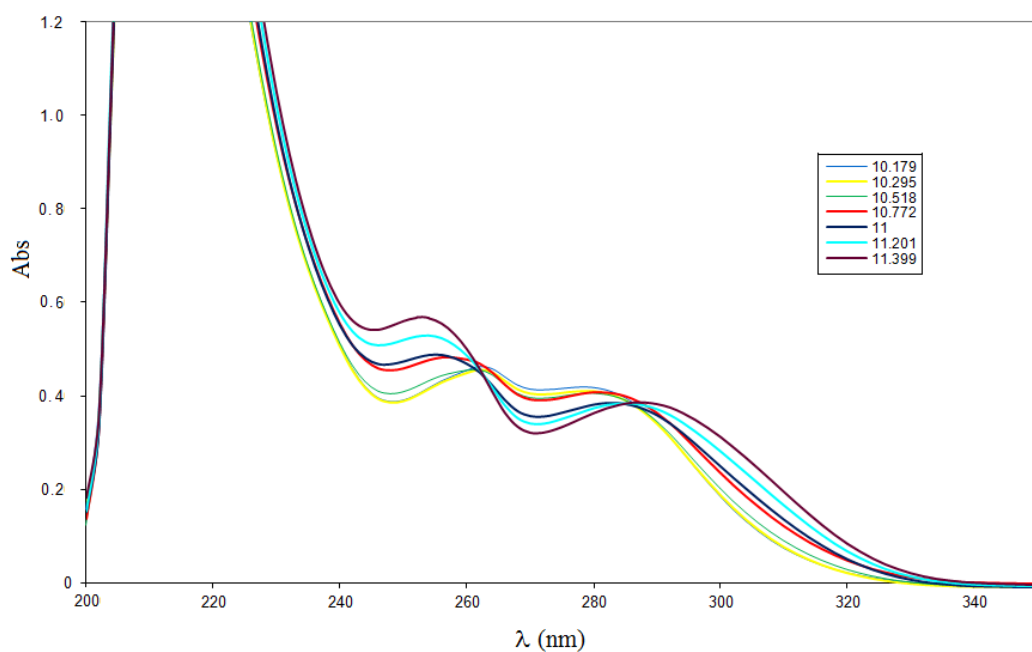

Figure 6.3: UV-Vis spectra of DQ58 ($[DQ58]_0$=0.08 mM) in KCl 0.2 M, registered from pH 10.179 to 11.399 with a 1 cm path length.

UV data have been processed at λ = 248, 264, and 304 nm, i.e. at the wavelengths where the absorption differences between the species present in solution are maxima. It was chosen not to evaluate the spectra at 224 nm and 210 nm, despite significant changes are observed by varying the pH, because at these wavelengths the absorbance values are too high and therefore not accurate. Ligand protonation constants obtained from the spectra elaborations are reported in Table 6.1; for comparison purposes, the potentiometric values are reported as well. It can be noticed that UV-Vis-derived $\log\beta$ values agree well with the corresponding potentiometric ones. Molar absorptivities of the ligand at wavelengths of interest were determined also, and are reported in Table 6.2.

Table 6.1: $\log\beta$ (uncertainty) of DQ58 obtained by both potentiometric and spectrophotometric techniques

	pH-pot	**UV-Vis**
H$_3$L	20.68 (2)	20.85 (2)
H$_2$L	17.43 (1)	17.62 (3)
HL	11.04 (1)	11.01 (2)

Table 6.2: molar absorptivities ε (uncertainty) of DQ58 at specific wavelengths

Wavelength (nm)	ε_{H3L} (mol$^{-1}\cdot$L$\cdot$cm^{-1})	ε_{H2L} (mol$^{-1}\cdot$L$\cdot$cm^{-1})	ε_{HL} (mol$^{-1}\cdot$L$\cdot$cm^{-1})	ε_{L} (mol$^{-1}\cdot$L$\cdot$cm^{-1})
248	6740 ± 43	6558 ± 39	3622 ± 35	7125 ± 38
264	1423 ± 22	3922 ± 30	4699 ± 49	3456 ± 41
304	5956 ± 47	2148 ± 37	1059 ± 21	4055 ± 45

6.1.2 Solutions containing DQ58+Cu(II)

The complexation equilibria between DQ58 and Cu(II) has been studied by pH-potentiometric measurements in the frame of a different thesis work [Suba 2013]. Since precipitation occurred at pH < 3, it has been possible to detect with a good accuracy only the monocomplex CuLH$^+$ ($\log\beta$ = 17.6 (3)). Therefore, spectrophotometric measurements on this system have been carried out, in order to clarify the metal coordination also at higher pH values. This was possible because at the lower concentrations explored by UV-Vis no precipitation was observed.

Figure 6.4 shows the spectra recorded for DQ58:Cu(II) solutions at a ligand-to-metal concentration ratio of 1:1. These spectra are different from those of the free ligand, as new absorption bands are visible: this is an indication of the complexes formation.

Furthermore, the main peak at 248 nm is due to pyridinic ring $\pi \rightarrow \pi^*$ transitions, and by increasing the pH from pH=2.17 to pH=6.10 the deprotonation causes a bathochromic shift till around 252 nm.
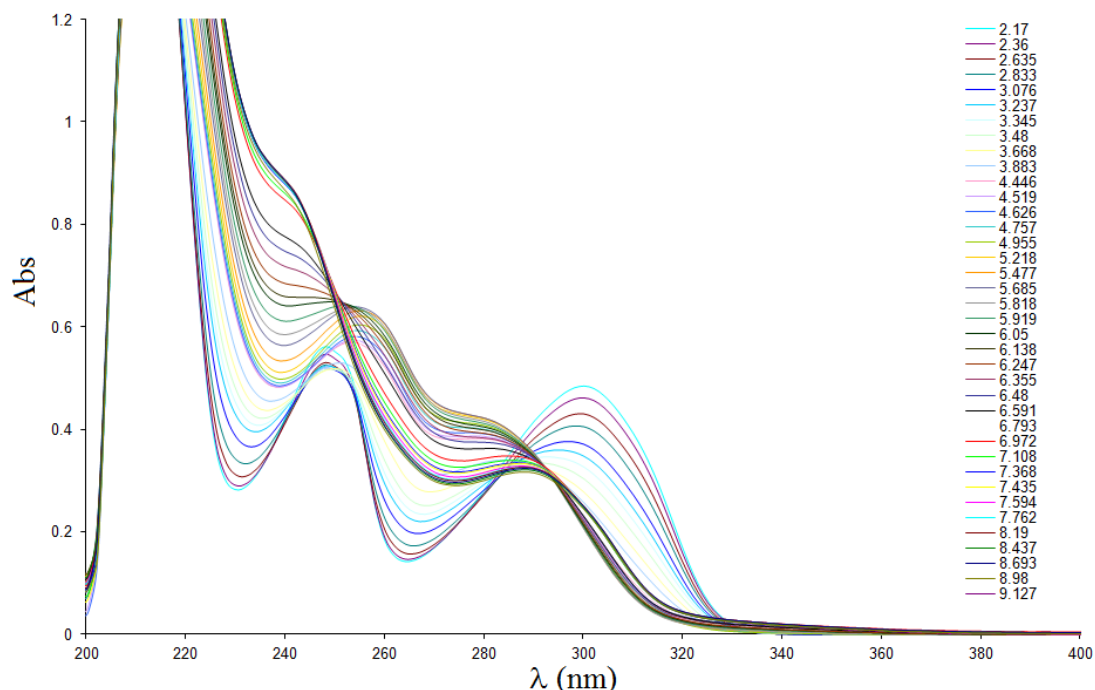

Figure 6.4: UV-Vis spectra of DQ58-Cu(II) solutions ([DQ58]$_0$=0.08 mM; [Cu^{2+}]$_0$=0.066 mM) in KCl 0.2 M, registered from pH 2.170 to 11.307 with a 1 cm path length.

Together with the spectra at the same ligand and metal concentrations, and different pH values, other spectra were recorder where the pH was kept constant and the metal was added to a ligand solution. Figure 6.5 shows the absorption spectra of the these solutions, whereas Figure 6.6 reports the graph Abs/[DQ58]$_0$ vs. [Cu]$_0$/[DQ58]$_0$. According to the latter graph, the bis-complex might be present in solution, because a slight slope change in the curve can be observed at [Cu]$_0$/[DQ58]$_0$ = 0.5. For more sure conclusions, and in order to obtain the stability constants of the complexes, the UV-Vis data have to be elaborated by PSEQUAD or by HYPERQUAD. These elaborations, anyway, are still in progress.
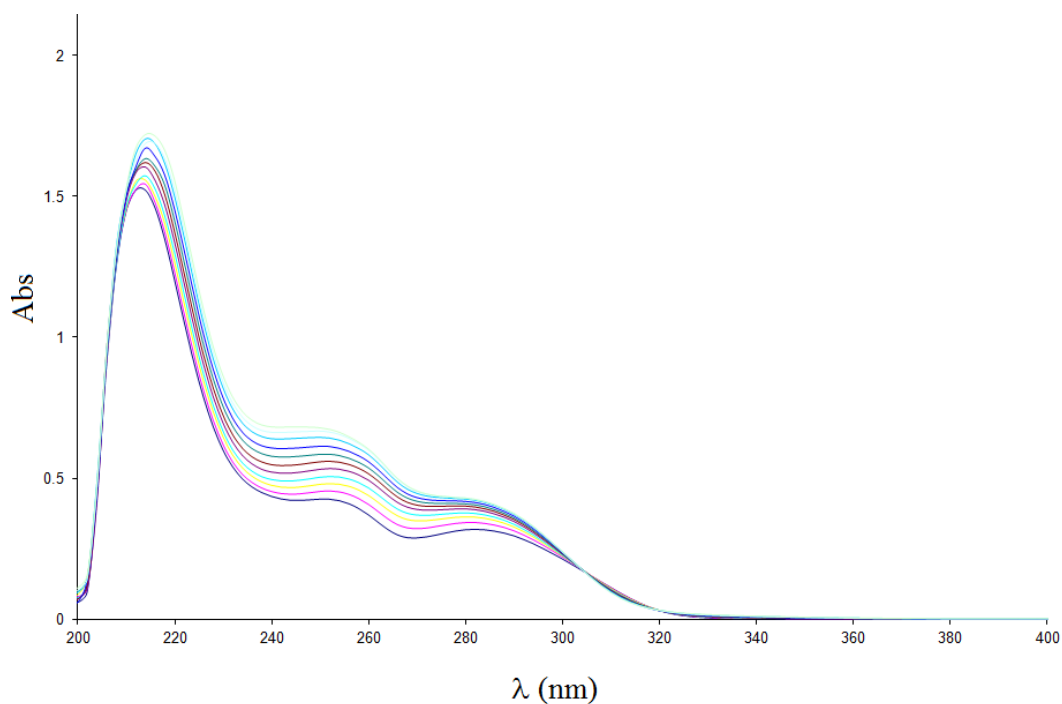
Figure 6.5: absorption spectra of DQ58-Cu(II) solutions obtained by increasing the Cu^{2+} concentration. See Table 4.6 for experimental details.
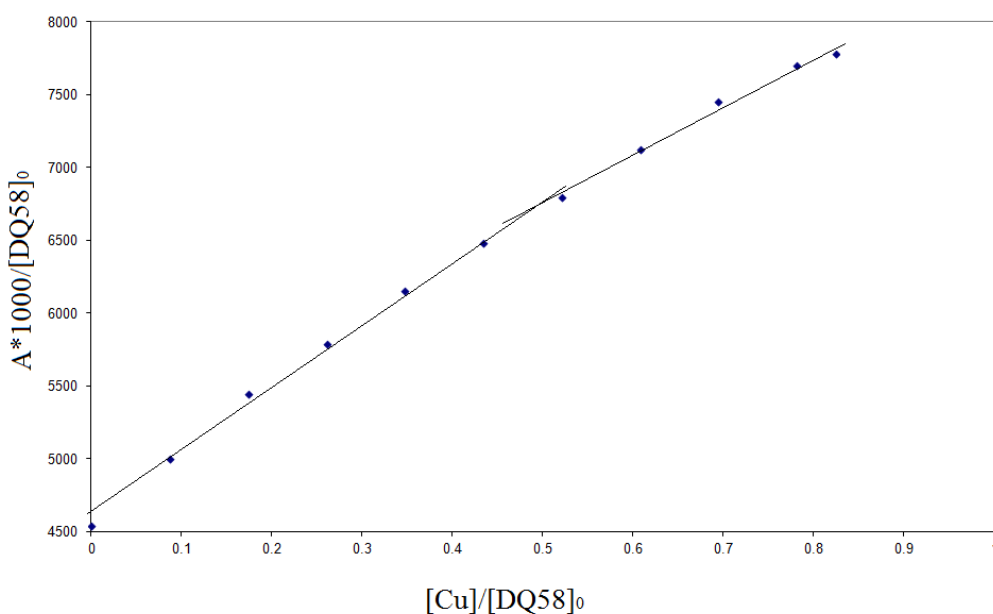

Figure 6.6: : A·1000/[DQ58]$_0$ vs. [Cu]$_0$/[DQ58]$_0$ calculated for each solution examined (dilutions have been taken into account)

6.1.3 Solutions containing DQ71508

The UV-Vis spectra of DQ71508 solutions are shown in Figure 6.7 (from pH 2.765 to 5.013), and Figure 6.8 (from pH 5.013 to 8.789). These pH range have been chosen (as for DQ58) according to potentiometric results in order to show the

presence of isosbestic points and therefore confirm the equilibrium between two differently protonated forms of the ligand at pH around each pK_A values.
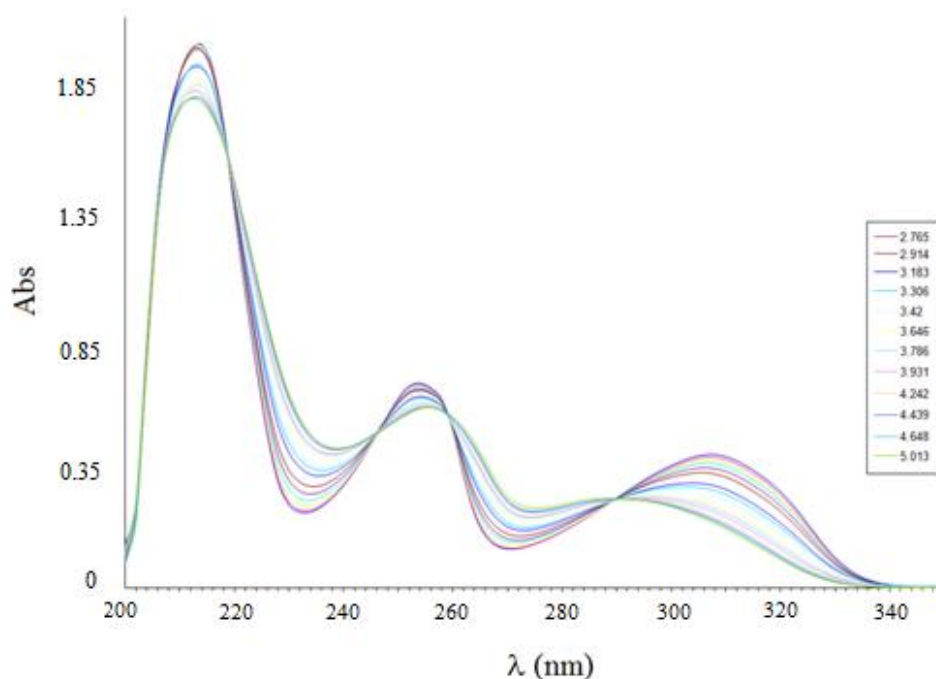

Figure 6.7: UV-Vis spectra of DQ71508 ([DQ71508]$_0$=0.08 mM) in KCl 0.2 M, registered from pH 2.765 to 5.013 with a 1 cm path length.
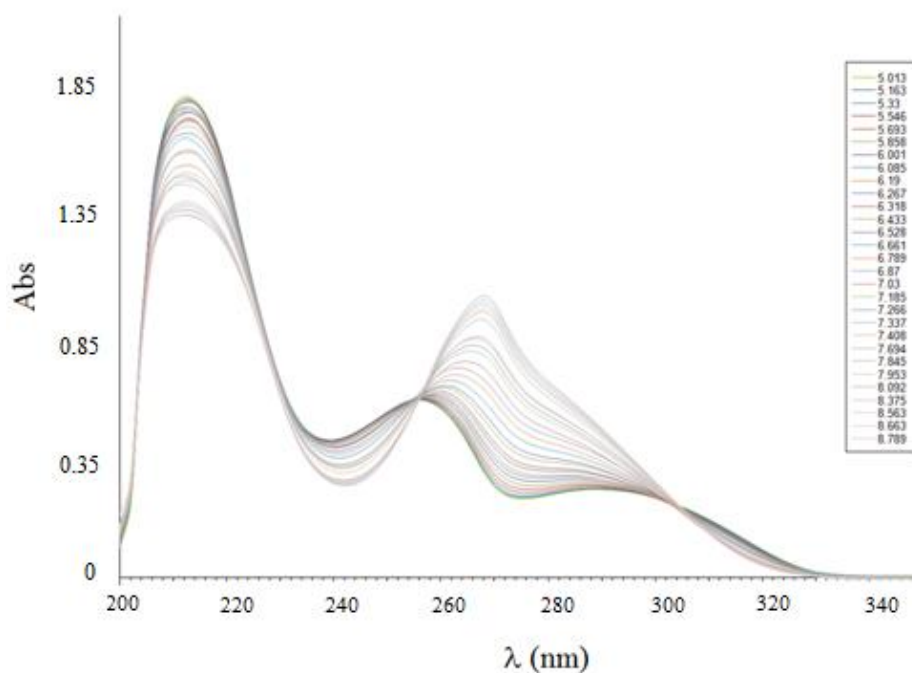

Figure 6.8: UV-Vis spectra of DQ71508 ([DQ71508]$_0$=0.08 mM) in KCl 0.2 M, registered from pH 5.013 to 8.789 with a 1 cm path length.

UV data have been processed at λ = 250, 268, and 316 nm, i.e. at the wavelengths that maximize the absorption differences between the species present in solution. Ligand protonation constants obtained from spectra evaluation are reported in Table 6.3 together with the corresponding potentiometric data. It can be observed that the correspondence between values obtained by the two techniques is excellent, and it is within the experimental uncertainty. Molar absorptivities of the ligand at wavelengths of interest were determined also, and are reported in Table 6.4.

Table 6.3: logβ (uncertainty) of DQ71508 obtained by both potentiometric and spectrophotometric techniques

	pH-pot	Uv-Vis
H$_2$L	9.99 (6)	9.95 (1)
HL	6.83 (2)	6.79 (1)

Table 6.4: molar absorptivities ε (uncertainty) of DQ71508 at specific wavelengths

Wavelength (nm)	ε_{H2L} (mol^{-1}·L·cm^{-1})	ε_{HL} (mol^{-1}·L·cm^{-1})	ε_L (mol^{-1}·L·cm^{-1})
250	6988 ± 43	6216 ± 41	4552 ± 38
268	1329 ± 23	3915 ± 33	10617 ± 49
316	4411 ± 28	1436 ± 17	813 ± 15

6.1.4   Solutions containing DQ71508+Cu(II)

Figure 6.9 shows the spectra recorded for DQ71508:Cu(II) solutions at a ligand-to-metal ratio of 1:1 and at various pH value. The peak which experience the maximum variation with pH is the one which at pH 2.2 resonates at 254 nm. It is due to pyridinic ring $\pi \rightarrow \pi^*$ transitions, and by increasing the pH the deprotonation causes a bathochromic shift till around 268 nm.
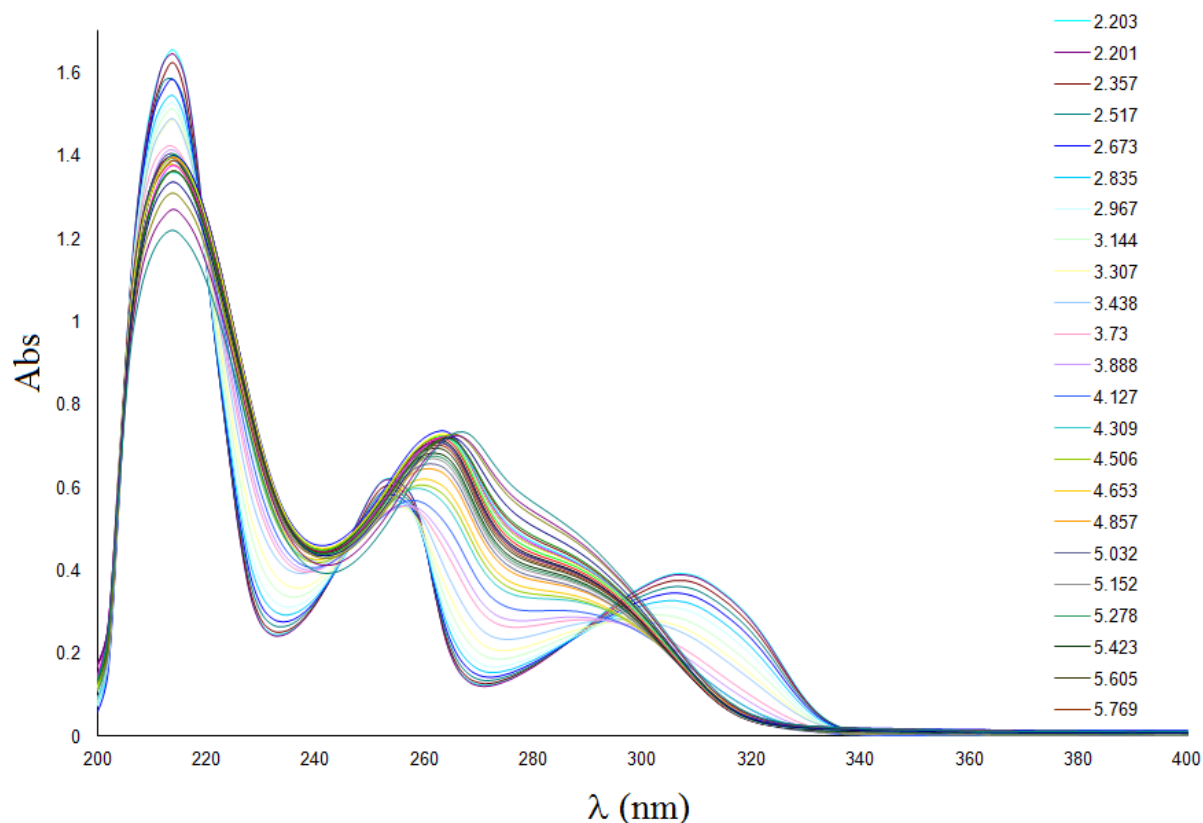
Figure 6.9: UV-Vis spectra of DQ71508-Cu(II) solutions ([DQ71508]$_0$=0.08 mM; [Cu^{2+}]$_0$=0.07 mM) in KCl 0.2 M, registered from pH 2.203 to 9.318 with a 1 cm path length.

As for DQ58-Cu(II), also for DQ71508-Cu(II) solutions other spectra were recorder where the pH was kept constant and the metal was added to a ligand solution. Figure 6.10 shows the absorption spectra of the these solutions (pH is kept constant at the value 6.10 ± 0.09), and Figure 6.11 reports the graph Abs/[DQ71508]$_0$ vs. [Cu]$_0$/[DQ71508]$_0$. It appears that the DQ71508-Cu(II) bis-complex might form, because a slight slope change in the curve can be observed at [Cu]$_0$/[DQ71508]$_0$ = 0.5. Here too, however, no definite conclusions can be drawn, and no stability constants of the complexes could be obtained up to now, because the UV-Vis data have not been elaborated yet.

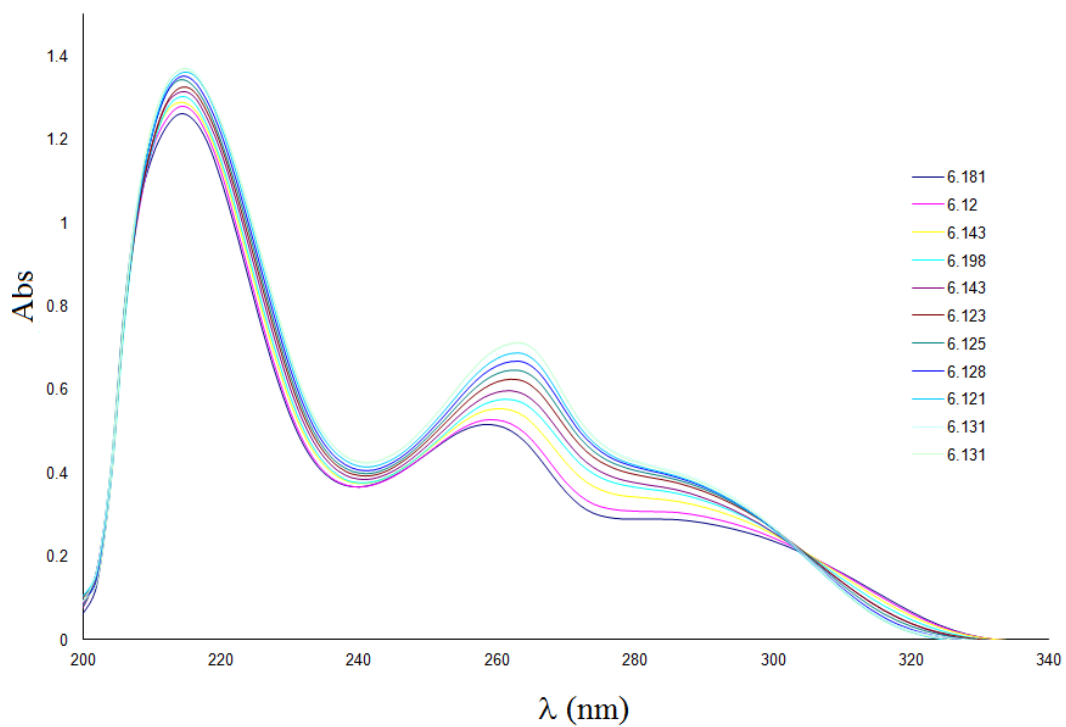**Figure 6.10: absorption spectra of DQ71508-Cu(II) solutions obtained by increasing the Cu^{2+} concentration.**
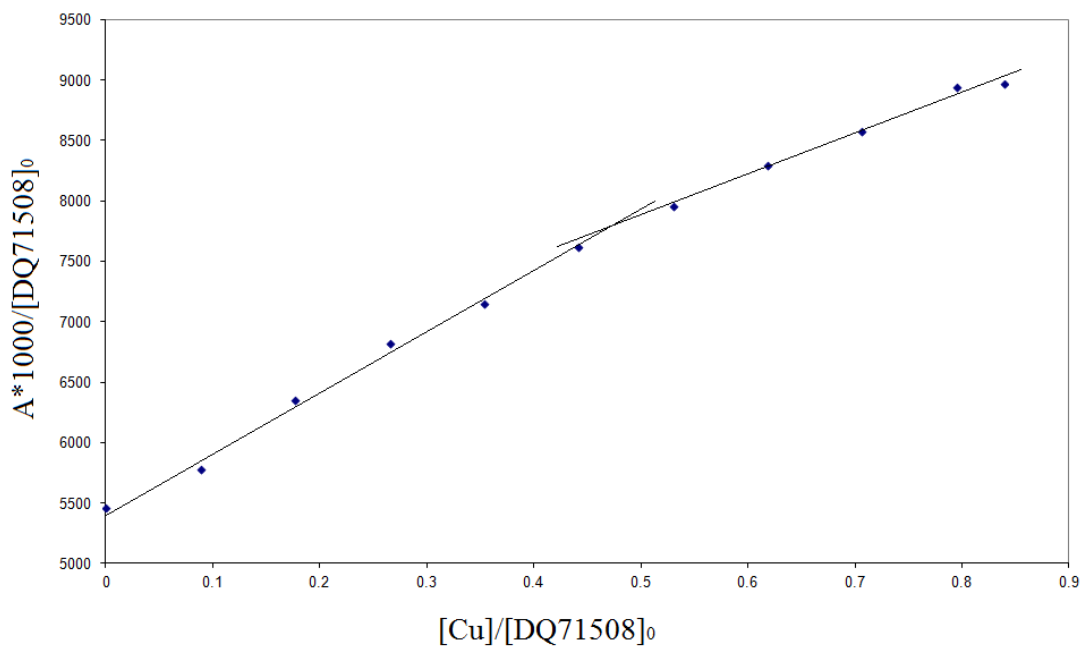

Figure 6.11: A·1000/[DQ71508]$_0$ vs. [Cu]/[DQ71508]$_0$ calculated for each solution examined (dilutions have been taken into account)

6.2 NMR MEASUREMENTS

6.2.1 Solutions containing DQ58 and DQ58+Zn(II)

Figure 6.12 shows the ^{1}H-NMR spectra of DQ58 solutions at three different pH values. These spectra show a single peak representative of the two equivalent protons in position 2 and 6 of the pyridine ring: only one peak is observed as the ligand is symmetric (see Figure 2.4). As expected, no signals belonging to the carboxylic, phenolic and pyridinic protons are observed, as they exchange very quickly with the protons of the water. By increasing the pH, there is a shift of the aromatic signal at higher fields, due to the gradual de-protonation of the acidic groups of DQ58 (according to the pK_A values reported in Table 5.2). In the spectrum recorded at more basic pH (spectrum *c*) there is a slight enlargement of the peak. This broadening may indicate the coexistence of more ligand forms at equilibrium. For DQ58, the most probable forms at equilibrium are the aromatic and the chinoid tautomeric forms. Therefore, the NMR indicate that for DQ58 the chinoid form can be more important, at least at pH larger than 6, than for the other HPCs investigated so far. NMR measurements at different frequency and/or temperature might permit to obtain more information about the kinetics and perhaps also the thermodynamics of the keto-enolic equilibrium for DQ58.

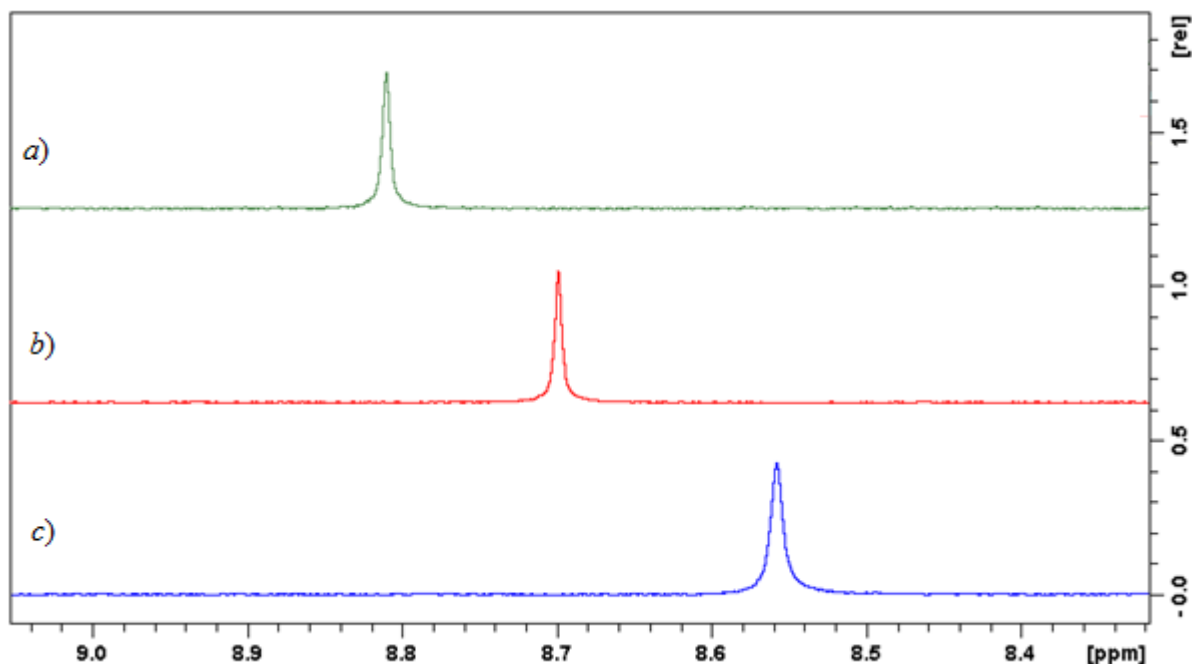
Figure 6.12: ^{1}H–NMR spectra for DQ58 ($1.478 \cdot 10^{-3}$ m) at different pH values: *a*) pH = 2.54; *b*) pH = 3.88; *c*) pH = 6.36 in D_2O. Only the region of interest (the aromatic one between 8.3 and 9.2 ppm) is shown in the spectra.

^{1}H–NMR spectra of Zn(II)+DQ58 solutions at different pH values are reported in Figure 6.13. In both spectra, the main signal can be attributed to both the free ligand and the monocomplex $ZnLH^+$, since they are expected to exchange very quickly and therefore they should give rise to only one signal, the position of which is a weighted mean value between the chemical shift of the free ligand and that of the complex; the mean is weighted on the concentration.

Additional minor peaks are detected in the spectra, especially at more basic pH, indicating the formation of additional inert species in solution. This finding does not agree with the potentiometric results, which indicate the formation of only one complex. Therefore, the latter data should be reconsidered, and/or NMR spectra should be repeated.
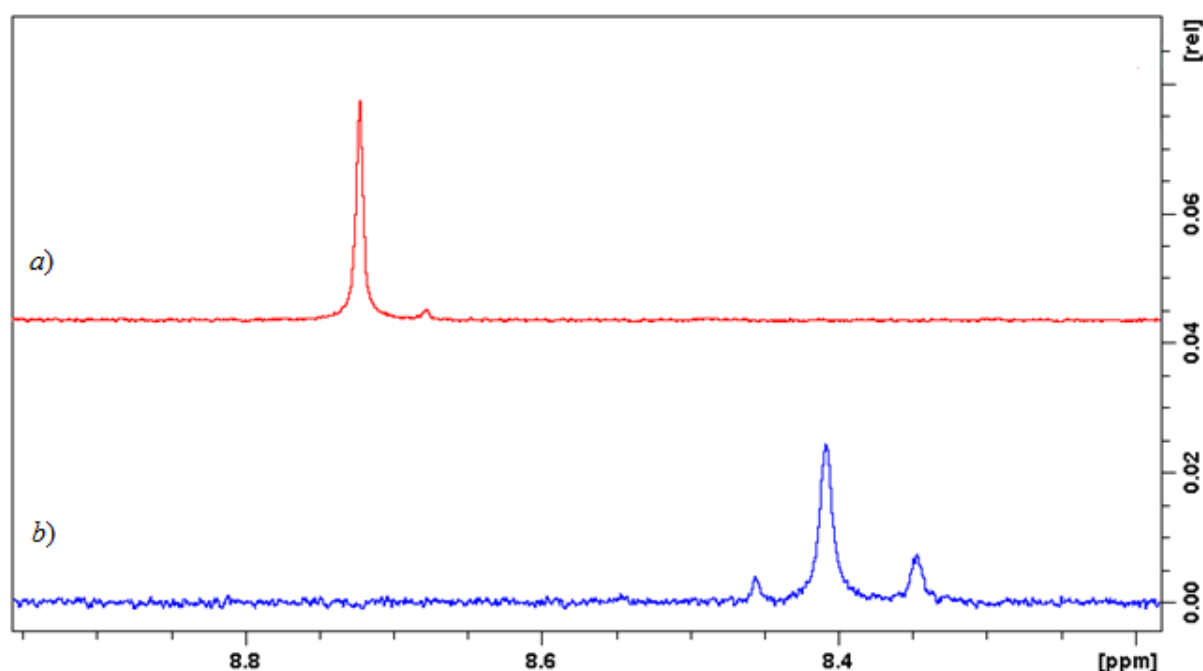

Figure 6.13: ^{1}H–NMR spectra for DQ58-Zn(II) ([DQ58]$_0$=1.478·10^{-3} m; [Zn^{2+}]$_0$=2.866·10^{-3} m) at different pH values: _a_) pH = 3.90; _b_) pH = 6.34 in D$_2$O. Only the region of interest (the aromatic one between 8.2 and 9 ppm) is shown in the spectra.

6.2.2 Solutions containing DQ71508 and DQ71508+Zn(II)

Figure 6.14 shows the ^{1}H-NMR spectra of DQ71508 solutions at three different pH values. In the aromatic area a single peak can be observed, which is attributed to the two equivalent protons in position 2 and 6 of the pyridine ring, as seen for DQ58. In the aliphatic region (not shown), another singlet appears (e.g. at 4.03 ppm for the solution at pH = 3.23), which is attributed to the 1-methyl protons.

By increasing the pH, a shift of both the aromatic and aliphatic protons towards lower ppm values is observed. This is caused by the increasing shielding due to the

progressive deprotonation of the acidic groups of DQ71508. This shift is much less pronounced for the signal of the methyl since it is less affected by acid-base equilibrium than are the aromatic protons.
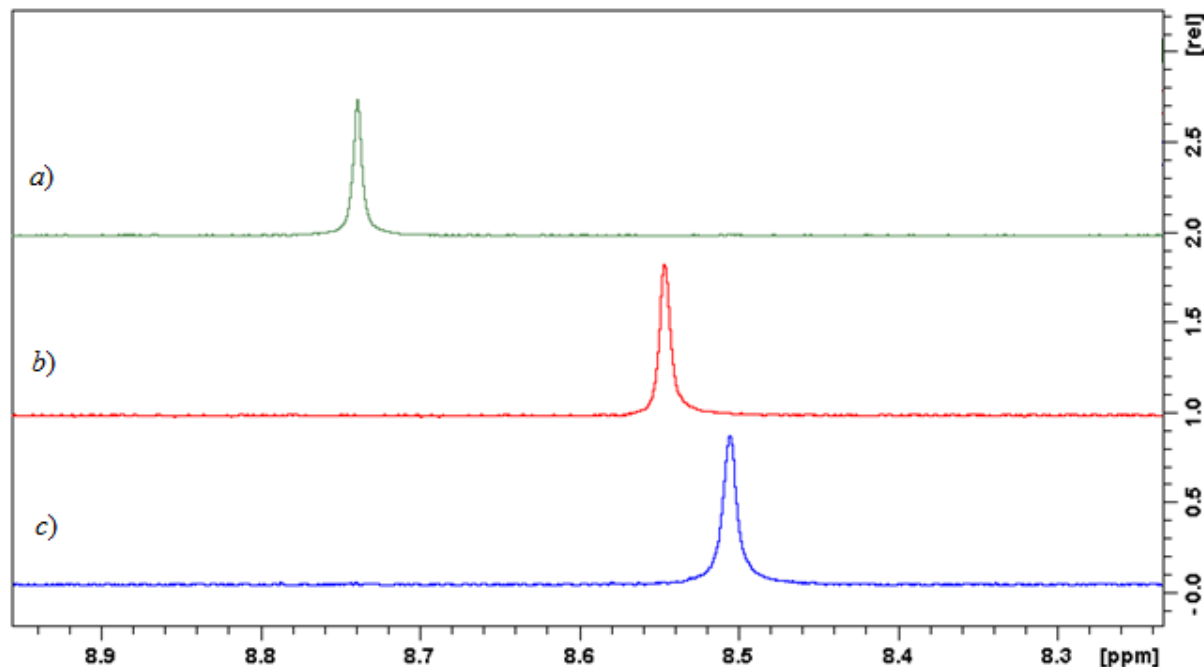

Figure 6.14: ^{1}H–NMR spectra for DQ71508 ($1.357 \cdot 10^{-3}$ m) at different pH values: *a*) pH = 3.23; *b*) pH = 5.24; *c*) pH = 6.36 in D$_2$O. Only the region of interest (the aromatic one between 8.2 and 8.9 ppm) is shown in the spectra.

^{1}H–NMR spectra of Zn(II)+DQ71508 solutions at different pH values are reported in Figure 6.15. As for DQ58, the main signal is an average weighted mean of the signals of the free ligand and of the complexes. In the spectrum registered at more acidic pH, the signal has the same chemical shift (8.74 ppm) as the free ligand at the same pH: this fact indicate the absence of complex formation, and agrees with the potentiometric results. In the spectrum at pH=6.43 the average signal is shifted up-field with respect to that of the free ligand at the same pH, indicating that Zn^{2+} has a more electrondonating effect than the proton. This evidence is coherent with the finding that the carboxylate pK_A of the free ligand is lower than that of the complex, and was observed also for DQ58-Zn^{2+} complexes. Differently than for DQ58, however, for DQ71508 no additional signals are observed in the spectra, i.e. the speciation obtained by NMR and by potentiometric titrations appear to be coherent in this case.
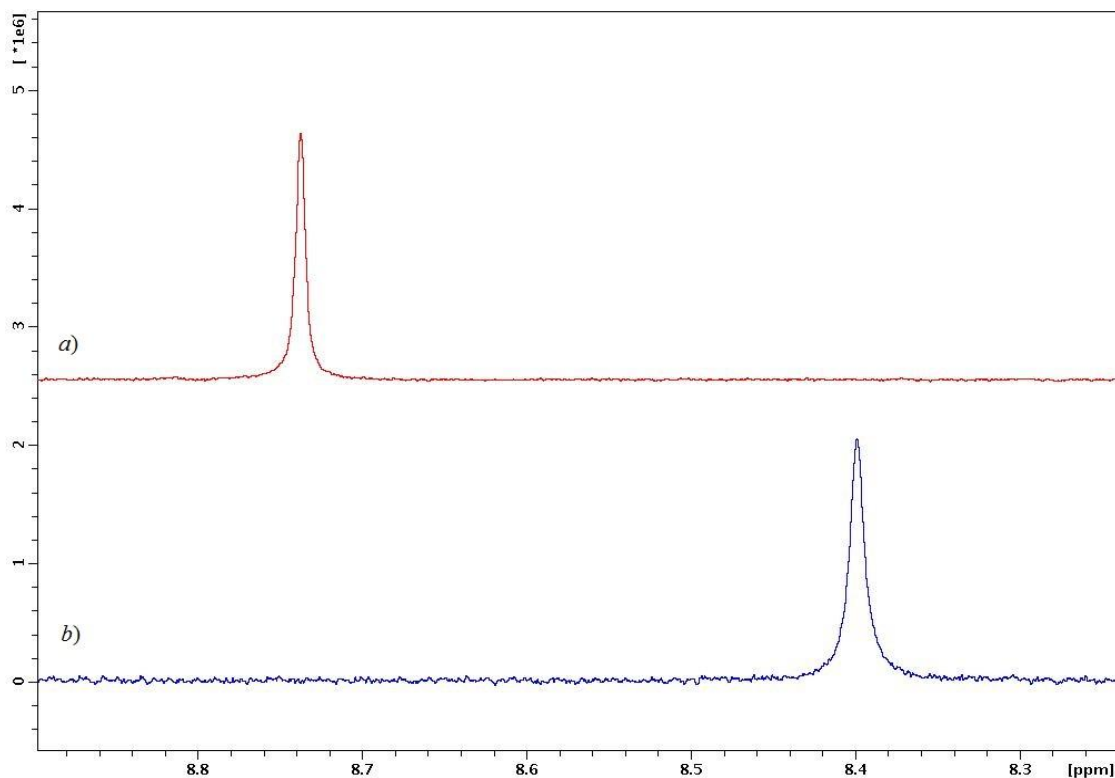
Figure 6.15: ^{1}H–NMR spectra for DQ71508-Zn(II) ([DQ71508]$_0$=1.357·10^{-3} m; [Zn^{2+}]$_0$=2.616·10^{-3} m) at different pH values: *a*) pH = 3.17; *b*) pH = 6.43 in D$_2$O. Only the region of interest (the aromatic one between 8.2 and 8.9 ppm) is shown in the spectra.

6.2.3   Solutions containing POA and POA+Al(III)

Figure 6.16 shows the ^{1}H-NMR spectra of POA solutions at three different pH values. The aromatic region of these spectra shows a single peak representative of the proton in position 6 in the pyridine ring (see Figure 2.4). Peaks are very narrow (the apparent broadness of the peaks in Figure 6.16 is due to the enlarged ppm scale). The aliphatic region (not shown) displays the singlets of the methyl group in position 2 (e.g. at 2.69 ppm for the solution at pH = 2.76) and of the methylenic group in position 5 (e.g. at 5.02 ppm for the solution at pH = 2.76).

By increasing the pH, there is a shift of all signals towards higher fields, due to the gradual de-protonation of the two acidic groups of POA. The chemical shift difference between spectra *a*) and *b*) is very low since there is no deprotonation in this pH range (2.76-4.22). The chemical shift difference for aliphatic protons is very small at all the investigated pH values, as these protons are only marginally affected by deprotonation of carboxylate, pyridinium and phenol.
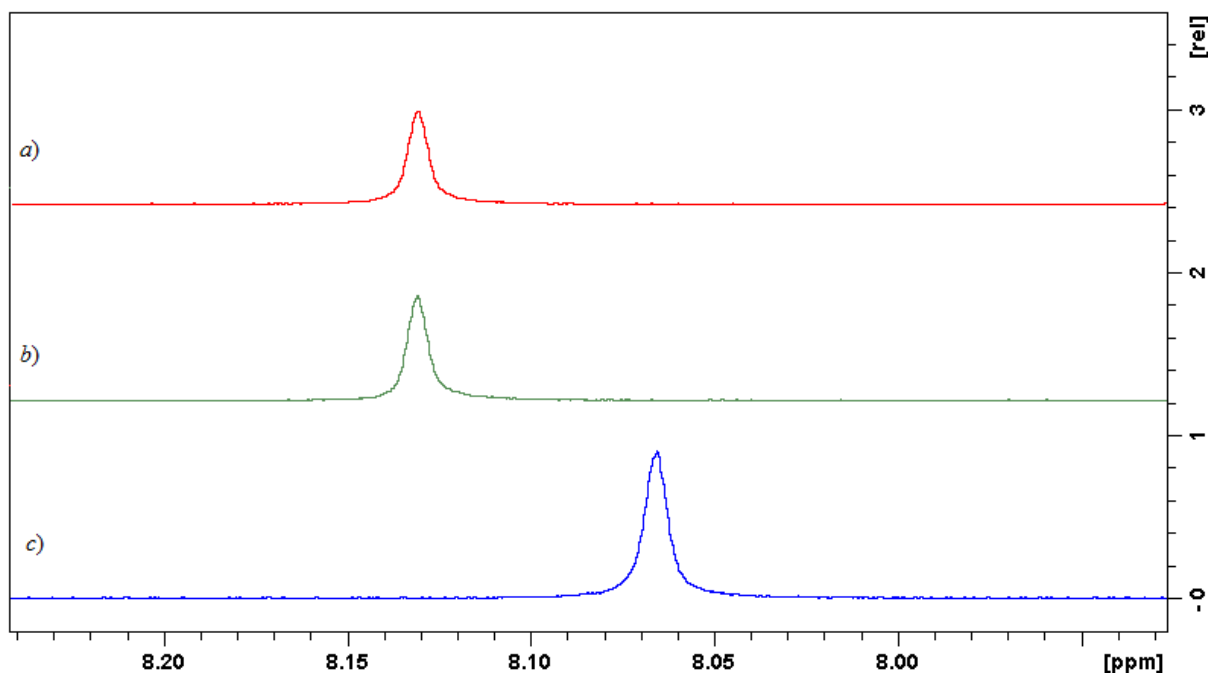
Figure 6.16: ^{1}**H–NMR spectra for POA (2.525·10^{-3} m) at different pH values:** *a*) **pH = 2.76;** *b*) **pH = 4.22;** *c*) **pH = 5.16 in D$_2$O. Only the region of interest (the aromatic one between 7.9 and 8.2 ppm) is shown in the spectra.**

^{1}H–NMR spectra of Al(III)+POA solutions at different pH values are reported in Figure 6.17. In each spectra, the most intense signal is attributed to the free ligand, because the chemical shift corresponds to that observed in the spectra of the free ligand (Figure 6.16). At the most acidic pH, a small additional peak can be detected together with that of the free ligand. At this pH, the main species expected in solution beside the free ligand is the complex AlLH^{2+}, as indicated by the distribution diagram of Figure 5.9. This new signal should therefore be attributed to this species. As seen for Zn(II), here too the complex signal is shifted up-field with respect to the free ligand peak, indicating a more pronounced electron-donating effect (or a minor electron-attracting effect) of aquo-Al^{3+} with respect to the proton. In the spectrum *b*) a new broad peak appears close to that of AlLH^{2+}: this indicates that at least one new complex is forming. From the distribution diagram of Figure 5.9, the new signal can be supposed to be AlL$_2$H$_2^+$. In the spectrum *c*), collected at more basic pH, the disappearance of the AlLH^{2+} signal can be observed. This data is coherent with the potentiometric results, which indicate that AlLH^{2+} should be negligible at pH larger than *ca*. 5. In the place of this signal, two other signals can be observed, which cannot be attributed easily as many species coexist in solution at these conditions.
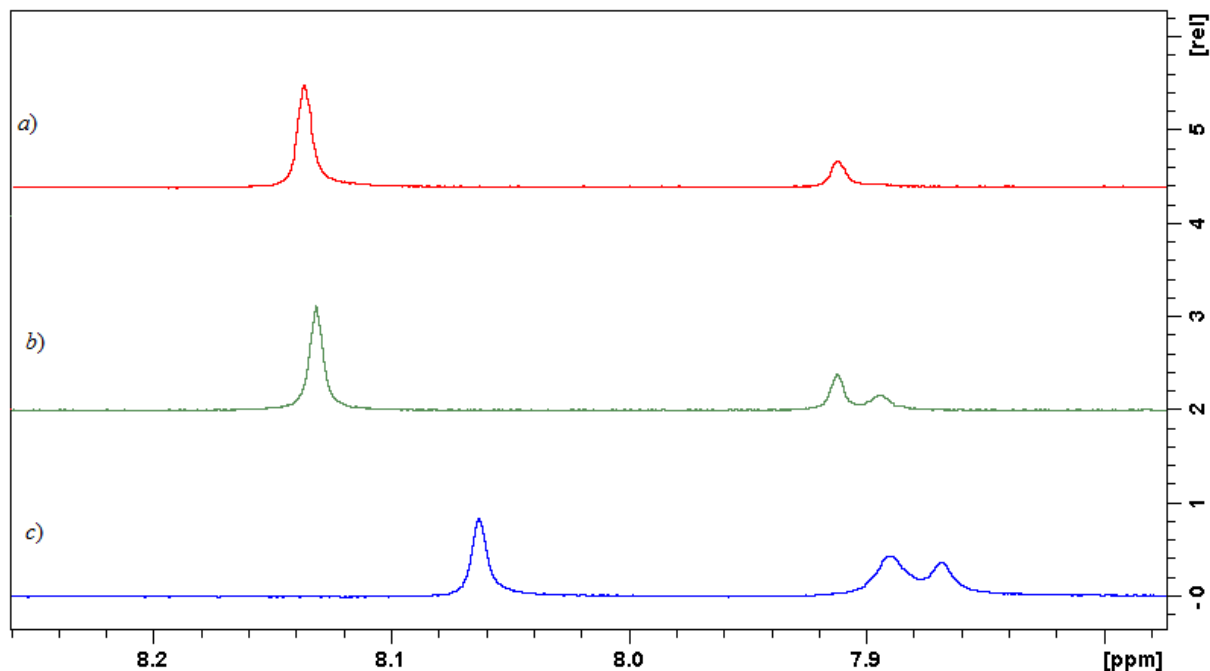
Figure 6.17: ^{1}H–NMR spectra for POA-Al(III) ([POA]$_0$=2.525·10^{-3} m; [Al^{3+}]$_0$=0.650·10^{-3} m) at different pH values: *a*) pH = 2.65; *b*) pH = 4.22; *c*) pH = 5.17 in D$_2$O. Only the region of interest (the aromatic one between 7.8 and 8.2 ppm) is shown in the spectra.

The integration values of the NMR aromatic signals of Figure 6.17 have been evaluated in order to obtain NMR semiquantitative data. These can be computed by dividing the area of the free ligand peak by the total area, and represent the percentage of ligand being in its free form. These values can be compared with those obtained from potentiometric measurements. All results are summarized in Table 6.5. The potentiometric values differ from the NMR ones (due to several reasons, e.g. isotopic effects), but only at the intermediate pH the difference is significant. The percentage of free ligand appears to have been overestimated: this might be both due to the overlap of a complex signal and the free ligand signal, or to the undetection of a severely broadened signal of the complexes. To this connection, bis Al(III)-HPCs complexes are eligible to give broad signals at NMR because the interconversion of their possible diastereoisomers is known to be rather quick [Crisponi 2012 (b)].

Table 6.5: free ligand percentage obtained by potentiometric results and ^{1}H-NMR spectra

pH	Potentiometry (%)	^{1}H-NMR (%)
2.65	85	80
4.22	54	77
5.17	46	40

7 CONCLUSIONS AND PERSPECTIVES

The research project, in which this thesis work was performed, regards the design, synthesis and study of hydroxypyridinecarboxylic acids (HPCs) as new chelating agents for iron and aluminium. The aim is to create new HPC derivatives bearing the same positive properties as the HPCs studied up to now, but showing at the same time a higher complexation strength towards the two toxic metal ions. At the present stage of the project, hydroxypyridinedicarboxylic acids (HPdCs) have been identified as possible candidates, and two HPdC derivatives have been chosen for the studies, 4-hydroxy-3,5-pyridinedicarboxylic acid (DQ58) and 4-hydroxy-1-methyl-3,5-pyridinedicarboxylic acid (DQ71508). The studies on DQ58 and DQ71508 which can be performed at first are purely chemical, and regard the solution speciation studies of solutions containing either ligand and either of the following metal ions: Fe(III), Al(III), Cu(II), Zn(II). Iron and aluminium should be studied in order to get the most important information, the metal-ligand affinity, which is likely correlated with the chelator efficiency *in vivo*. Copper and zinc speciation are important as well, because their metal-chelator affinity can be correlated with possible toxic side effects induced by the chelator (furthermore, if the zinc- and copper-ligand affinity were adequate, the chelator might be of interest for a metal-targeting therapy in Alzheimer disease).

Among the eight possible combinations of ligand+metal systems which the chosen ligand and metal ions produce, the following were studied during this thesis work: DQ58-Zn(II), DQ71508-Zn(II), DQ71508-Cu(II), and (in part) DQ58-Cu(II). For each Zn(II) system and for DQ71508-Cu(II), potentiometric data have been obtained, in which the final ligand-metal titrations have been preceded by the titrations of the ligand and of the metal alone, and by the acid-base titrations. The easy of potentiometry to undergo systematic and random errors requested the potentiometric apparatus to be continuously and accurately checked through calibrations and parameters comparison. Potentiometric titrations curves indicated the formation of very few complexes, which include only the 1:1 ligand-to-metal complex having one or two different protonation states. For all the above four systems, UV-Vis data have been obtained as well. ^{1}H NMR and EPR spectra have been recorded for ligand-Zn(II) and ligand-Cu(II) solutions, respectively.

No definitive result can be given, because most UV-Vis and all EPR spectra have not been elaborated yet, i.e., corresponding final results are still missing. These results can be very important, because they would allow to clarify the metal-ligand speciation at physiological pH. In fact, UV-Vis appeared to reduce or overcome the precipitation problem encountered in all ligand-metal potentiometric titrations

starting from acidic pH values. Nevertheless, the obtained potentiometric data indicate that the Cu(II) and Zn(II) complexes should be very weak at physiological pH, thus possibly causing no essential metal depletion during a chelation therapy regiment. On the other hand, the potentiometric results obtained in other thesis works [Cassini 2012, Feltracco 2013], indicate that DQ58 and DQ71508 are good but not excellent iron and aluminium chelators, i.e., their Al(III) and Fe(III) complexation strength is high but still significantly lower than that of other chelators presently in use (such as Deferiprone). Were these results confirmed, it would result that DQ58 and DQ71508 cannot be proposed either for the aluminium and iron chelation therapy, or for the metal-targeting therapy for copper and zinc.

Beside the above described research project, another HPC has been considered, 4-pyridoxic acid (POA), due to its biological relevance and to the interesting possibility to employ a well-known non-toxic compound as chelator. The following metal-POA have been studied in this thesis: POA-Zn(II) and POA-Al(III). Potentiometric data on POA-Zn(II) indicated no complex formation, or the formation of very weak complexes which could not be detected in solution. On the other hand, the solution speciation of POA-Al(III) demonstrated to be rather complicated, and many complexes coexist in solution with ligand-to-metal stoichiometric ratios 1:1, 2:1, and 3:1, and with different protonation states. The complexes formed in solution are stable, so that the hydroxide precipitation is prevented by a ligand moderate excess. However, the Al(III) affinity of POA is not as high as it is for other chelators presently in use.

As work perspectives, the missing spectroscopic data have to be elaborated. Some results on the metal-ligand systems not included in this thesis, but included in the project, are being processed as well, and will allow to gain a full speciation picture of the systems examined in this project.

BIBLIOGRAFIA

Abdulla 1979

Abdulla, M.; Svensson, S.; Norden, A.
Antagonistic effect of zinc in heavy metal poison.
Proceedings of management and control of heavy metals in the environment, CEP consultants, Edinburgh, UK (1979).

Albert 1967

Cotton, F.A.; Wilkinson, G.
Chimica Inorganica.
Ambrosiana (ed.), II edizione (1967).

Alfrey 1980

Alfrey, A.C.; Hegg, A.; Craswell, P.
Metabolism and toxicity of aluminium in renal failure.
Am. J. Clin. Nutr., **33**, 1509–1516 (1980).

Anderegg 1990

Anderegg, G.; Raeber, M.
J. Chem. Soc. Commun., 1194 (1990)

Arnal 2012

Arnal, N.; Tacconi de Alaniz, M.J.; Marra, C.A.
Biochim. Biophys. Acta, **1820,** 931–939 (2012).

Bergeron 1993

Bergeron, R.J.; Streiff, R.R.; Creary, E.A.; Daniels, R.D.J.
Blood, **81**, 2166 (1993)

Bertini 2008

Bertini, I.; Cavallaro, G.
Biol. Inorg. Chem., **13**, 3-14 (2008).

Brilla 2005

Brilla, L.R.; Conte, V.
Effects of a novel zinc-magnesium formulation in hormones and strength.
http://www.snac.com/research.htm (2005)

Bunton 1961

Bunton, C.A.; Shiner Jr., V.J.
Isotopo effects in deuterium oxide solution.
Journal of the American Chemical (1961)

Bush 1994

Bush, A.I.; Pettingel, W.H.; Multhaup, G.D.; Paradis, M.; Vonsattel, J.P.; Gusella, J.F.; Beyreuther, K.; Masters, C.L.; Tanzi, R.E.
Science **265**, 1464-1567 (1994).

Cassini 2012

Studio complessometrico di nuovi potenziali farmaci chelanti per alluminio (III) e ferro (III): acido 4–idrossi–3,5–piridindicarbossilico e N–acetilglutammil–

[cisteinil(5–metilen–8–idrossichinolina)–
metossiglicina]–metossile
Tesi di laurea, Università degli Studi di Padova (2012)

Charles 1976   Charles, F.; Baes, Jr; Mesmer, R.E.
The hydrolysis of cations.
Wiley (1976).

Coates 1967   Coates, E.; Rigg, B.; Saville, B.; Skelton, D.
J. Chem. Soc., 5613 (1965).

Cohen 1934   Cohen, E.; Elvehijem, C.A.
The relation of iron and copper to the cytochrome
andoxidase content of animal tissue.
*J. Biol. Chem,***107** (97) (1934).

Cotton 1968   Cotton and Wilkinson.
Chimica Inorganica.
Casa editrice Ambrosiana (1968).

Crisponi 2008   Crisponi, G.; Remelli, M.
Coord Chem Rev, **252**, 1225-1240 (2008)

Crisponi 2012 (a)   Crisponi, G.; Nurchi, V.M.; Bertolasi, V.; Remelli, M.;
Faa, G.
Chelating agents for human diseases related to
aluminium overload.
Coord. Chem Rev., **256**, 89–104 (2012).

Crisponi 2012 (b)   Crisponi, G.; Dean, A.; Di Marco, V.B.; Lachowicz,
J.I.; Nurchi, V.M.; Remelli, M.; Tapparo, A.
Different approaches to the study of chelating agents
for iron and aluminium overload pathologies
Anal. Bioanal. Chem., 1618-2642 (2012)

Dean 2009   Dean, A.; Ferlin. M.G.; Brun, P.; Castagliuolo, I.;
Yokel, R.A.; Badocco, D.; Pastore, P.; Venzo, A.;
Bombi, G.G.; Di Marco, V.B.
1,6–Dimethyl–4–hydroxy–3–pyridinecarboxylic acid
and 4–hydroxy–2–methyl–3–pyridine-carboxylic acid
as new possible chelating agents for iron and
aluminium
Dalton Trans., 1815–1824 (2009)

Dudev 2000   Dudev, T.; Lim, C.
J. Am. Chem. Soc., **122**, 11146-11153 (2000)

Dudev 2006   Dudev, M.; Wang, J.; Dudev, T.; Lim, C.

Factors governing the metal coordination number in metal complexes from Cambridge structural database Analyses
J. Phys. Chem B, **110**, 1889-1895 (2006)

Durrant 1970 Durrant, P.J.; Durrant, B.
Advanced inorganic chemistry, II edition.
Longman (ed) (1970).

Edward 1995 Edward, J.T.; Ponka, P.; Richardson, D.R.
Partition–coefficients of the iron(III) complexes of pyridoxal isonicotinoyl hydrazone and the correlation to iron chelation efficacy
Biometals, **8**, 209–217 (1995)

Eigen 1963 Eigen, M.; Bunsenges, Ber.
Phys. Chem., **67**, 753 (1963).

Feltracco 2013 Studio complesso metrico e caratterizzazione in vitro di un nuovo potenziale farmaco chelante per alluminio e ferro
Tesi di laurea, Università degli Studi di Padova (2013)

Floyd 1933 Floyd, R.A.; Carney, J.M.
The role of metal ions in oxidative process and aging.
Taxicol. Health **9** (1,2), special issue (1933).

Frisardi 2010 Frisardi, V.; Solfrizzi, V.; Capurso, C.; Kehoe, P.G.; Imbimbo, B.P.; Santamato A.; Dellegrazie, F.; Seripa, D.; Pilotto, A.; Capurso, A.; Panza, F.
J. Alzheimers Dis., **20**, 17-30 (2010).

Gaeta 2005 Gaeta, A.; Hider, R.C.
The crucial role of metal ions in neurodegeneration: the basis for a promising therapeutic strategy
British Jornal of Pharmacology, **146**, 1041–1059 (2005)

Ganrot 1986 Ganrot, P.O.
Metabolism and possible health effects of aluminium.
Environ. Health Perspect., **6**, 363–441 (1986).

Geser 2008 Geser F.; Lee VM-Y; Trojanowski, J.Q.
Frontotemporal Dementias.
The molecular and genetic basis of neurologic and psychiatric disease, Ed. Rosenberg R, et al. (2008).

Graddon 1964 Graddon, D. P.; Weedon, D. G.
Austral J. Chem., **17**, 607 (1964).

Guengerich 2009   Guengerich, F.P.
J. Biol. Chem., **284** (2009).

Hahn 1990   Hahn, F.N.; McMurry, T.J.; Hugi, A.; Raymond, K.N.
Coordination chemistry of microbial iron transport. 42.
Structural and spectroscopy characterisation of
diastereometric Cr(III) and Co(III) complexes of
desferrithiocin
J. Am. Chem. Soc., **112**, 1854–1860 (1990)

Housecroft 2005   Housecroft, C.E.; Sharpe, A.G.
Inorganic chemistry, second ed.
Pearson Education Limited (2005).

Hugy 1985   Hugy–Cleary, D.; Helm, L.; Merbach, A.E.
Variable–temperature and variable–pressure ^{17}O–NMR
study of water exchange of hexaaquo–aluminium(III) .
Helv. Chim. Acta, **68**, 545–554 (1985).

Hunt 1983   Hunt, J.P.; Fredman, H.L.
prog. Inorg. Chem., **30**, 359 (1983).

Irving 1967   Irving, H.M.; Miles, M.G.; Petit, L.D.
Anal. Chim. Acta, **38**, 475–482 (1967)

Keberle 1964   Keberle, H.
Ann. N.Y. Acad. Sci., **119**, 758 (1964)

Kiss 1996   Kiss, T.; Farkas, E.
The bioinorganic chemistry of aluminium
Persp. Bioinorg. Chem., **3**, 199–250 (1996).

Kontoghiorghes 1995   Kontoghiorghes, G.J.
Toxicol. Lett., **80**, 1-18 (1995)

Kontoghiorghes 2000   Kontoghiorghes, G.J.; Pattichi, K.; Hadjigavriel, M.;
Kolnagou, A.
Transfusional iron overload and chelation therapy with
deferoxamine and deferiprone (L1)
Transfusional Science, **23**, 211–223 (2000)

Kozlowski 2012   Kozlowski, H.; Luczkowski, M.; Remelli, M.;
Valensin, D.
Coord. *Chem. Rev.,* **256**, 2129-2141 (2012).

Lattmann 1997   Lattmann, R.; Acklin, P.
Substituted 3,5–diphenyl–1,2,4–triazoles and their use
as pharmaceutical metal chelators

International Patent WO 97/49395 (1997)

Lee 1996

Lee, J.D.
Chimica Inorganica
Piccin (1996).

Lipinski 1997

Lipinski, C.A.; Lombardo, F.; Dominy, B.W.; Feeney, P.J.
Adv. Drug Del. Rev., **23** (1997)

Liu 2002

Liu, Z.D.; Hider, R.C.
Med. Res. Rev., **22**, 26–64 (2002)

Maccà 1995

Maccà, C.
Gran questo incompreso. Un suggerimento per un più efficace approccio didattico
CnS, 1995, **17** (5/6), 86–88 (1995)

Martin 1986

Martin, B.R.
The chemistry of aluminium as related to biology and Medicine.
Clin. Chem., **32**, 1797–1806 (1986).

Masters 1985

Masters, C.L.; Simms, G.; Weinman, N.A.; Multhaup, G.; McDonald, B.L.; Neyreuther, K.
Proc. Natl. Acad. Sci. U.S.A. **82**, 4245-4249 (1985).

Nussbaum 2003

Nussbaum, R.L.; Ellis, C.E.
Alzheimer's disease and Parkinson's disease.
N. Engl. J. Med., **348**, 1356-1364 (2003).

Ohman 1988

Ohman, L.O.
Equilibrium and structural studies of silicon(IV) and Aluminium(III) in aqueous solution. 17. Stable and metastable complexes in the H–Al^{3+}–citric acid .
Inorg. Chem., **27**, 2568–2570 (1988)

Pories 1966

Pories, W.J.; Strain, W.H.
Zinc and wound healing.
Zinc metabolism. A.S. Prasad (Ed). Charles C. Thomas, Springfield (IL) (1966).

Prejbenau 2011

Prejbenau, R., Ahmadi, M.; Scurtu, M.; Vermesan, D.; Olariu, L.
Influences of zinc and manganese overdoses in biosystems
Rev. Chim, **62**, 750-752 (2011)

Rockenbauer 1996

Rockenbauer, A.; Korecz, L.

	Appl. Magn. Reson., **10**, 29-43 (1996)
Rockenbauer 2001	Rockenbauer, A.; Szabó-Plánka, T.; Árkosi, Zs.; Korecz, L. *J. Am. Chem. Soc.* **123**, 7646-7654 (2001)
Rossotti 1961	Rossotti, F.J.C.; Rossotti, H. The determination of stability constants and other equilibrium constants in solution New York–Toronto–London, Mc Graw–Hill Book Company Inc. (1961)
Rotzinger 2005	Rotzinger, F.P. *Chem. Rev.*, **105**, 2003-2037 (2005)
Silverthom 2007	Silverthorn, D.U. Fisiologia, Un approccio integrato Ambrosiana (ed.), III edizione (2007)
Suba 2013	Két piridinkarbonsav réz(II) komplexeinek egyensúlyi vizsgálata Thesis work, University of Szeged (2013)
Suzuki 1981	Suzuki, K.T.; Maitani, T. *Biochem. J.*, **199**, 289-295 (1981).
Swaddle 2005	Swaddle, T.W. Kinetic evidence for five–coordination in $Al(OH)aq.^{2+}$ ion *Science*, **308**, 1450–1453 (2005).
Terry 1987	Terry, R.D.; Hansen, L.A.; DeTeresa, R.; Davies, P.; Tobias, H.; Katzman, R. Senile dementia of the Alzheimer type without neocortical neurofibrillary tangles. *J Neuropath Exp Neurol*, **46**,262-268 (1987).
Wilkins 2002	Wilkins, R.G. Kinetics and mechanism of reactions of transition metal complexes. Wiley-VCH (2002).
Willis 1983	Willis, M.R.; Savory, J. Chemical toxicology and clinical chemistry of metals. S.S.B. (ed.); Savory, J. (ed.) (1983).
Wilson 1977	Wilson, R.L. Iron, zinc, free radicals and oxygen tissue disorders and cancer control.

Iron methabolism. R. Porter (Ed). Ciba Found. Symp, **51**, 331-354 (1977).

Wilson 1987   Wilson, R.L.
Vitamin, selenium, zinc and copper interactions in free radical protection against ill-placed iron.
Proc. Nutr. Soc.I, **46**(27) (1987).

Wolfe 1990   Wolfe, L.C.
Desferrithiocin
Semin. Haematol., **27**, 117–120 (1990)

Yumoto 2009   Yumoto, S.; Kakimi, S.; Ohsaki, A.; Ishikawa, A.
J. Inorg. Biochem., **103**, 1579-1584 (2009).

Zatta 1995   Zatta, P.; Zambenedetti, P. et al.
La chimica dell'alluminio e i sistemi biologici. Dati certi e questioni aperte.
La chimica e l'industria, **77**, 797–802 (1995)

Zatta 2009   Zatta, P.; Drago, D.; Bolognin, S.; Sensi, S.L.
Trends Pharmacol. Sci., **30**, 346-355 (2009).